Alliages base Cobalt en surfusion sous champ magnétique intense : propriétés magnétiques et comportement à la solidification

Jun Wang

西北工業大學 NORTHWESTERN POLYTECHNICAL UNIVERSITY

UNIVERSITÉ DE GRENOBLE

THÈSE

Pour obtenir le grade de

DOCTEUR DE L'UNIVERSITÉ DE GRENOBLE

préparée dans le cadre d'une cotutelle entre l'*Université de Grenoble* et la *Northwestern Polytechnical University*

Spécialité : **PHYSIQUE DES MATERIAUX**

Arrêté ministériel : le 6 janvier 2005 -7 août 2006

Présentée par **Jun WANG**

Thèse dirigée par **Eric Beaugnon** et **Jinshan LI**

préparée au sein des **Consortium de Recherche pour l'Emergence de Technologies Avancées (CNRS/CRETA) et du State Key Laboratory of Solidification Processing (NWPU)** dans l'**Ecole Doctorale de Physique de l'Université de Grenoble et la Graduated School of Northwestern Polytechnical University**

Alliages base Cobalt en surfusion sous champ magnétique intense : propriétés magnétiques et comportement à la solidification

Thèse soutenue publiquement le **24 septembre 2012**,
devant le jury composé de :

Mme Yudong ZHANG
Ingénieur de Recherche, Université de Metz, Rapporteur
M. Jacques FOULETIER
Professeur, Université Joseph Fourier
M. Jacques NOUDEM
Professeur, Université de Caen
M. Eric BEAUGNON
Professeur, Université Joseph Fourier
M. Pingxiang ZHANG
Professeur, Northwest Institute for Nonferrous Research, Rapporteur
M. Guo YAN
Dr., West Superconducting Technologies Co. Ltd
M. Xianghong LIU
Dr., West Superconducting Technologies Co. Ltd
M. Jinshan LI
Professeur, Northwestern Polytechnical University

Université Joseph Fourier / Université Pierre Mendès France / Université Stendhal / Université de Savoie / Grenoble INP

ABSTRACT

This work is devoted to the investigation of the magnetic field effect on the magnetic properties and solidification behavior of undercooled Co based alloys in high magnetic field. Co based alloys are promising candidates to be undercooled below or approaching their Curie point in strong magnetic field due to their small temperature difference between liquid line and Curie point. In this dissertation, a high temperature undercooling facility with magnetization measurement system is built in a superconducting magnet, and is used for in situ measurement of the magnetization of the undercooled melts and to studying the undercoolability and solidification microstructure evolution in magnetic field. The deep undercooled Co melt is strongly magnetized in magnetic fields, and its magnetization is even larger than the magnetization of heated solid at the same temperature. The magnetization of undercooled Co-B near eutectic alloy is related with overheating temperature while the undercooled Co-Sn melt is always in paramagnetic state. Mean undercooling and recalescence extent of different metals and alloys are affected by external magnetic field. In uniform magnetic field, the undercooling of Cu is enhanced while the undercoolings of Co and Co-Sn keep constant. However, the recalescence extents of Co and Co-Sn alloys are reduced, and with the increasing Co content, the effect becomes larger. Magnetic field promotes the precipitation of αCo dendrite phase and the formation of anomalous eutectics in solidified microstructure of undercooled Co-Sn alloys. The microstructure evolution processes are affected by magnetic field depending on the field intensity and undercooling. This work opens a new way to investigate the magnetic properties of deeply undercooled metallic melts and non-equilibrium solidification in strong magnetic fields.

Résumé

Ce travail est dédié à l'étude de l'effet des champs magnétiques sur les propriétés magnétiques et le comportement à la solidification d'alliages à base de Cobalt en surfusion sous champ magnétique intense. Les alliages à base Co sont d'excellents candidats pour obtenir une surfusion en dessous ou proche du point de Curie sous champ intense en raison du faible écart entre ce point de Curie et la température du liquidus. Dans cette étude, un dispositif haute température de surfusion intégrant une mesure magnétique a été construit dans un aimant supraconducteur, et est utilisé pour la mesure in situ de l'aimantation de liquides surfondus et pour l'étude du sur-refroidissement et de l'évolution de la microstructure de solidification en champ intense. Le cobalt liquide en surfusion est fortement magnétique sous champ, et son aimantation est même supérieure à celle du solide au chauffage à la même température. L'aimantation de l'alliage proche eutectique Co-B en surfusion dépend de la température de surchauffe, tandis que le Co-Sn en surfusion est toujours paramagnétique. La surfusion moyenne et l'étendue de la recalescence de différents métaux et alliages est affectée par un champ externe. En champ magnétique uniforme, la surfusion du Cuivre est amplifiée, tandis que la surfusion du Cobalt et de Co-Sn reste identique. Cependant, l'étendue de la recalescence du Cobalt et de Co-Sn est réduite, et l'effet est d'autant plus important pour des teneurs supérieures en Cobalt. Le champ magnétique promeut la précipitation de la phase dendritique αCo et la formation d'eutectique anormal dans la microstructure des alliages Co-Sn surfondus. Les processus d'évolution de la microstructure sont affectés par le champ magnétique, et dépendent de l'intensité du champ et de la surfusion. Ce travail offre de nouveaux horizons dans l'étude des propriétés magnétiques d'alliages métalliques en forte surfusion et dans l'étude de la solidification hors équilibre sous champ magnétique intense.

ACKNOWLEDGEMENTS

This thesis research would not have been possible without kind helps and supports from many individuals. First of all, I am deeply indebted to my thesis supervisors, Dr. Eric BEAUGNON and Dr. Jinshan LI. Dr. Eric BEAUGNON, as a caring mentor, he is always there whenever I need guidance and support. His interest, intuition, and ideas have been an invaluable source of inspiration. His enthusiasm, humorous and optimism are inspiring me continuously. Dr. Jinshan LI, since I first met him in 2005, he always keeps a paternal eye on me. His encourage and edification has been endless source of motivation for me. His enthusiasm, decisive, and optimism are encouraging me all the time. I want to thank them for all the time they have spent with me explaining the most obscure concepts, for helping me view results with new sights and for teaching me how to think about by myself. It has been my greatest pleasure and most important experience to work under their guidance.

I owe my special thanks to Dr. André SULPICE for helping me in many ways for my research and daily life. I am very grateful to Dr. Sophie RIVOIRARD and Dr. Rui HU, for their helps in building the experimental setup and many fruitful discussions. I am grateful to Dr. Jean-louis SOUBEYROUX for helping me to use the levitation induction melting furnace, Dr. Xavier CHAUD for helping in using furnace and internet connection, Dr. Laureline PORCRA for helping me to use microscope, Dr. Philippe ODIER for helping me perform DTA analysis, Dr. Sebastien PAIRIS for assistance in using SEM and Dr Olivier LEYNAUD for assistance in using XRD. I would like to thank Paul CHOMETON for helping me build the furnace and teaching me to use the SEM, Pierre Frédéric-Sibeud for assistance in my experiments and Marie-Dominique Bernardinis for kind help in my research and daily life.

I would like to express my gratitude to all the members in CRETA. For their friendship, cooperation and many discussions on various topics. Especially, I am grateful to Bianca FRINCU, Alexandre VASSA, Mélissa MIKOLAJZYK, Ghislain BUGNICOURT, Baptiste DELHOMME, Sarah PETIT, Nathalie DECHOUX, Thomas GARCIN, Sylvain GARRIER, Gildas DIGUET, et al. I would like to show my sincerely thanks to members in Institute of Rare Metal Materials and Processing

(RM2P). It is my great pleasure to study and work with Dr. Hongchao KOU, Dr. Xiangyi XUE, Dr. Hui CHANG, Dr. Hong ZHONG, Dr. Tiebang ZHANG, Dr. Bin TANG, Dr. Zhongbo ZHOU, Dr Hongbao YU, et al in RM2P.

I also want to thank my Chinese friends who accompany with me in France: Zhaosheng WANG (MCBT), Qingyang WANG (MCBT), Tao WU (LNCMI), Houxiu XIAO(LNCMI), Yuepeng ZHANG(NANO), Peng LIU(NANO), Qiao LI(Grenoble III) and Danxiang XU(Grenoble III).

Finally, I would like to express my deepest gratitude to my mother, sister and family for their unconditional love and encouragement. I am also grateful to my wife Pei and lovely daughter Liuliu. It is my great happiness to share the life with them together.

The support from the China Scholarship Council (CSC), Service Scientifique Ambassade de France en Chine and French-Chinese International Associated Laboratory LAS2M are acknowledged.

TABLE OF CONTENTS

CHAPTER 1 INTRODUCTION

1.1 General review

With the development of cryogenic and superconducting technologies, it is quite easy to generate high static magnetic fields above 10T by using cryogen-free superconducting magnets, which can be used for a long term without filling with expensive liquid helium to obtain 4K or lower temperature [COEY09, WEB1]. Thus, the application of cryogen-free superconducting magnet has reduced the cost for maintain high magnetic field and greatly promoted the application of magnetic fields in advanced materials processing, and also in the research of fundamental magneto science.

Magnetic field, especially for high magnetic field, as clean, powerful and non-contacting energy, has received much attention in material processing area, as it can act on atomic behaviors and affect such as atom arrangement, matching and migration and changes the thermodynamic state of materials hence exert powerful influence on microstructures and properties of materials [BUSC03]. As an extreme processing method, magnetic fields were firstly used in physical research and now gradually developed to be used in chemistry, biology, and materials science, etc.

The application of magnetic field on materials processing has been a subject of much attention since two decades, and becomes a new direction of materials science-electromagnetic processing of materials (EPM). Present research indicates that the application of magnetic field can change the thermodynamic state of phase transitions of materials and influence the phase transformation process [GARC10]. In solid state phase transitions, heat treatment under the magnetic field can change the morphology of the microstructure [MOLO04, XION08]. For crystal with magneto anisotropy, the grain can be aligned when heat treated under magnetic field, and can make bulk textured materials [DERA91, RIVO09]. Very recently, the solidification of materials under magnetic field has become a hot topic. The solidification process has great importance on the final properties, and the application of magnetic field in the solidification process can change the morphology, distribution and growth velocity of the precipitated phases and obtain in-situ formed composites, gradient materials and anisotropic materials with unique structure and excellent properties [BAN08,

CHEN11, LI09a, LIU11b, REN06, SAVI81, TOUR00, YASU01]. Non-equilibrium solidification is a very important research area and has many potential applications. Due to the limitation of the experimental facilities, the non-equilibrium solidification under magnetic field has been little investigated. Deep investigation on the magnetic properties of undercooled melt, undercoolability, and microstructures of undercooled melt solidified under strong magnetic field is an essential way for underlying the mechanism of solidification of deep cooled melt under strong magnetic field.

1.2 Materials processing under strong magnetic field

1.2.1 Texture of materials under strong magnetic field

The grain of materials tends to align along the easy magnetization axis, which is the typical characteristic of the magnetic field effect during heat treatment. It is rather mature for the investigation of texture mechanism under magnetic field, and the magneto crystalline anisotropy is attributed to account for this. Under high magnetic field, even non-ferromagnetic materials can be textured during the solidification process, indicating the magnetic field can be used to control the morphology of the solidified crystal. In 1981, Savitsky et al [SAVI81] found that the MnBi phase aligned along the magnetic field direction during solidification of Bi–Mn alloy in a 2.5T magnetic field, and magnetocrystalline anisotropy was the main reason according to magnetic property measurements. De Rango et al. [DERA91] extended the investigation to the solidification of paramagnetic $YBa_2Cu_3O_7$ material and obtained texture crystal structure in a 5T magnetic field, seen in Fig 1-1. Asai [ASAI89] found MnBi phase precipitated along the direction of the magnetic field in MnBi alloy while perpendicular alignments in Al-Si-Fe alloy during solidification in a high magnetic field. Based on the traditional magneto theory, Asai, et al. [ASAI07] incorporated magnetization energy to describe the texture behavior under magnetic field. There are three conditions required for texturing for non-ferromagnetic materials: the crystal must have magnetocrystalline anisotropy, the magnetocrystalline energy must be larger than the thermal fluctuation energy and constrain of medium must be weak enough for the rotation of the crystal even with weak magnetization energy.

Most recently, some new valuable experiment results have been found which can be used as new theories or just enrich the old ones. For example, based on the

investigation of texturing of different materials under magnetic field, R. Tournier believed that there exist unmelted crystals with magnetocrystalline anisotropy in the melt which play a very important role on the texturing process. With the finding of new results and introducing of new experimental methods, we believe that the texturing theory will be further developed in the future.

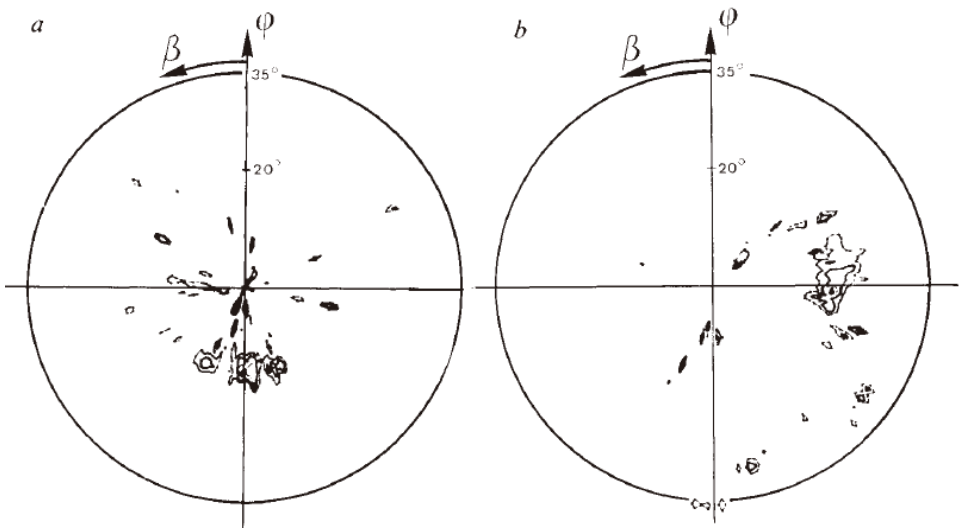

Fig 1-1 Textured $YBa_2Cu_3O_7$ solidified under 5T magnetic field [DERA91]

1.2.2 Controlling the melt flow by strong magnetic field

The flow in the alloy melt can affect the transfer of heat and solute, and influence the crystal growth process. Due to the temperature gradient and concentration gradient, the density difference in different zone can generate convection flow under gravity field. When the magnetic field is applied, the Lorentz force generated by electromagnetic introduction can damp the convection process. In 1953, when Tiller et al. [TILL53] proposed the famous constitutional undercooling theory, they pointed out that alloys solidified under strong magnetic field can eliminate the solute distribution in the solidification interface front caused by convection, and formed homogeneous material. In 1966, Utech and Flemings [UTEC66] eliminated the solute band in semiconductor single crystal by restraining the convection flow with magnetic field, and evidently decreased the macrosegregation during the growth of the semiconductor single crystal. In 1983, Oreper and Szekely [OREP83] found that the intensity of the magnetic field determined the suppression effect of nature convection, and also the size and shape of the system also played a very important role. In 1990, by investigation of the unidirectional solidification of doped semiconductor, Motakel

[MOTA90] estimated the general relationship between diffusion controlled growth and magnetic field intensity. Then, Kang et al [KANG94a, KANG94b] found the Lorentz force was very small when the convection effect was very weak under magnetic field, and the effect of magnetic field on suppressing the convection was very weak. In this case, low convection model should be used to describe the convection in magnetic field. Based on the present results, we can find that the magnetic field has complicated effect on the solute distribution, and the suppressing mechanism may be different for different system and magnetic field.

Except for the suppression effect of magnetic field on the melt convection, it can also induce the flow of the melt. In 1993, Moreau et al. [MORE93] found the dendrites became coarse when 0.55T magnetic field was applied in the unidirectional solidification of Bi-Sn alloy, and they introduced thermoelectric effects to explain this variation. Tewari et al. [TEWA94] found the same effect and the cellular microstructures were severely distorted when 0.45T magnetic field was applied during the unidirectional solidification of Pb-Sn alloys. Li et al. [LI09b] found a low magnetic field can reduce thermal electromagnetic flow in unidirectional solidification process by numerical simulation, and found magnetic field can cause the interface instability and form ring like microstructure by protuberance in the interface in the unidirectional solidification of Al-Cu alloy (seen in Fig 1-2).

Fig 1-2 Solidified microstructure of Al-0.85wt.%Cu alloy in the mush zone [LI09b]

1.2.3 Phase transitions under strong magnetic field

The same as temperature and pressure, as an extreme physical means, strong magnetic field can affect the phase transition process of materials, especially for the phase transitions accompanied with large magnetic susceptibility difference or

ferromagnetic phase transitions. The present investigation of the effect of magnetic field on phase transition process mainly focuses on the solid state phase transition process of austenite/martensite, including effect of magnetic field on equilibrium phase diagram [KOCH00], formation of martensite [FUKU09], and decomposition kinetics of austenite [GARC10], the texturing and elongation effect of ferrite grain during heat treatment in magnetic field [ZHAN05], the phase structure variation by magnetic field treatment, e.g. the microstructure of bainite and martensite without magnetic field will transform to fine grained bainite microstructure in strong magnetic field [GARC09].

Because of the large magnetic susceptibility difference of martensite (ferromagnetic) and austenite (paramagnetic), martensite undergoes much more effect by external magnetic field. Using molecular theory, Joo et al [JOO00, JOO04] has calculated the effect of strong magnetic field on phase diagram of Fe-Fe_3C, seen in Fig 1-3, the results indicated that austenite/ferrite transition temperature increased with the increasing magnetic field intensity and phase transition temperature increased 20°C by 12T magnetic field. By building thermal expansion measurement facilities in strong magnetic field, Garcin et al [GARC09] found the austenite/ferrite transition temperature increased linearly with the external magnetic field in Fe-C-Mn alloys, and the volume fraction of ferrite increased under external magnetic field. Kakeshita et al [KAKE85] found strong magnetic field promoted martensite transformation, and impulse magnetic field accelerated the martensite transition in Fe-24.9Ni-3.9Mn alloy, and reduced the nose temperature of the TTT diagram and shortened the incubation time.

1.2.4 Levitation of diamagnetic materials in strong magnetic field

Gradient field generated by strong magnetic field can levitate diamagnetic material, which was an important finding in materials processing in magnetic field. In 1991, Beaugnon et al [BEAU91] firstly found the levitation effect of diamagnetic material in high magnetic fields. In levitation state, the magnetic force exerted on the levitation medium is in equilibrium with gravity, e.g. the levitated frog and strawberry

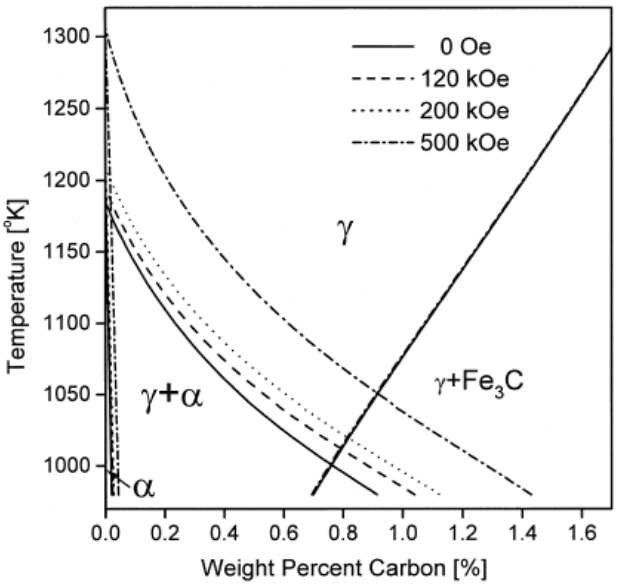

Fig 1-3 Fe-C phase diagram associated with the γ/α andγ/Fe_3C transformation for various applied magnetic fields [JOO00]

shown in Fig 1-4. For the matter in levitation state, magnetic field can take effect on its every atom or molecular, which means the matter can be treated in a zero gravity state. Thus, this effect can be used as a new technique in materials processing, e.g. container free crystal growth, which can prevent the contamination of the pollutions from the container and can also avoid the solute segregation caused by the gravity force.

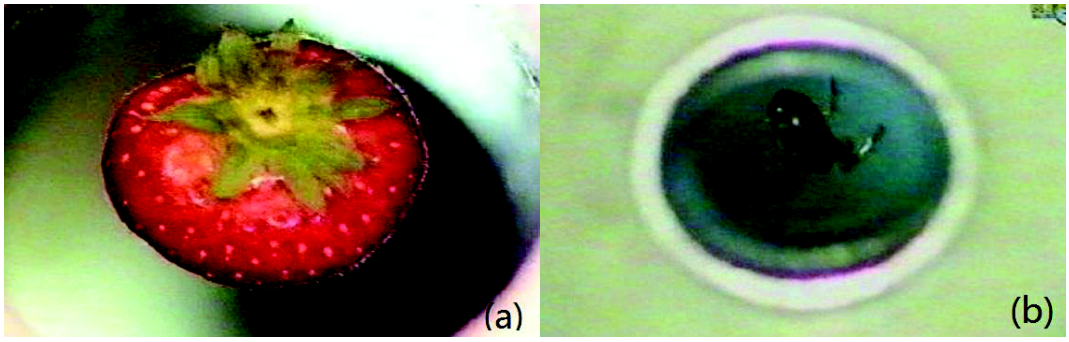

Fig 1-4 Magnetic field levitation of (a) a strawberry and (b) a frog

The magnetic field can also generate other effects for diamagnetic materials. N. Hirota et al [HIRO95] found rise and fall of surface level of diamagnetic water solutions in high magnetic field, exhibiting wave like arrangement, and this effect was called Moses effect (Seen from Fig 1-5). Westeon et al [WEST10] found the surface morphology changed during dissolve process of bluestone into water in non-homogeneous magnetic field, and this effect was due to the magnetic

susceptibility difference caused by solute concentration variations on the surface in magnetic field.

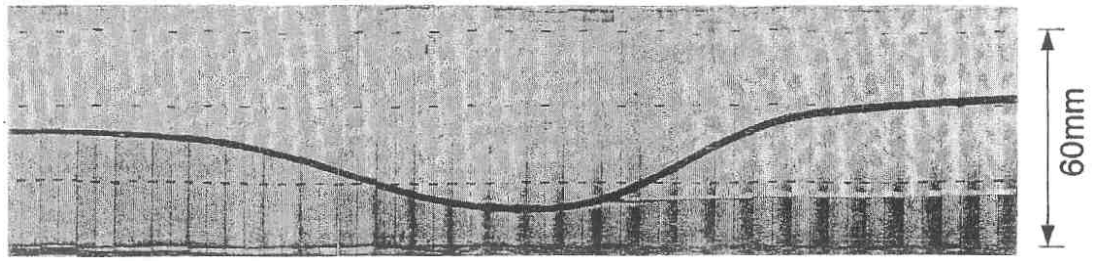

Fig 1-5 Rise and fall of surface level of water solutions in high magnetic field [HIRO95].

1.3 Solidification behavior under strong magnetic field

The solidification process of materials plays an important role in determination of final microstructure and properties. The effect of magnetic field on the solidification process is always stronger than solid state transformation process. Except for controlling melt flow, changing the solute distribution profile during solidification, strong magnetic field can also take strong effects on changing phase transition temperature, and solidified microstructure.

1.3.1 Effect of magnetic field on the solidification thermodynamics

Strong magnetic field can exert intense magnetic energy to atomic or molecular scale of matters without contamination, and changes the thermodynamic state. The thermodynamic effect of application of magnetic field is the magnetic Gibbs energy exerted on the system. No matter for pure metal or alloys, for the solidification process from liquid to solid, the magnetic properties variation between liquid and solid phase suggests magnetic field can change the thermodynamic equilibrium of the solidification process. Fig 1-6 is schematic diagram for the Gibbs free energy of transitions containing ferromagnetic phase. The application of magnetic field increases the driving force for phase transition, and shifts the phase transition point to high temperature range.

The total Gibbs free energy (ΔG_{total}) of pure metals or alloys in strong magnetic field can be expressed as:

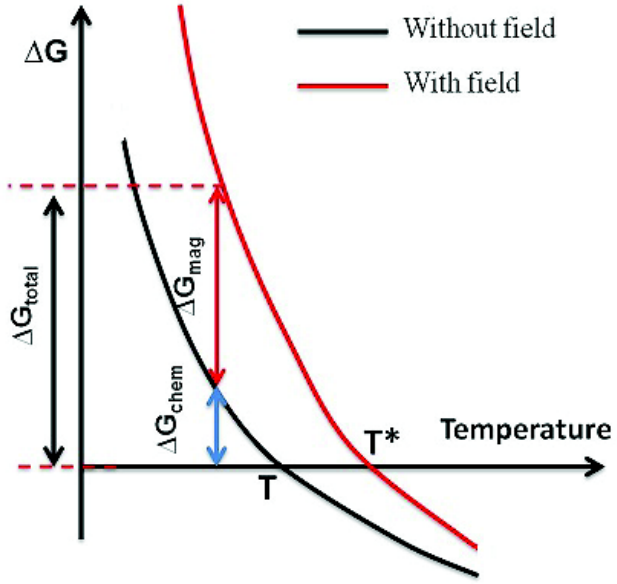

Fig 1-6 Schematic free energy-temperature diagram representing the effect of magnetic field on the relative contribution of the chemical and the magnetic free energy with and without the application of external magnetic field.

$$\Delta G_{total} = \Delta G_{chem} + \Delta G_{mag} \tag{1-1}$$

Where ΔG_{chem} and ΔG_{mag} are the chemical Gibbs free energy difference between solid and liquid phase per volume and external field caused Gibbs free energy difference per volume, respectively.

Under equilibrium condition, the melt solidifies at the melting point without magnetic field. When the nucleation is avoided during solidification process, the melt comes into undercooled state. Generally, when the undercooling is not so large, a linear model proposed by Turbull [TURB69] can be used to calculate Gibbs free energy:

$$\Delta G_{chem} = \frac{\Delta H_f \Delta T}{T_E} \tag{1-2}$$

When the undercooling is very large, the chemical Gibbs free energy of solidification process can be expressed by empirical model proposed by Dubey and Ramachandrarao [HERL94]:

$$\Delta G_{chem} = \Delta G_{LS}(T) = \frac{\Delta H_f \Delta T}{T_E} - \frac{\Delta c_P(T_E)\Delta T^2}{2T}[1 - \frac{\Delta T}{6T}] \tag{1-3}$$

The Gibbs free energy caused by external magnetic field can be calculated by:

$$\Delta G_{mag} = -\int_0^{H_{ex}} \mu_0 (M^S - M^L) dH_{ex} \tag{1-4}$$

And for nonferromagnetic alloys, it can be simplified as:

$$\Delta G_{mag} = -\frac{1}{2}\mu_0 \Delta\chi^{S-L} H_{ex}^2 \tag{1-5}$$

In case of low undercoolings, during solidification, $\Delta G_{total}=0$, and we can receive:

$$\Delta T = \frac{\Delta\chi^{S-L} B^2}{2\mu_0 \Delta H_m} T_m \tag{1-6}$$

Where H_{ex}, M^S, M^L, ρ and μ_0 are the external magnetic field, magnetization of solid and lquid, density and vacuum magnetic permeability. And ΔH and ΔS are enthalpy and entropy difference during solidification process, respectively.

In magnetic field, equilibrium solidification temperature is affected by the magnetic susceptibility of solid/liquid phase. Li et al [LI10a, LI10b] has measured the melting point and equilibrium solidification temperature of different metals and alloys by building a DTA apparatus in strong magnetic field. Their results indicated that with the increasing magnetic field, the melting point of pure Bi and Al kept constant in magnetic field while the equilibrium solidification temperatures were changed by the magnetic field, and the equilibrium temperature for Bi increased while it decreased for pure Al.

1.3.2 Effect of magnetic field on the solidified microstructure

The application of magnetic field during solidification process can directly control the convection flow in the melt and also affect the final solidified microstructure and phases. Except for the well known texture effect during solidification in magnetic field, many more new phenomena have been found during the solidification of materials these years.

Liu et al [LIU07] have successfully fabricated MnSb/Sb–MnSb hypereutectic gradient composites by controlling the field gradient and cooling rate. Wang et al [WANG09] found that the field intensity can change the solidified microstructure in near eutectic Mn-90.8wt%Sb alloys, their results found the solidified microstructure was purely eutectics without magnetic field, and MnSb/Sb precipitated in the solidified microstructure when 4.4T magnetic field was applied. MnSb and Sb phases would be precipitated at the same time when the field increased again, and the volume fraction of primary phase increased with the field intensity. During the investigation of Al-Si alloys, Liu et al [LIU11c] found strong magnetic field could reduce the space between secondary dendrites arms and lamellar distance, and this was due to the

constrain effect of magnetic field for the solute movement in the solid-liquid interface, which controlled the diffusion of solute atoms. X. Li et al [LI06, LI07c, LI09a] have introduced a unidirectional facility to a superconducting magnet, and systematically investigated the unidirectional solidification behavior in high magnetic field. Their results found that the high magnetic field caused the breakdown of a planar interface into cellular undulations and the formation of an irregular shape and also found the magnetic force and thermoelectric magnetic force were mainly responsible for the interface irregularity and also induced the instability of the interface.

1.4 Solidification of undercooled melt under strong magnetic field

1.4.1 Investigation on non-equilibrium solidification

By avoiding heterogeneous nucleation, the metallic melt can solidify at temperature below its equilibrium melting point, which is called undercooling solidification. The temperature difference between the equilibrium melting temperature and actual nucleation temperature is called undercooling (ΔT). Once nucleation happens in the undercooled melt, fast solidification process starts in the undercooled melt, and the latent heat release speed is much larger than the heat release to the environment. The system is instantly heated to maximum temperature, $T_{R,}$ and this process is called recalescence. Recalescence process stops when rapid solidification finishes, and turns to slow cooling process. The remaining liquid solidifies by the slowly heat release to environment. Different from traditional rapid quenching technique, solidification from undercooled melt is a thermodynamic undercooling, which can make a bulk volume liquid solidify fast, and the undercooling is easy to control. This is good for deeply investigating the solidification microstructure evolution process with undercooling and the physical properties of undercooled melt.

Rapid solidification from deeply undercooled melt has become a research topic since 1950s. Up to now, the non-equilibrium solidification theory is relatively mature. During the solidification process, nucleation happens first, and the driving force for nucleation, called Gibbs free energy, increases with the undercooling. According to classical nucleation theory, the static homogeneous nucleation rate in the undercooled

melt can be expressed as:

$$I_t^{\hom} = K \exp(-\frac{a\sigma_{lS}^3}{k_B T(\Delta G_V)^2}) \quad (1\text{-}7)$$

Where K is a constant, determined by the physical properties of the undercooled melt, a is a morphology factor of crystal, and σ is the interface energy of solid/liquid interface. k_B is the Boltzman constant. When heterogeneous nucleation happens in the undercooled melt, the static nucleation rate is:

$$I_t^{het} = K \exp(-\frac{a\sigma_{lS}^3 f(\theta)}{k_B T(\Delta G_V)^2}) \quad (1\text{-}8)$$

Where $f(\theta)=[(2+\cos\theta)(1-\cos\theta)^2/4]$, and θ is the wetting angle between the crystal and the nucleation etchant.

For the undercooled melt, it takes time for the system to change, and in case of atomic distribution is slower than the environment variation, the nucleation kinetics should be considered for nucleation. Zeldovich et al [ZELD43] proposed that the formation of critical nucleation took some nucleation time, and nonstatic nucleation or kinetic nucleation happened in this system. The nucleation rate can be expressed as:

$$I_t^{\hom} = I_s^{\hom} \exp(-\frac{\tau}{t}) \quad (1\text{-}9)$$

Where τ is incubation time for nucleation and t is the time.

For the undercooled melt, one stable nuclei is enough for triggering solidification process of the whole sample, and this process can be expressed as [CHRI03]:

$$IsVt = 1 \quad (1\text{-}10)$$

Where V is volume of alloy melt for homogeneous nucleation or the whole catalytic surface for heterogeneous nucleation.

The static state disappears when nucleation happens in the melt, and then the rapid growth of crystals comes. Recently, many new theoretic models concerning free dendrites growth have been developed. In 1953, Chalmer proposed the famous constituent undercooling theory to determine the condition for planar interface growth [TILL53]. However, incorporating the equilibrium thermodynamic theory to solve non-equilibrium kinetic process has intrinsic limitations. To solve this problem, using linear stability analysis, Mulins and Sekerka built a new theory (called MS theory) by considering surface tension, thermal and solute transfer difference between solid and liquid phase [MULL63, MULL64]. At large undercoolings, thermal diffusion length at the solid-liquid front is of the same order as the perturbed wave length, in this case

MS theory is no more suitable for the description of the stability of interface. Trivedi and Kurz [TRIV86] have extended MS theory to the solidification of deeply undercooled melt and built the absolute stability theory for planar interface growth.

For describing the dendrite growth in the undercooled melt, many models were proposed worldwide, and the model developed by Boettinger, Coriell and Trivedi, called BCT model [BOET00], was proved to fit well with experimental results and has been one of the most widely used model. BCT model was built based on Ivantsov function for description of diffusion field, minimum wave length for instable growth of dendrite tip, and a growth velocity dependent solute redistribution coefficient and liquidus line slope. According to this model, the undercooling of the dendrite tip can be divided into four parts:

$$\Delta T = \Delta T_t + \Delta T_C + \Delta T_R + \Delta T_K \tag{1-11}$$

Where ΔT_t is thermal undercooling, ΔT_C is constituent undercooling, ΔT_R is curvature undercooling, and ΔT_K is kinetic undercooling. T_t, ΔT_R and ΔT_K can be expressed as:

$$\Delta T_t = \frac{\Delta H}{C_p} I_v(P_t) \tag{1-12}$$

$$\Delta T_R = \frac{2\Gamma}{R} \tag{1-13}$$

$$\Delta T_K = \frac{v_s}{\mu} \tag{1-14}$$

Where C_p is specific heat of liquid phase, $I_v(P_t)$ is Ivantsov function (where $P_t=ER/2\alpha L$, is thermal Peclet number), μ is the function of alloy thermo physical parameters and temperature, Γ is Gibbs-Thomson coefficient. According to Aziz's research results [AZIZ82], considering solute trapping effect on the solute distribution and liquidus line slope, ΔT_C can be expressed as:

$$\Delta T_C = m_L C_0 \left[1 - \frac{m/m_0}{1-(1-k) I_v(P_C)} \right] \tag{1-15}$$

Where m_0 is equilibrium liquidus line slope, and $I_v(P_C)$ is Ivantsov function (where $P_C=vsR/2D_L$ is solute Peclet number). Solute distribution coefficient and liquidus line slope can be expressed as:

$$k = \frac{k_0 + (a_0 / D)V}{1 + (a_0 / D)V} \tag{1-16}$$

$$m = m_0[1 + \frac{k_0 - k(1 - \ln(k / k_0))}{1 - k_0}] \tag{1-17}$$

Thus, the total undercooling can be written in the following form：

$$\Delta T = \frac{\Delta H}{C_P} I_v(P_t) + m_L C_0 \left[1 - \frac{m \ / m_0}{1 - (1 - k) I_v(P_C)}\right] + \frac{2\Gamma}{R} + \frac{V}{\mu} \tag{1-18}$$

The radius of the dendrite tip is:

$$R = \frac{\sigma / (\Delta S \sigma^*)}{\frac{P_t \Delta H}{C_P} \xi_t + \frac{2m^{'} P_C C_0 (k-1)}{1 - (1-k) I_v(P_C)} \xi_C} \tag{1-19}$$

Where

$$\xi_t = 1 - \frac{1}{\sqrt{1 + \frac{1}{\sigma^* P_t^{\,2}}}} \tag{1-20}$$

$$\xi_C = 1 + \frac{2k}{1 - 2k - \sqrt{1 + \frac{1}{\sigma^* P_C^{\,2}}}} \tag{1-21}$$

And the alloy composition of the solid and liquid phase in the dendrite tip can be written as:

$$C_L^* = \frac{C_0}{1 - (1 - k) I_v(P_C)} \tag{1-22}$$

$$C_S^* = \frac{k C_0}{1 - (1 - k) I_v(P_C)} \tag{1-23}$$

Using the above equations, the undercooling in the dendrite tip, radius of the dendrite tip and solute distribution coefficient and liquidus line, and even the composition of the solid and liquid phases in the dendrite tip can be calculated.

1.4.2 Effect of magnetic field on nonequilibrium solidification of undercooled melt

As a strong physical means, magnetic field can act on atomic scale of matters, and plays an important role in phase transformations. For the solidification of undercooled melt, the question arises whether the magnetic field can affect the nucleation process and determines the final microstructure has become an important topic, but up to now, only a few experiments have been carried out concerning to this area.

According to the knowledge of magnetic hydromechanics, the application of strong static magnetic can suppress the thermal and solute convection in the melt, and then can affect the nucleation process. In 1992, Hasegawa and Asai [HASE92] have investigated the effect of strong magnetic field on the undercoolability of pure Cu. Their results found that the undercooling of Cu increased when a 0.5T magnetic field was applied, and the instability was also strengthened. In 2004, Yasuda et al [YASU04, YASU05] built an electromagnetic levitation melting facility in a 10T superconducting magnet, and found static magnetic field could stabilize the undercooled Cu and CuAg melt while having no effect on the undercooling (seen in Fig 1-7). For paramagnetic Ni melt, they found the melt was quite unstable and fluctuates in 5T magnetic field. Zhang et al [ZHAN10a, ZHAN10b] have investigated the undercooling behavior of Cu and Ge in magnetic field, and found that the mean undercooling of Cu was increased by the application of magnetic field while the mean undercooling of Ge was independent of magnetic field. From the above results we can see that it is not easy to obtain deep undercooling in the magnetic field, and the maximum undercooling obtained is much smaller than the undercooling obtained by common undercooling methods without magnetic field. Until now, there are very limited research results concerning the effect of magnetic field on the solidified microstructure of the undercooled melt.

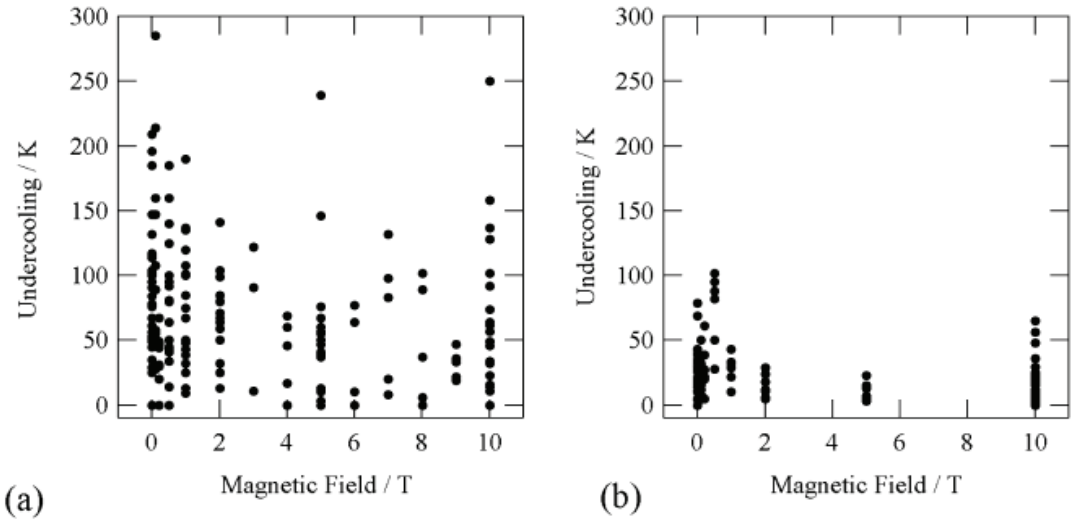

Fig 1-7 Undercooling of the nucleation in the copper and the Cu-1at%Ag alloys [YASU04].

1.4.3 Magnetic properties of undercooled melt

The Curie temperature, T_C, of metallic materials is always bellow its liquidus line temperature T_L. The atoms are constrained in solid state matter, thus traditional theories think that the long range ferromagnetic ordering is constrained only in solid matters. Actually, the magnetic ordering has been found in liquid ^{3}He. When the temperature is lower than 2.7mk, ^{3}He forms Femi liquid, and this super liquid has the similar Cooper pairs, which forms two ^{3}He atomic pair by BCS mechanism [VOLL84]. If one can undercool the metallic melt below its Curie temperature, it is possible to obtain ferromagnetic melt. When the ferromagnetic melt is processed in a strong magnetic field, many unique experimental results will be found. Now, with the development of supercooling and superconducting technology, it is possible to undercool a metallic melt below its Curie point in strong magnetic field.

Co based alloy posses excellent magnetic properties, and its Curie temperature is the highest among all the metallic materials, e.g. the curie temperature of Co is 1394K which is the highest Curie temperature among all the materials in nature. Because of the minimum temperature difference between the liquidus line and Curie temperature, $\triangle T=T_L-T_C$, Co based alloys are the most promising candidates for obtaining deep undercooling below their Curie temperature. Since the end of last century, Herlach et al [HERL07] in Germany have done a lot of research work for obtaining ferromagnetic liquids.

Whether we can obtain a ferromagnetic liquid in other systems except for ^{3}He has

long been a controversial scientific topic. In 1968, Bush et al [BUSC68], firstly reported the ferromagnetic long range formation in a undercooled Au-Co melt around its eutectic point, and ferromagnetic behavior disappeared when the temperature was 70 ºC above the melting point. Then Nakagawa et al [NAKA69] doubt Bush's results, and by directly measuring the magnetic susceptibility of the melt, the Curie temperature determined for Au-Co(30 and 40 at%) were 400 and 600ºC, respectively, which were much lower than the melting point, indicating it was impossible to obtain ferromagnetic liquid above the melting point. After, based on theoretic calculations, many researchers [FEIJ80, HEMM77, KALA78, VaAKA84] found that ferromagnetic liquid can exist, when the Heisenberg ferromagnetic exchange function is strong enough.

In 1994, Reske et al [RESK95] firstly undercooled Co-Pd alloy below its Curie point using electromagnetic levitation technique, and the magnetization of Co-Pd undercooled melt rapidly increased when the temperature was approaching Curie point during cooling (seen in Fig 1-8), and the Curie temperature by extrapolating the data was 6 K lower than the value obtained for the solid state.

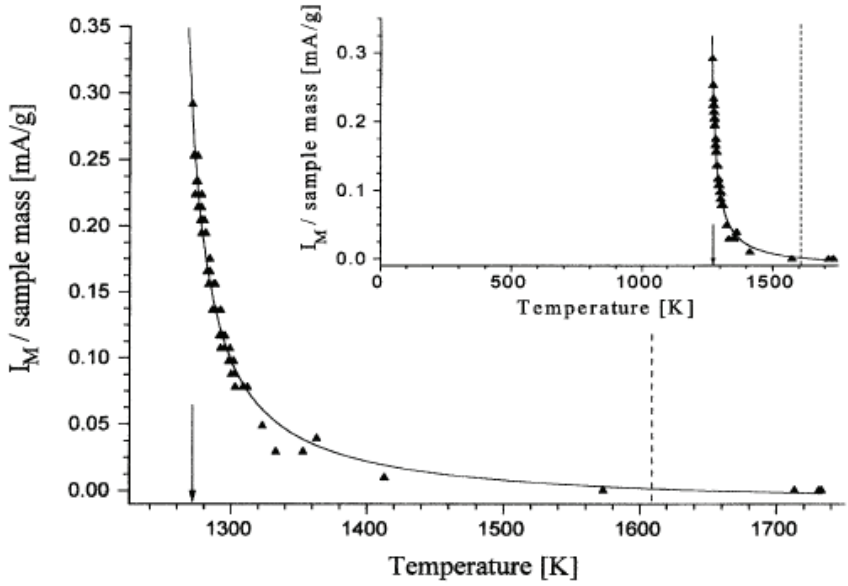

Fig 1-8 Change of the magnetization, ΔM, as a function of temperature T in the undercooled liquid regime for $Co_{80}Pd_{20}$ measured with a modified Faraday balance [RESK95]

Platzek et al [PLAT94] found the Co-Pd undercooled melt was attracted by Co-Sm hard magnet when undercooled the melt approaching Curie temperature, which has certified the increase of the magnetization of the liquid (seen in Fig 1-9).

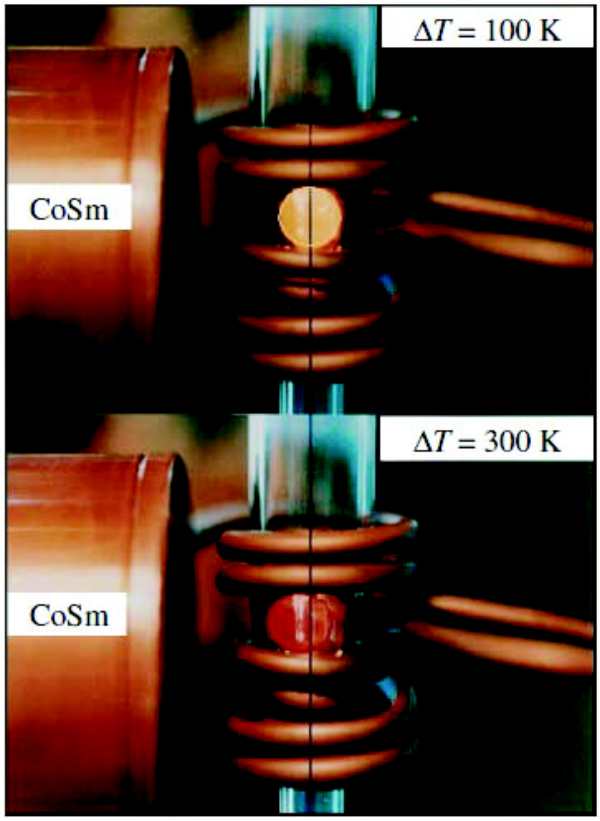

Fig 1-9 Levitated undercooled melt at at a temperature above T_C (top Fig) and below T_C (bottom Fig) close to a CoSm hard magnet [PLAT94]

Then by reducing the sample size, Albrecht [ALBR97] has succesfully undercooled Co-Pd melt below its Curie temperautre, and firstly observed the ferromagnetism in liquid of alloy melt. Herlach et al [HERL03] have investigated the effect of long range ferromagnetic ordering on the nucleation temperature in undercooled melt, and found when approaching Curie temperature, the transition from non-ferromagnetic to ferromagnetic could affect the energy for nucleation in undercooled melt. Reutzel et al [REUT04] have measured the magnetic properties of undercooled Co and Co-Au alloys, and found the magnetization of undercooled melt increased rapidly when close to the Curie temperature. Using classical nucleation theory, Holland-Moritz et al [HOLL04, HOLL07] found the nucleation temperature of Co-Pd alloys was consistent with the experimental results when the Co content was smaller than 70% (seen in Fig 1-10) while the theoretical nucleation temperature was lower than experimental temperature when Co content was higher than 70%. The authors have calculated the contribution of ferromagnetic transition on Gibbs free energy based on molecular theory, and found the calculation was in agreement with the experimetnal results. Their results indicated that ferromagnetic transition

promoted the nucleation in the undercooled melt and once close to the Curie point, the melt tends to crystallize. Recently, Zhou and Hu et al [ZHOU11a, ZHOU11b] have undercooled Co-Pd alloys to the undercooling of 415K, which is 100K below its Curie point, and this has brought a great challenge to the present theory on the effect of ferromagnetic transition on the nucleation in the undercooled melt.

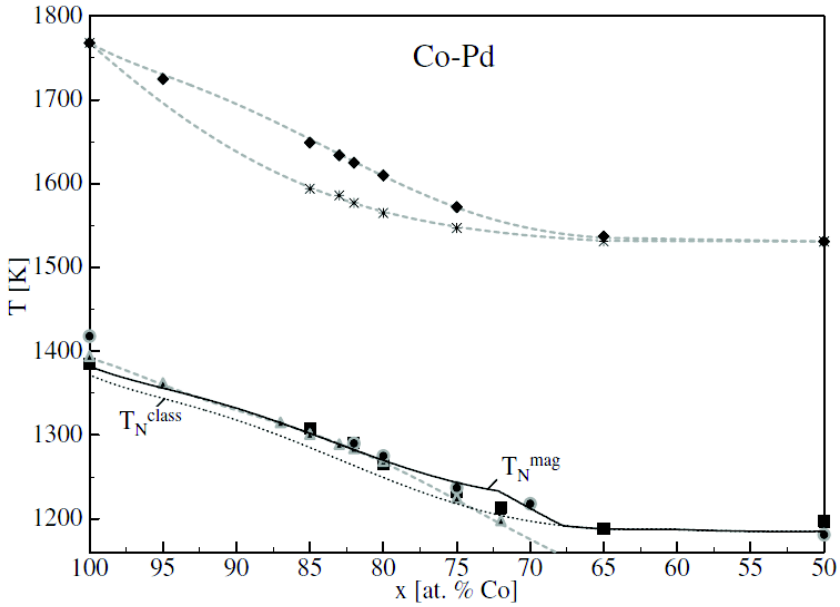

Fig 1-10 The calculated nucleation temperature for undercooled Co-Pd melt without (the dashed gray line) and (the solid line) with taking into account the ferromagnetic transition. The triangle and square symbols are the experimental data [HOLL04].

1.4.4 Magnetorheological behavior for ferrofluids under magnetic field

It is very difficult to obtain ferromagnetic liquid, Rosensweig et al [ROSE66, ROSE87, ROSE96] have developed ferrofluids by introducing very fine ferromagnetic particles into colloids. A collodidal magnetic fluid, or ferrofluid, consists typically of a suspension of a nanosized ferromagnetic particle in a nonmagnetic carrier fluid. A surfactant covering the particles prevents particle to particle agglomeration, and Brownian motion prevents particle sedimentation in gravitational or magnetic fields. Although called ferrofluid, actually they are in paramagnetic state, and that is because ferrofluid cannot maintain magnetism when the external magnetic field is removed. But due to their structure, they are in a superparamagnetic state. When a paramagnetic ferrofluid is submitted to a strong enough magnetic field, a lotus like surface morphology will be formed. This typical

effect is called normal field instability. The formation of peaks and valleys on the surface can reduce the energy caused by the magnetic field. Ferrofluid has very large magnetic susceptibility and even a small square hard magnet is enough to generate lotus like surface (seen in Fig 1-11).

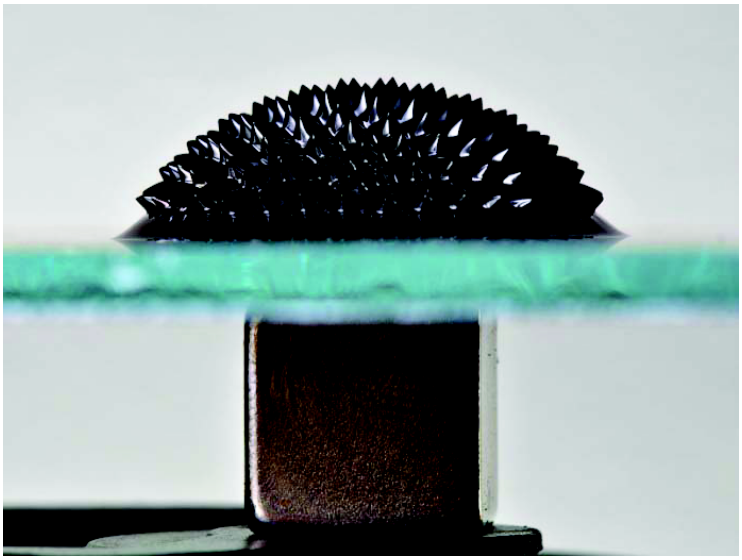

Fig 1-11 Unique morphology formed for ferrofluids when close to magnetic field [WEB2].

1.5 Motivation

High magnetic field has become a new physical means for materials processing, especially for the solidification process in strong magnetic field, and many new experimental results have been found concerning to this area. Until now, the investigation of non-equilibrium solidification process in magnetic field was constrained to the undercoolability, and the undercooling obtained was far from the maximum undercooling that can be obtained without magnetic field. The studies about solidification process in magnetic field only focus on small undercooling conditions, and the research results are mainly concerned by crystal orientation and phase separation. Since deep undercooling is a non-equilibrium solidification process, it is very difficult to achieve this process in high magnetic fields. Until now, there are only a few research papers referring to this area and there is no report about obtaining the same maximum undercooling as that without magnetic field.

In strong magnetic fields, some alloys, e.g. Co based alloys, are promising candidates to be undercooled below or approaching their Curie point. Up to the present, the reports are only carried out in the fields smaller than 0.5T. The application of strong magnetic fields (e.g.>10T) when the alloy is undercooled

approaching its Curie point is sure to have important affect on the formation of ordering structure in the melt, thus affecting the solidification process. During the investigation of superundercooling solidification, one can find undercooling can determine the final solidified microstructure. Also, the application of magnetic field in this process will also generate many new phenomena, especially when the undercooling is close to the Curie point.

Based on the above research background, in this study, we try to build an undercooling platform in a superconducting magnet, using glass fluxing and combining cyclic heating method to achieve deep undercooled Co based alloy melts. Then, we investigate magnetic field intensity and gradient on the undercoolability of Co based alloys. Using a modified Faraday balance, the magnetization measurement facility is used to measure the magnetic properties of undercooled melt in strong magnetic field. Based on the above experimental results, considering solidification theory and knowledge of EPM, we have studied the microstructure evolution process and anomalous eutectic formation mechanism in magnetic field. The main research content is listed as follows:

(1) To design an undercooling experimental platform in a superconducting magnet and achieve supercooling of metals and alloys in magnetic field. Using modified Faraday balance to measure the magnetic properties of the undercooled melt in real time.

(2) To study the magnetic properties of undercooled melt in gradient magnetic fields. Using the facilities designed to measure the magnetization of undercooled pure Co, Co-Sn alloys and Co-B alloys, and to analyze the effect of undercooling and magnetic field on the magnetic properties of these metal and alloys.

(3) To investigate the effect of magnetic field on the undercoolability of metals alloys. The metals, pure Cu and Co, and Co-Sn alloys are chosen to investigate the effect of static and gradient magnetic field on the undercoolability of diamagnetic, ferromagnetic and paramagnetic alloys.

(4) The microstructure evolution process in strong magnetic fields. Using Co-Sn alloys to investigate the microstructure formed at different undercoolings and different magnetic fields, and analyze the effect of magnetic field on the dendrite growth and eutectic formation process.

CHAPTER 2 EXPERIMENTAL MEANS

Magnetic field with intensity larger than 10T is very easy to be generated due to the development of superconducting technology, providing convenient and efficient means for materials processing by directly building experimental platforms in the magnet. In order to obtain very large undercooling, metals and alloys need to be heated a few hundred degrees above their melting point and held for a certain period to eliminate impurity elements and avoid heterogeneous nucleation. Up to now, the induction melting method is a quite simple and commonly used way for receiving large undercooling. However, due to the complicated electric-magnetic environment, installing a induction heating furnace in a magnet always cause the vibration of the sample and affect the undercooling and the accuracy of measured temperature. Thus, in the present research, we built a furnace using SiC heating element for the undercooling platform. By tuning the position of the heater, the undercooling platform can change between homogeneous to gradient magnetic field. Incorporating a high accuracy balance for measuring the magnetic force exerted on the sample, a magnetization measurement system was built for undercooled melt.

2.1 Solidification of undercooled melt under strong magnetic field

2.1.1 Experimental setup

A common undercooling experiment system includes heating system, on-line temperature measuring, controlling system and vacuum system. For building undercooling facility in the magnet, the constrained space of the magnet bore and the magnetic force exerted on the facilities should be carefully considered. Yasuda et al [YASU04] have designed an induction levitation melting furnace using simultaneous imposition of alternating and static magnetic fields for obtaining large undercooling. However, the undercooling obtained by the furnace was not stable and vibrated with the cycling heating times, and also the maximum undercooling was not large enough compared with undercooling limits in experiments without magnetic field. Thus, in order to obtain a large undercooling in a high intensity static and gradient magnetic

field, we used the following solutions.

(1) Superconducting magnet

The present undercooling platform is installed in a helium free superconducting magnet with maximum intensity 12T produced by Cryogenic Ltd (Seen in Fig 2-1). It takes only 12-15 minutes to obtain its maximum field strength which is relatively very fast compared with traditional magnet. The magnet has a bore in 50mm diameter, and 480mm in length. When the furnace is put in the working space, the maximum temperature zone is 20cm from the top surface of the magnet. The diameter of the sample is smaller than 6mm, thus the field gradient caused by the sample size within the area of maximum field is relatively small.

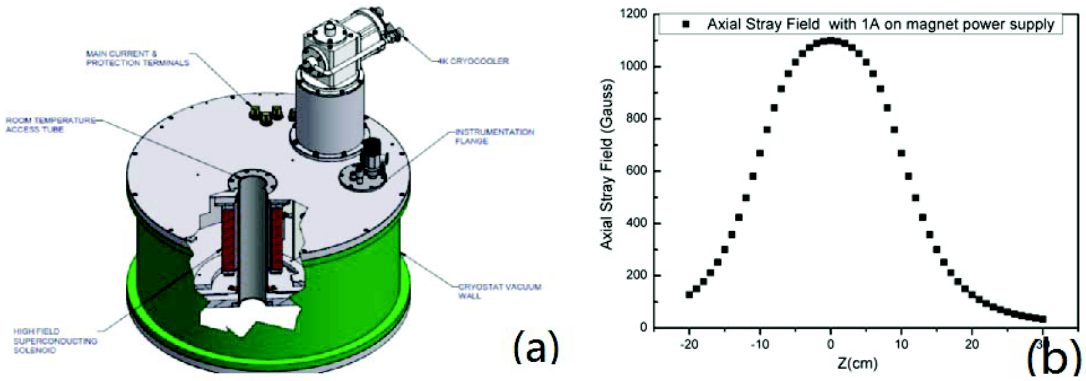

Fig 2-1 (a) Schematic diagram of the magnet, (b) Magnetic profile along the vertical direction of the magnetic field. The data is measured when the imposed current is 1A, and the maximum field, 12T, is obtained when the current is 109.5A.

(2) Heating system

In order to meet the demand for obtaining high overheating, we use a high density SiC spiral type heating element (I Squared R Element CO. INC.). The heating element with diameter 25mm outside and 15mm inside can be heated up to 1650°C, seen in Fig 2-2. The double wall water cooled jacket is used to cool the system between the heating element and magnet. Between the water cooled jacket and SiC heater, 6mm thick refractory wool is used for heat insulation. A direct current power supply (DC-55V×78A) is used as heating power. The maximum heating rate can be up to 100℃/min, and the maximum cooling rate is up to 150℃/min when the temperature is above 800℃. The length of the heating zone is 10cm, and the temperature fluctuation in the maximum heating zone is less than ±3℃ within 2cm heating zone, which can guarantee temperature homogenization of the sample.

(3) Controlling system for heating

The heating system is controlled by a ‘S type’ thermal couple installed in the

homogeneous heating zone below the sample crucible. A temperature controller (Eurotherm 3504) is used to automatically tune the DC power supply, and the system is controlled by Itool software installed in a PC.

To ensure the linearity of the heating and cooling, 3 segments PID parameters are calibrated and used as the controlling parameter, which could control the thermal history of the sample precisely.

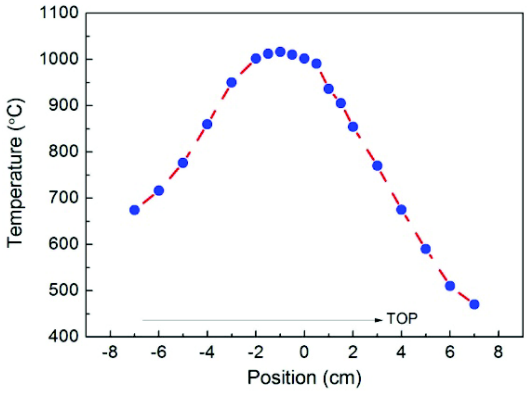

(a) (b)

Fig 2-2 (a) Picture of SiC heater used and (b) temperature profile when the maximum temperature is 1010℃.

(4) Temperature measuring system

The temperature of the melt is measured on-line by a two-color pyrometer (Germany, IMPAC-ISR50-LO). An optic fiber head installed with the pyrometer is used to avoid the magnetic field effect on the precision of the pyrometer. The characteristic parameters of pyrometer are shown in Table 2-1.

Before measuring the temperature, the pyrometer is calibrated by a 'S type' thermocouple, and the emissivity slope is tuned to make sure the measured temperature is within ±2℃.

Table 2-1 Parameters of ISR50-LO 2-color pyrometer

Type	Range	Resolution	Spot size	Response time	Emissivity slope
ISR50-LO(MB25)	800-2500℃	±4℃	3 mm	≥10 ms	0.8～1.2

2.1.2 Undercooling procedures

Glass fluxing combined with cyclic overheating is used to achieve large

undercooling in superconducting magnet. The sample is encapsulated in molten glass slag, and combination of cyclic heating by holding at given overheating and cooling are used to purify the molten alloys. The controlling parameters affecting the undercooling are: overheating temperature, holding time, cyclic heating times and cooling rate.

B_2O_3 is chosen as the purifying glass slag, and high purity SiO_2 quartz tube with a hemisphere bottom shape is used as heating crucible. By heating for many cycles with the controlling system, the melt is cooled to a given undercooling when the maximum undercooling is in a rather stable state. After recalescence, rapid quenching is used to cool the sample and avoid solid state phase transition. The schematic diagram of the system is shown in Fig 2-3(a), and a typical heating program is shown in Fig 2-3(b).

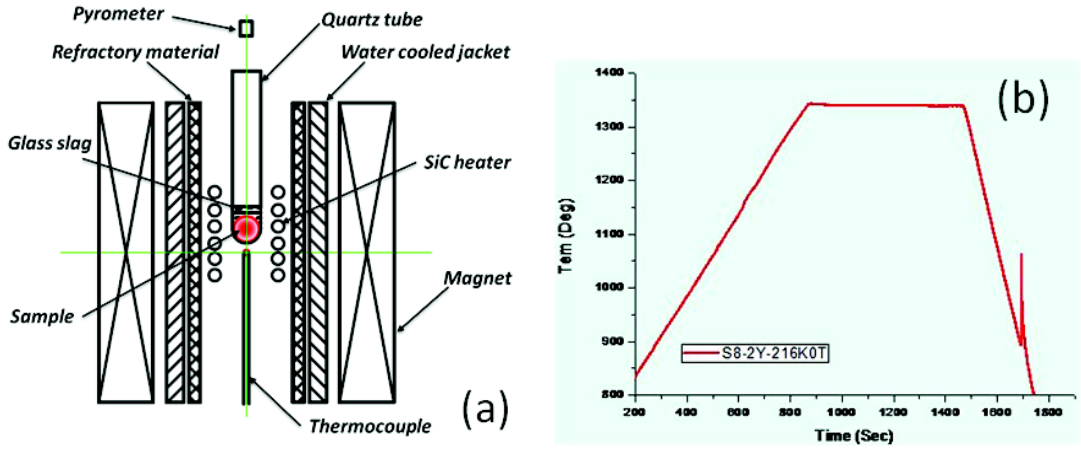

Fig 2-3 (a) Schematic diagram of the undercooling facility under magnet and (b) typical temperature profile as a function of time.

2.2 Magnetic susceptibility measurement under strong magnetic field

2.2.1 Experimental setup

Fig 2-4 shows the schematic diagram of the force acting on a ferromagnetic or paramagnetic material ($\chi>0$) in a magnet. The arrows in horizontal direction show the radial force from the center of the magnetic bore to the magnetic wall while the vertical ones show the force along the magnetic bore.

In the magnet center region (point O), the field is larger when the sample is closer to magnet wall. Thus, a sample with a positive magnetic susceptibility will deviate from the magnet axis and finally contact with the edge and the heating element.

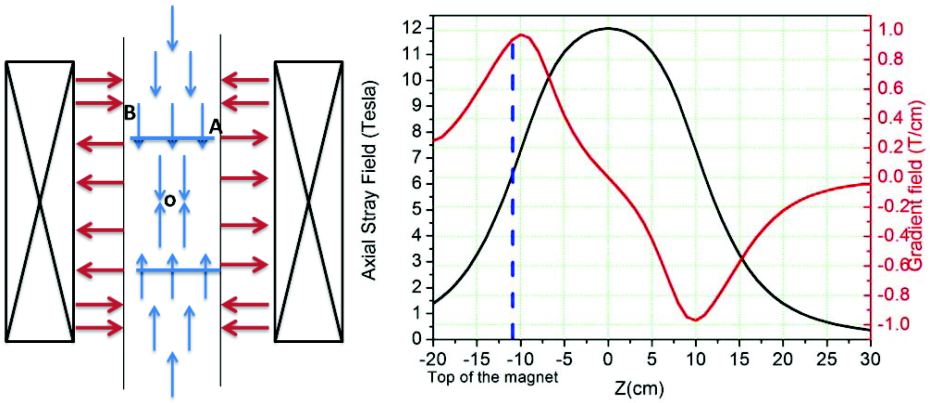

Fig 2-4 (a)Schematic illustration of radial (red) and axial (blue) forces applied on a ferromagnetic or paramagnetic material, in the room temperature bore of a superconducting magnet, (b)field gradient along the vertical direction of the magnet, the dot line represents the field profile at the position of point A in (a).

Under this condition, due to the friction and perturbance, any measurement for the magnetic force acting on the sample is not accurate. Above the maximum field region, the field gradient reaches its maximum value at point A, and the magnetic force exerted on sample is still in the radial direction. But above point A, there exists an equilibrium zone B, where the magnetic force exerted on the sample in the radial direction is to the center of the magnet, which means that the sample will be automatically centered in the magnet, without any contact with the heating element. Although the field intensity in this area is much smaller than the maximum field, it is still large enough for magnetic force measurement by electronic balance. In the present investigation, B is 5mm above the maximum field gradient region A, and when a 1T magnetic field is applied, the field intensity in the position A is about 0.61T, and in the position B is about 0.52T.

The sample with positive magnetic susceptibility will undertake magnetic force downward to the vertical direction. And for a freely suspended sample below the balance, the magnetic force can be calculated by:

$$F_z = \frac{\chi}{2\mu_0} VB\frac{dB}{dZ} = mM\frac{dB}{dZ} \tag{2-1}$$

Where χ is mass susceptibility (cm^3/g, CGS Unit)，M is the magnetization per gram (emu/g，CGS Unit), V and m are volume and mass. In Eq.(2-1), the magnetic field gradient is expressed in $Oe^2 \cdot cm^{-1}$ (BdB/dz) or $Oe \cdot cm^{-1}$ (dB/dz). When the magnetic field is applied, the measured mass corresponds to the addition of force exerted on the sample, sample holder, quartz crucible, glass slag and the gravity of the whole system.

Then we can express the measured results：

$$F_z = (m_{measured} - m_{background})g \quad (2\text{-}2)$$

Where m_{measured} and $m_{\text{background}}$ are the measured magnetic force on the sample and the background including the gravity of the system and magnetic force exerted on the sample holder, quartz crucible and glass slag, respectively. And g is acceleration of gravity constant in $\text{cm}\cdot\text{s}^{-2}$. The background signal mainly corresponds to the negative contribution of diamagnetic quartz tube and sample holder. Compared with the ferromagnetic sample, the background can be neglected. However, when the alloy is in a weak paramagnetic state, e.g. high temperatures above its Curie point, accurate measurement of the background becomes very important.

During the measurement, the sample is put 95mm above the maximum field region, and the field gradient calibrated by pure Ni is 0.93T/cm. And the magnetization of the sample can be directly calculated by the following equation:

$$M = 1.2653\frac{(m_{measured} - m_{background})}{mB} \quad (2\text{-}3)$$

Where M is in emu/g, m is in g, and B is in T.

2.2.2 Calibration and background correction

The magnetization of ferromagnetic materials is very sensitive to temperature, and large error can be obtained when the temperature of the sample is not homogeneous or incorrect. Thus, to ensure the accuracy of the temperature, two factors are considered in this paper. Firstly, tune the position of the heating element precisely. The temperature within the maximum heating zone is within ±3℃ in 20mm, and the diameter of tested sample is within 6mm, which means the temperature gradient can be controlled to be very small when the sample is put in the maximum temperature zone. Secondly, the heating and cooling rate used is 5℃/min. The low rate can make sure that the temperature varies homogeneously during measurement.

Before testing, the mass of the sample and sample holder (including quartz crucible and glass slag) can be directly removed by the reset to ‘0’ function of the balance. Then the measured data totally comes from the field effect, and also the background from the force exerted on the sample holder is included. The background

caused by the magnetic force can be measured by carrying the experiments without sample at the same heating program. Considering the difficulty in measuring temperature when there is no sample, pure diamagnetic Cu is used to determine the temperature during the scan of the background since Cu has very negligible effect on the background due to its low magnetic susceptibility.

Fig 2-5 is the background by measuring Cu in 1T magnetic field. It can be seen from the figure that, the background caused by magnetic field has very limited effect on the measuring results. From the measuring range, the variation of the mass is within 15mg, and this will be important for the accuracy of measurement at high temperatures when the magnetic susceptibility of sample is very small. And in this case, the background should be subtracted before calculation.

Strong magnetic field is generated by electric magnetic effect, and the stability of current in superconducting coil will directly affect the field stability, and thus affect the magnetization measurement process. Besides, the heat flow within the heating element can also lead to the vibration of the measurement. The environment for the facility, e.g. temperature, humidity and perturbance can affect the precision of electronic balance. In the present experimental system, the noise caused by the environment at 1500ºC is within ±1mg, indicating the system is in a good precision.

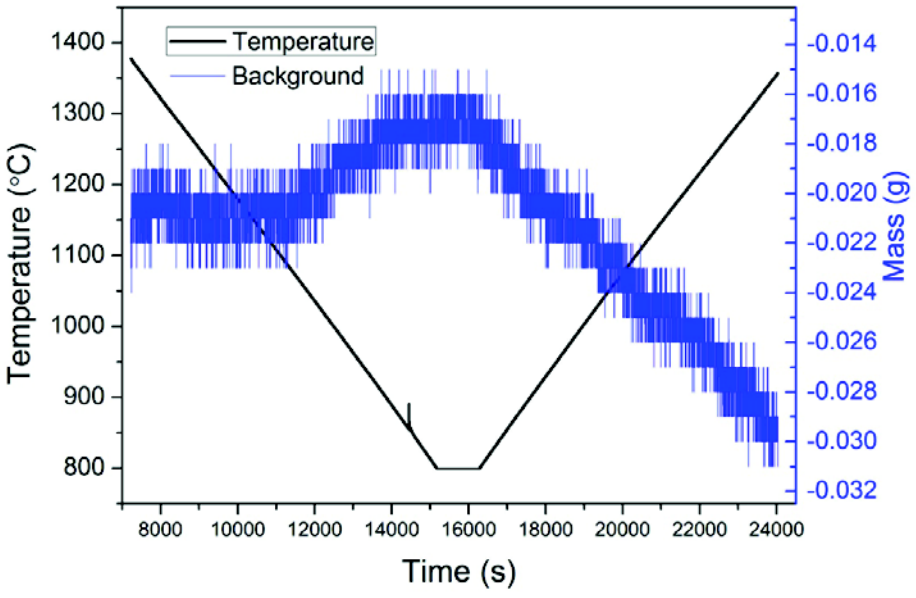

Fig 2-5 Measured data for pure Cu with 1 T magnetic field.

2.3 Sample preparation and structure characterization

2.3.1 Sample preparation

Co based alloys are the most promising candidates to be undercooled below their melting point due to their small difference between the Curie temperature and melting point. In this paper, pure Co, Co-(Sn, B) binary alloys are chosen for investigation, and for comparison, pure Cu is selected for the study of undercoolability. Pure Co has the highest Curie temperature in the exiting materials, which is up to 1121℃. And for binary Co-Sn alloys, the eutectic point according to phase diagram shown in Fig 2-6 is $Co_{79.5}Sn_{20.5}$ at.%. In this paper, three near eutectic point composition, $Co_{79.5}Sn_{20.5}$ at.%, $Co_{76}Sn_{24}$ at.% and $Co_{72}Sn_{28}$ at.% are chosen for investigation. For Co-B alloy, the near eutectic composition, $Co_{83}B_{17}$ at.%, is chosen for investigation.

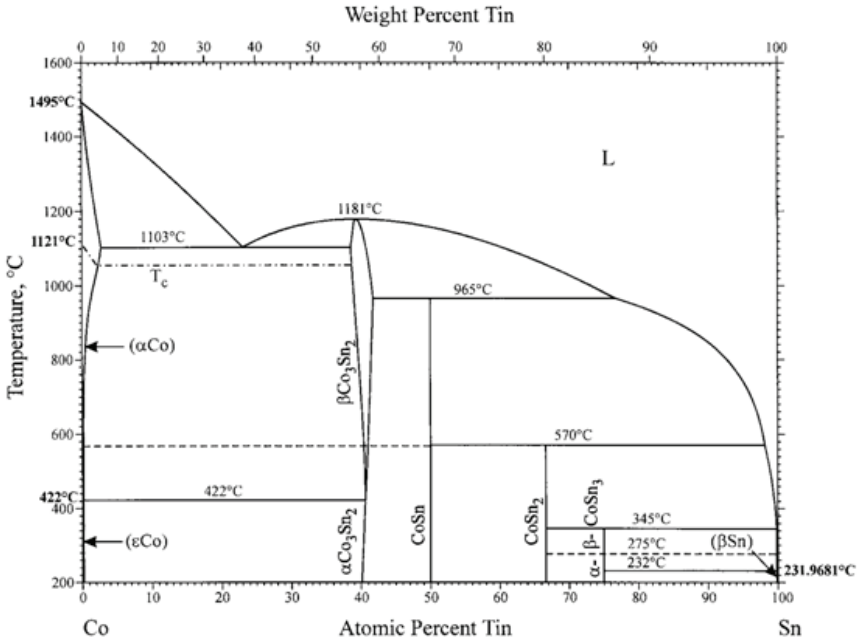

Fig 2-6 Phase diagram of Co-Sn binary alloys [OKAM06].

Pure materials Cu, Co, Sn and B with purity larger than 99.99 wt.% are used as raw material. Co-Sn binary alloys are prepared by a cold crucible levitation melting method, Co-B alloys are prepared by high vacuum arc melting furnace. The samples are cut in pieces about 1g in weight by a precision cutting machine. The glass slag used for undercooling experiment is pure B_2O_3.

2.3.2 Microstructure characterization

After solidification, samples used for microstructure observation adopt the following procedures: the samples are firstly cut along and perpendicular to the direction of the magnetic field, then encapsulated by epoxy resign in transverse and longitudinal direction. The electrolyte polishing method is used for polishing the sample. The electrolyte used is Electrolyte A2 (Struers). The parameters used are: voltage: 20V, polishing time: 10s, temperature: 25℃.

The optic microstructure is observed by a Zeiss® SIP 40715 optic microscope. Two kinds of scanning electron microscope JEOL 56-LV(installed with EDS, 138eV, PGT®) and Zeiss Ultra Plus field emission scanning electron microscope (equiped with INCA OXFORD EDX and EBSD) are used for high magnification observation. The XRD analysis is carried out by a Siemens D5000 X-ray Powder Diffractometer with a Co Kα radiation.

In order to have good observation results, the following procedures are used for preparing EBSD samples.

(1) sample cutting

The sample is cut by a precision cutting machine (Struers, Accutom-5). During cutting, the cutting speed is restrained below 0.05mm/s. After cutting, the sample is encapsulated with epoxy resign and polished.

(2) polishing process

Mechnical polishing combined with chemical polishing methods are used for polishing. The polishing process is detailed in Table 2-2.

Table 2-2 Procedures for EBSD sample preparation. The force used during polishing is from 5 to 10N.

Steps	Method	Speed (r/min)	Time (min)
1	MP(SiC-Paper 600)	300	3
2	MP(SiC-Paper 1200)	300	3
3	MP(SiC-Paper 4000)	300	5
4	MP(MD-DAC 3μm)	200	10
5	MP(MD-NAP 1μm)	200	10
6	CP (MD-Chem+OP-U)	200	10

CHAPTER 3 MAGNETIC PROPERTIES OF UNDERCOOLED CO-BASED ALLOYS IN MAGNETIC FIELD

When the molten melt comes into the undercooled state, even without nucleation, a large amount of short range orders (SRO) exist in the undercooled melt. The amount and scale of SRO also change with the increased undercooling. In 50th last century, it is commonly believed that SRO was determined by the crystalline phase. With further investigation, researchers found that the melt had its specific SRO and did not have any direct relationship with the solidified phase [HERL07]. For ferromagnetic metals and alloys, ferromagnetic to paramagnetic transition happens when temperature is higher than the Curie temperature during the heating process, and the melt comes into paramagnetic state. During the cooling process, magnetic SRO is supposed to form when the melt is cooled below its melting point [REUT04]. Present research indicates that the magnetic ordering in the undercooled melt can undergo paramagnetic to ferromagnetic transition, and ferromagnetic liquid maybe formed. That is to say, at a certain undercooling when the melt is below the Curie temperature, the magnetic ordering can directly transform from paramagnetic state to ferromagnetic state. Rosensweig [ROSE66] found that ferrofluid is in a superparamagnetic state without magnetic field, and the magnetic domains are out of order. When close to a magnetic field, ferrofluid can be magnetized and generate many unique pattern with peaks and valleys. In this chapter, by installing a modified Faraday balance with undercooling facility in a superconducting magnet, the magnetic properties of pure Co, Co-Sn and Co-B binary alloys are investigated in high magnetic field.

3.1 Magnetic properties of undercooled pure Co

The heating traces of pure Co sample for magnetization measurement shown in Fig 3-1 are as follows: (1)Cooling1: firstly cool down from 1560°C to 800°C at 5°C /min, (2)Heating2: then heat to 1560°C at 5°C /min, (3)Cooling3: finally cool down to 800°C at 5°C/min. The low heating and cooling rate is to ensure the time needed for data acquisition of fast speed balance (Mettler Toledo PR503). The stabilization time

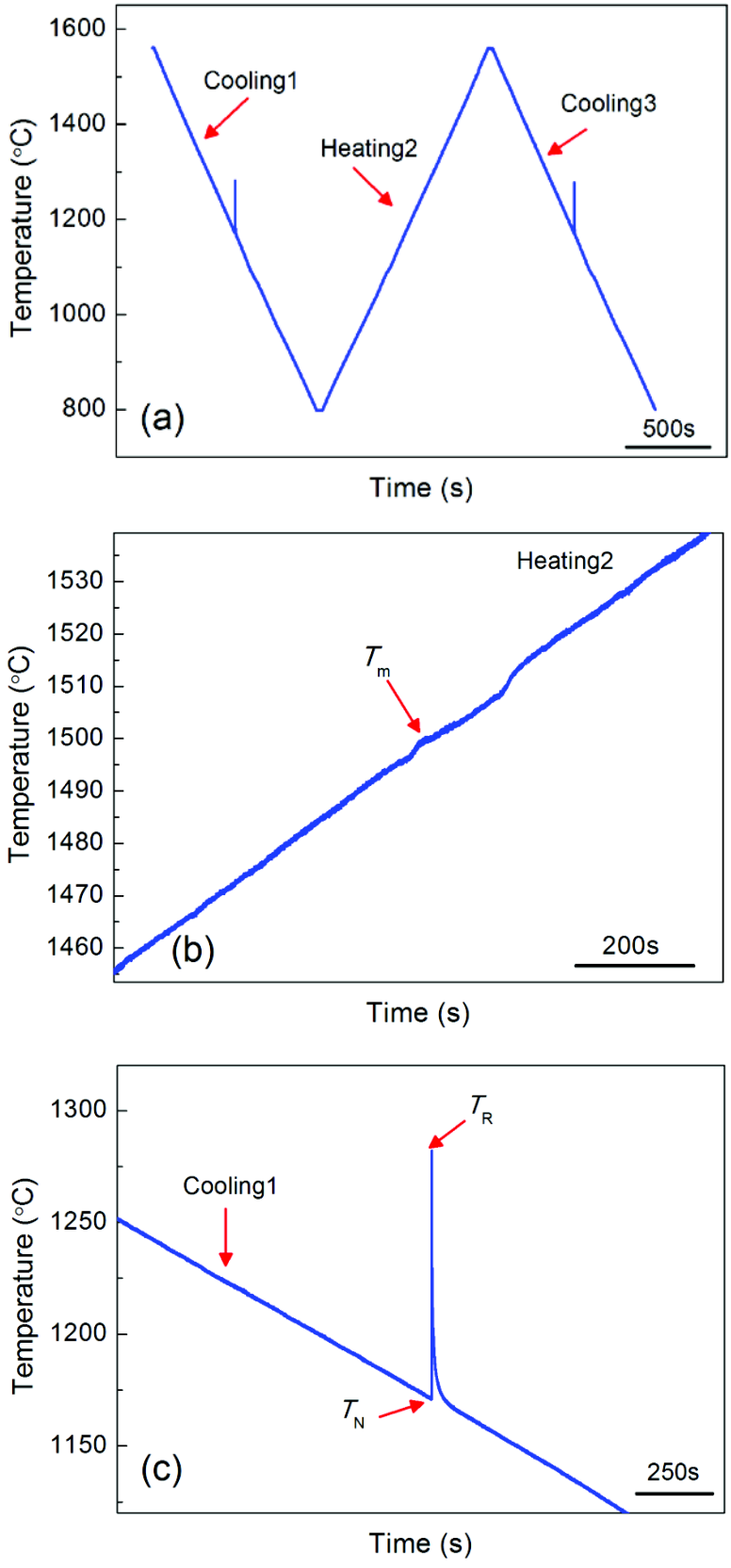

Fig 3-1 Heating traces of pure Co for magnetization measurement.
(a) whole temperature profile of three consecutive processes, (b) enlarged figure around melting point in Heating2, and (c) enlarged recalescence range in Cooling1.

of the balance is 1.5s, and the temperature variation within this time range is 0.125°C, indicating the present balance is fast enough to receive accurate magnetization value at the present heating and cooling rate. The melting point determined by pyrometer (shown in Fig 3-1(b)) is 1499°C which is consistent of the melting point of pure Co. And the sharp temperature increase during cooling process (shown in Fig 3-1(c)) indicates the alloy is nucleated at 1170°C, a relatively large undercooling can permit the investigation of the magnetization of deeply undercooled melt.

Fig 3-2 is the magnetization-temperature curve of pure Co in 0.52T magnetic field of the sample heated according to the trace in Fig 3-1(a). As we can see from Fig 3-2(a), the magnetization of pure Co is almost overlapped for the three consecutive heating processes, indicating the good reproducibility of the measurement. During heating process, the magnetization decreases with increasing temperature and a catastrophic decrease happens when approaching the Curie point. Because of the existence of remaining short range order above the Curie point, the magnetization curve always reveals a remaining tail in an external magnetic field, which progressively decreases to regular paramagnetism. When the temperature is above the Curie point, the metal is in paramagnetic state, and the magnetization decreases continuously with the increasing temperature. A steep decrease of the magnetization at 1498°C due to the melting of Co can be observed (seen in Fig 3-2 (b)), which is consistent with the results measured by pyrometer (shown in Fig 3-1(b)). During the cooling process, the magnetization increases with the decrease temperature and no obvious change happens at melting point. Then the alloy melt comes into the undercooled state. The magnetization of the undercooled melt is almost overlapped compared with the magnetization curve during heating. When the temperature bellows 1275°C (T_0 in Fig 3-2(c)), the magnetization of the undercooled liquid starts to increase faster, as seen in Fig 3-2(c), indicating the magnetization of the liquid is higher than the solid. The difference increases with the increasing undercooling before the nucleation temperature at 1170°C. The magnetization of the undercooled liquid at 1170°C, M_{liquid}=3.4emu/g, which is more than 30% larger than that of the magnetization of solid where M_{solid}=2.6emu/g. Due to the rapid temperature increase in the recalescence process, the balance can not accurately measure the data due to its slow stabilization time for receiving a correct data in the fast solidification process. However, we still can see the trend: rapidly decrease until the maximum temperature after nucleation at T_R, which is consistent with the temperature measured by

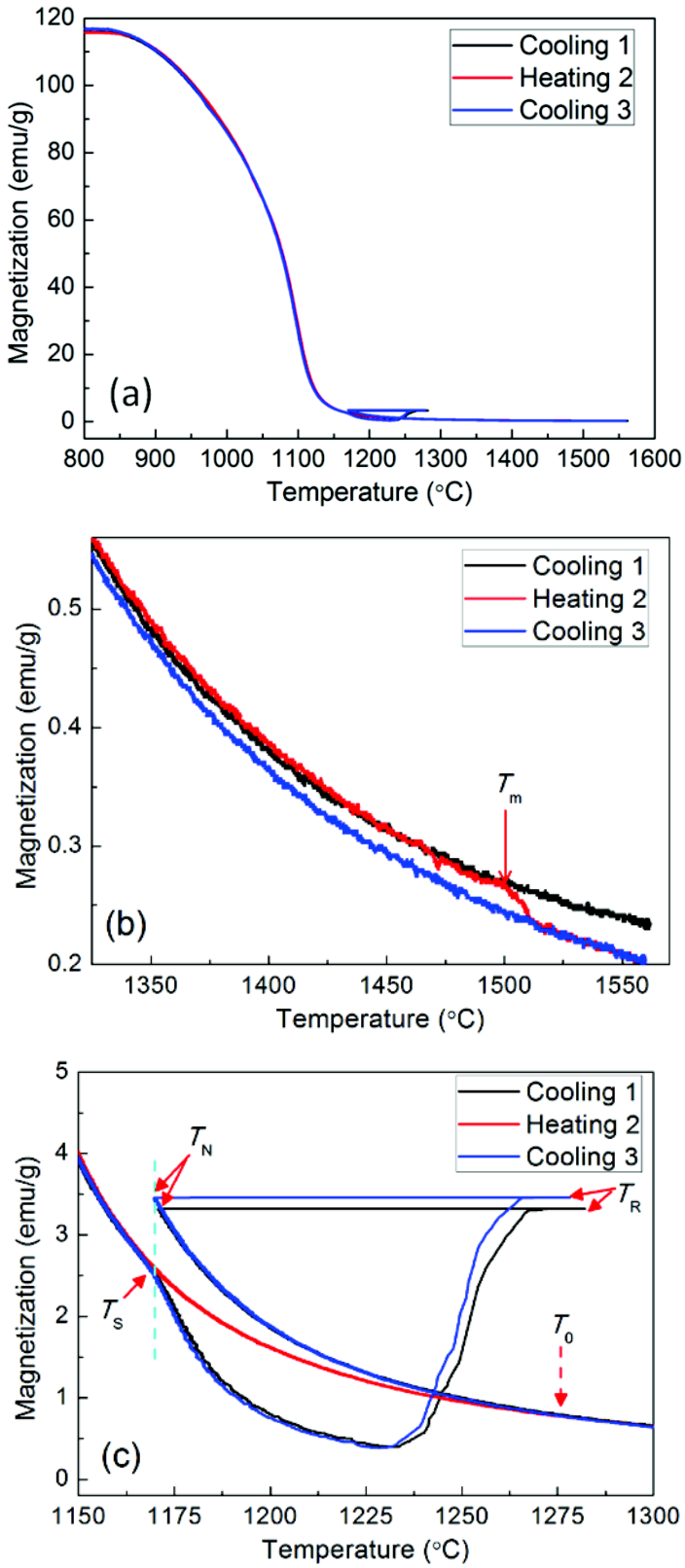

Fig 3-2 Magnetization as a function of temperature curves of pure Co measured in 0.52T magnetic field, and the field gradient at the sample position is 774Gauss/cm. (a) magnetization of three consecutive processes shown in Fig 3-1, (b) magnified Figure of the temperature range close to melting point in (a), and (c) magnified Figure of the temperature range close to recalescence temperature in (a).

pyrometer. And after the rapid solidification progress is finished, the magnetization curve comes back to the value measured during heating process when the temperature slows down to 1170°C again (T_S).

Above the Curie temperature, a ferromagnetic material becomes paramagnetic and obeys the Curie-Weiss law as [BUSC03]:

$$\chi = \frac{C}{T - \theta_p} \tag{3-1}$$

Where χ, C and θ_p are magnetic susceptibility (cm^3/g), Curie constant (cm^3K/g) and the asymptotic or paramagnetic Curie temperature (K), respectively. When T=θ_p, the susceptibility diverges which implies that one may have a nonzero magnetization in a zero applied field, exactly corresponding to the definition of the Curie temperature. Thus, paramagnetic Curie temperature (θ_p) is considered approximately equal to Curie temperature (T_C) [CULL08]. The Curie constant can be expressed as:

$$C = \frac{Np^2\mu_B^2}{3k_B} \tag{3-2}$$

Where N and k_B are Avogadro constant and Boltzmann constant, p and μ_B are effect Bohr magneton and Bohr magneton, respectively.

In the paramagnetic regime above the Curie temperature, the inverse magnetic susceptibility is in a linear relationship with temperature. Fig 3-3 is the inverse magnetic susceptibility as a function of temperature curve of pure Co in 0.52T magnetic field. It can be seen that the curve is linear above melting point, indicating the perfect paramagnetic state. While during cooling process, there is no typical variation of the slope even when the melt comes from overheated to undercooled state at beginning. The slopes of the two curves are different below the melting point and a intersection is observed at 1275°C (marked as T_0 in Fig 3-3) where we find the same magnetization of solid and liquid. We can also see that the slope of the curve is not definitely constant and especially when the temperature approaches the Curie point. One possible explanation is that the magnetic short range orders exist in the low overheating and undercooled melt which cause the deviation of the melt from the ideal paramagnetic state. Diamagnetism is caused by the orbital moment of electron, thus it is inevitable to generate diamagnetic properties since everything has this moment [KITT05]. When the Curie-Weiss law is used to determine the paramagnetic Curie temperature and other magnetic parameters, a temperature independent constant χ_0 is introduced to Eq. (3-1) and a new form is [AMOR84]:

Table 3-1 Curie-Weiss fitting of the magnetic susceptibility of pure Co during heating and cooling process, the magnetic field and the magnetic gradient is 0.52T and 774Gauss/cm, respectively.

Parameter	χ_0 (10^{-3}cm^3/g)	C (10^{-3}cm^{3}K/g)	θ_P (°C)	R-square	$\mu_{eff}(\mu_B)$
Heating (S)	-0.0129	23.5	1130	0.9999	3.33
Cooling (L)	-0.0111	20.4	1148.5	0.9999	3.10

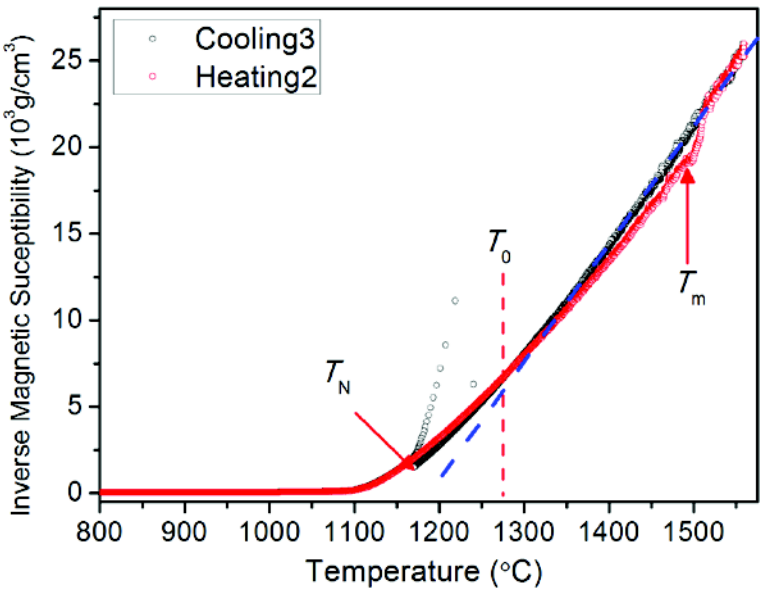

Fig 3-3 Inverse magnetic susceptibility as a function of temperature of pure Co during heating and cooling process under 0.52T magnetic field

$$\chi = \chi_0 + \frac{C}{T - \theta_P} \tag{3-3}$$

By directly fitting with Eq.(3-3) for Co during heating and cooling using the data in Fig 3-2 (the fitting curves are shown in Fig 3-4), the parameters are calculated and shown in Table 3-1. The paramagnetic Curie temperature of pure solid Co determined is θ_P(S)=1130ºC (with an error of ±6ºC), and the effective Bohr magneton number μ_B=3.33, which is nearly coincide and in good agreement with earlier measurements by Kamp [KAMP88] and Reutzel [REUT04]. While the paramagnetic Curie temperature of the undercooled melt is θ_P(L)=1148.5ºC (with an error of ±3ºC), and the effective Bohr magneton number is μ_B=3.10. Compared with solid state, the Curie temperature of the undercooled melt increases 18.5ºC, and the magneton moment is smaller than that in solid state.

Fig 3-5 is the magnetization-temperature curve of pure Co measured in 6.23T magnetic field during heating and cooling process. Under large magnetic field, the

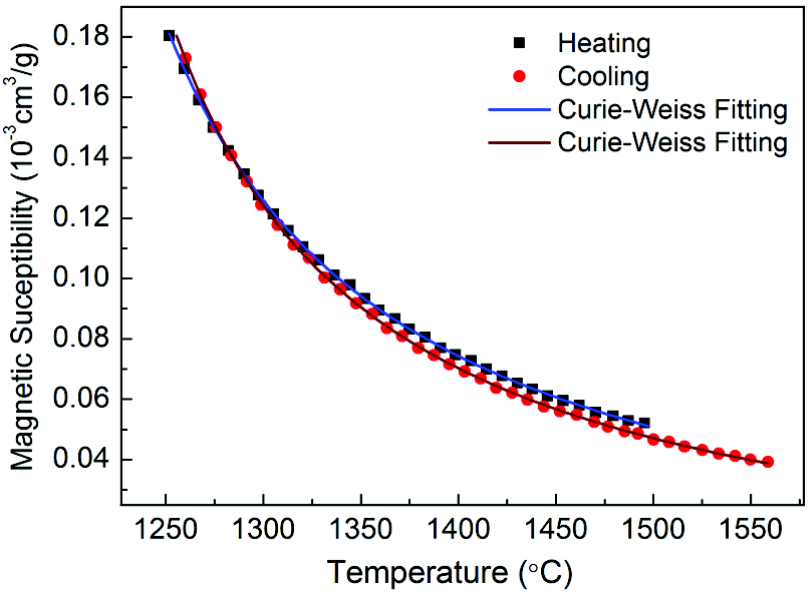

Fig 3-4 Fitting results based on Curie-Weiss law of pure Co. Since when the temperature is approaching the Curie point, either the solid or undercooled Co is not in a real paramagnetic state due to remaining magnetic ordering. Thus the data range used for fitting is far above Curie point, here we starts from 1250ºC.

Table 3-2 Curie-Weiss fitting of the magnetic susceptibility of pure Co during heating and cooling process, the magnetic field and the magnetic gradient is 6.23 T and 9294Gauss/cm, respectively

Parameter	χ_0 (10^{-3}cm^3/g)	C (10^{-3}cm^{3}K/g)	θ_P(ºC)	R-square	μ_{eff}(μ_B)
Heating (S)	-0.0085	24.35	1120.5	1	3.39
Cooling (L)	-0.0075	22.76	1132.5	0.9998	3.28

magnetization of the melt is rapidly increased when approaching the Curie temperature. When belows a critical temperature, T_0 (1350ºC at the present state), the magnetization of undercooled melt starts to increase faster than solid, and the difference increases with the increasing undercooling between the undercooled melt and heated solid at the same temperature before the undercooled melt is solidified at T_N=1163.5 ºC.

Table 3-2 is the fitting results according to Eq.(3-3), it can be seen that the calculated paramagnetic Curie temperature based on Curie-Weiss law for the sample solidified in 6.23T magnetic field is lower than that in 0.52T magnetic field. The Bohr magneton number determined for solid Co, μ_B=3.39, which is consistent with the value determined in 0.52T shown in Table 3-1. And for undercooled liquid, μ_B=3.28, which is smaller than the solid state but larger than the value obtained in 0.52T magnetic field.

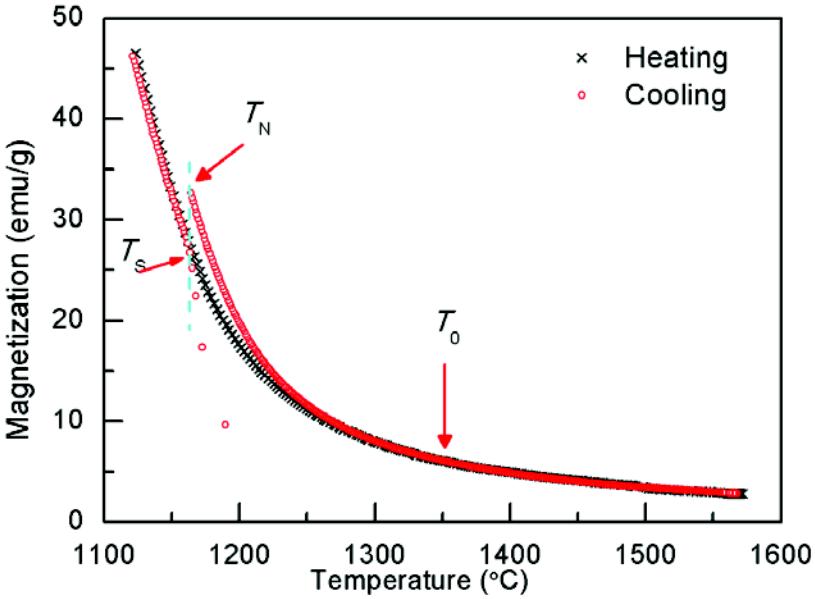

Fig 3-5 Magnetizations as a function of temperature curves of pure Co measured in 9294Gauss/cm gradient magnetic field and the field intensity is 6.23T at the sample position. The black crossing and red circle represent the heating and cooling process, respectively. Due to the large magnetic force exerted on the sample below the Curie temperature in the magnetic field, the magnetization curves are stopped before saturation as the value outweighed the measuring weight of the balance.

Fig 3-6 presents the picture of the solidified sample, and a lotus-like surface with many peaks and valleys is shown. This unique morphology is the characteristics of ferrofluid when it is put close to a magnetic field. And for pure metal, we are the first to find this unique phenomenon. When a magnetic field is applied to a ferrofluid, the magnetic moments of the particles orient along the field lines almost instantly. The magnetization of the ferrofluid responds immediately to the changes in the applied magnetic field and when the applied field is removed, the moments randomize quickly [ROSE87]. In a gradient field, the whole fluid responds as a homogeneous magnetic liquid which moves to the region of highest flux. This means that ferrofluids can be precisely positioned and controlled by an external magnetic field. The forces holding the magnetic fluid in place are proportional to the gradient of the external field and the magnetization value of the fluid. This means that the retention force of a ferrofluid can be adjusted by changing either the magnetization of the fluid or the magnetic field in the region. However, for undercooled liquid, there are no ferromagnetic particles in the melt and one probable reason is the long range order existing in the melt can be magnetized in strong external field, leading to the change of the magnetic nature of the melt. It is widely accepted that, ordering

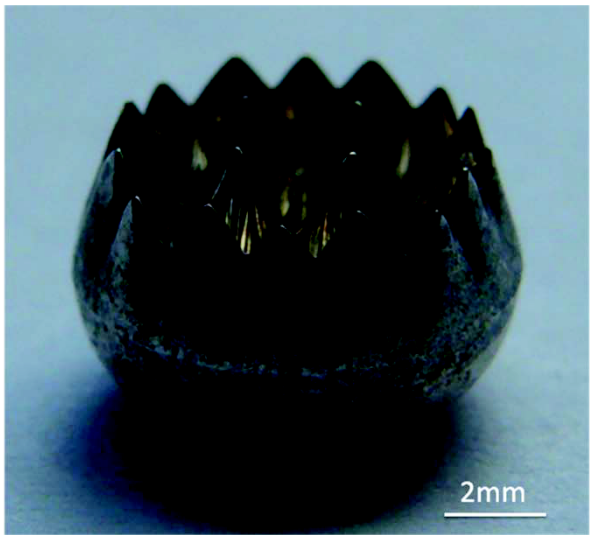

Fig 3-6 Macro-Photograph of undercooled pure Co solidified under 9294Gauss/cm gradient field, the field intensity at the sample position is 6.23T

structures tend to form in the undercooled melt, which can act as the pre-nucleation sites. And the length scale and number of ordering structure are related with the nature of the liquid and undercooling. Thus for undercooled liquid, the undercooling related orders can act as the ferromagnetic particles in ferrofluid and form 'molecular liquid' with many ferromagnetic orders inside. For the undercooled melt in magnetic field, the morphology of the melt is affected by surface tension, gravity, viscosity of the melt and intensity of the external magnetic field. Without magnetic field, pure metal solidified under surface tension and gravity effect will form spherical shape. When something in liquid state is put in a strong magnetic field, even for diamagnetic water, its surface morphology will change due to the Moses effect [HIRO95]. The metallic melt containing ferromagnetic orderings can be strongly affected by the external magnetic field. In case of ferrofluid, even it is put close to a small hard magnet, very special surface with lots of peaks and valleys can be formed due to the effects of surface tension, gravity and magnetic strength, and this effect is called normal field instability [ABOU00]. Compared with ferrofluid, which is a mixture of colloids and nano-scaled ferromagnetic particles, undercooled metallic melt can be treated as a mixture of purely random packed atoms and short range or even long range chemical orders. For ferromagnetic alloys, orders in the melt can be ferromagnetic. However, the length scale maybe much smaller (even smaller than the length of magnetic domain) than the particles in ferrofluid. Thus, the theory which is suitable for the ferrohydrodynamics of ferrofluid may not suitable for the undercooled metallic melt with ferromagnetic long range orders. In fact, ferrofluid is in a superparamagnetic

state due to tiny nano-sized ferromagnetic particles. While for the present undercooled melt, even the scale of magnetic orderings are smaller than superparamagnetic blocking orderings, the melt cannot come into superparamagnetic state due to the temperature is still above the Curie point. And the breakup of the surface equilibrium to form unique peak structure could be attributed to the magnetization of ferromagnetic long range orderings in the melt. As we can seen from Fig 3-5, even above Curie point, the undercooled melt can be strongly magnetized which can provide the energy needed for forming unique surface morphology.

Fig 3-7 shows the magnetization-temperature curves of pure Co measured at low magnetic field, 0.13T (the field gradient is 194Gauss/cm). It can be seen that the magnetization of the undercooled melt presents the same trend as that measured in 6.23T magnetic field. The whole magnetization curves are overlapped for Co no matter in solid state or overheated state, and the discrepancy happens only when the melt comes into the undercooled state. One interesting point existing in the curves is a turning point at 1086 ºC (marked by the circle in Fig 3-7), and the sharp transition indicates the paramagnetic to ferromagnetic transition happens at this point. Albrecht et al [ALBR97] also have measured the Curie temperature of pure Co liquid, however their results showed the Curie temperature of the melt, 1121ºC, which was lower than the Curie temperature of its solid state, 1127 ºC.

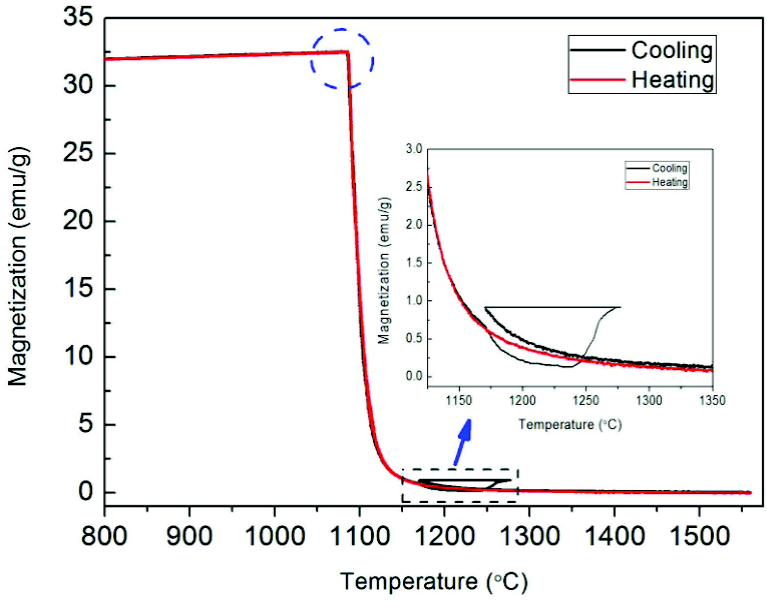

Fig 3-7 Magnetization as a function of temperature curves of pure Co measured in 194Gauss/cm gradient magnetic field, and the field intensity at the sample position is 0.13T, the black and red lines represent the cooling and heating process, respectively.

Theoretically, it is possible for the existence of ferromagnetic liquid, and also the undercooling experiments of Co-Pd by Reske [RESK95] have proved the existence of long range magnetic ordering. The thermally driven oscillation amplitudes of atoms in the metallic melt may hinder the establishment of a permanent long range magnetic ordering at high temperatures. The undercooling of the melt and the external magnetic (intensity and gradient) can directly affect this process. With the increasing undercooling, the temperature of the melt decreases gradually while the viscosity increases. The thermally oscillation amplitudes of atoms are weakened, while the possibility for the formation of long range magnetic orders increase. The external magnetic field can stabilize the ferromagnetic orders and let them perfectly align since there are no effective blocks for the ordering in the liquid. After the alloy solidifies, the equiaxed crystal microstructure is formed and the magnetic domain is constrained in the grain. The latent heat release during solidification can change the alignment of the domain and the strain induced by rapid solidification can also reduce the magnetic properties of alloys. Thus when the undercooling surpass certain value, it is possible for the liquid melt to have larger magnetization than it in the liquid state. In deeply undercooled melts, the icosahedral short-range order was proved to be exist in pure Fe [SCHE02], Ni [SCHE02], Zr [SCHE02] and Co [HOLL02] by neutron diffraction experiments. And to have a fully understanding of the highly magnetization of undercooled liquid Co, more precise experiments, for example directly using neutron diffraction method to investigate the structure of deeply undercooled Co melt in strong external magnetic are required in future.

3.2 Magnetic properties of undercooled binary Co-B alloy

Unlike pure Co, the magnetic phase in Co-B binary alloys is αCo (the maximum solubility for B in Co is 0.163%), and the magnetization is typically affected by the solubility of B. Except the ferromagnetic αCo phase, Co_3B is another phase which is non-ferromagnetic in near eutectic Co-B alloys. Thus the magnetic properties of Co-B near eutectic alloys are affected by the solubility of B in αCo and also the relative volume fraction of αCo and Co_3B. In undercooled melt, the clusters always have the same structure as the solidified phases [HERL07], thus when an external magnetic field is applied, the undercooled melt can be strongly affected and show some unique behaviors.

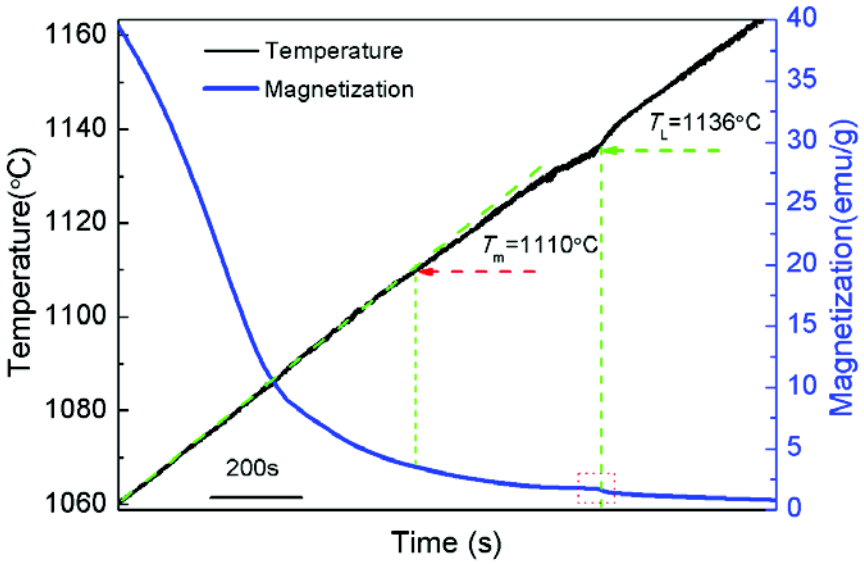

Fig 3-8 Time vs. temperature and time vs. magnetization curve of $Co_{83}B_{17}$ alloy during heating. The field intensity and gradient at the sample position are 388Gauss/cm and 0.26T, respectively.

Fig 3-8 shows the temperature and magnetization profile of $Co_{83}B_{17}$ alloy during heating taken at 5ºC /min in 0.26T magnetic field (field gradient at the sample position is 388Gauss/cm). The deviation from the linear heating line at 1100 ºC shows the melting of the alloy. The melting process is finished at 1136 ºC, where we can see an inflexion point. The magnetization curve shows the same trend, no obvious difference is shown at the melting point and a typical decrease point at the fully liquid temperature (rectangle areas in Fig 3-8). Fig 3-9 is the magnetization curves of $Co_{83}B_{17}$ alloy measured in 0.065T magnetic field during heating and cooling process. It can be seen that the magnetization curves are overlapped only above the melting point. When the alloy is undercooled below its melting point, the magnetization starts to deviate, and the magnetization of liquid melt is smaller than that of solid state at the same temperature. At 1046ºC the magnetization of solid during heating and magnetization of undercooled melt during cooling is the same. Below 1046 ºC, the magnetization of undercooled melt is larger than that of solid, and the discrepancy becomes larger until the melt solidifies at 1033.5ºC. After the recalescence, the magnetization of the solid Co-B alloy is stable around 17emu/g and it is larger than that during heating.

Fig 3-10 is the inverse magnetic susceptibility as a function of temperature curves of $Co_{83}B_{17}$ alloy during heating and cooling process under 2.08T magnetic field. It can be seen that, the inverse magnetic susceptibility of $Co_{83}B_{17}$ alloy solidified after heating at different overheating temperatures, 1325ºC(Fig 3-10(a)) and 1500ºC (Fig

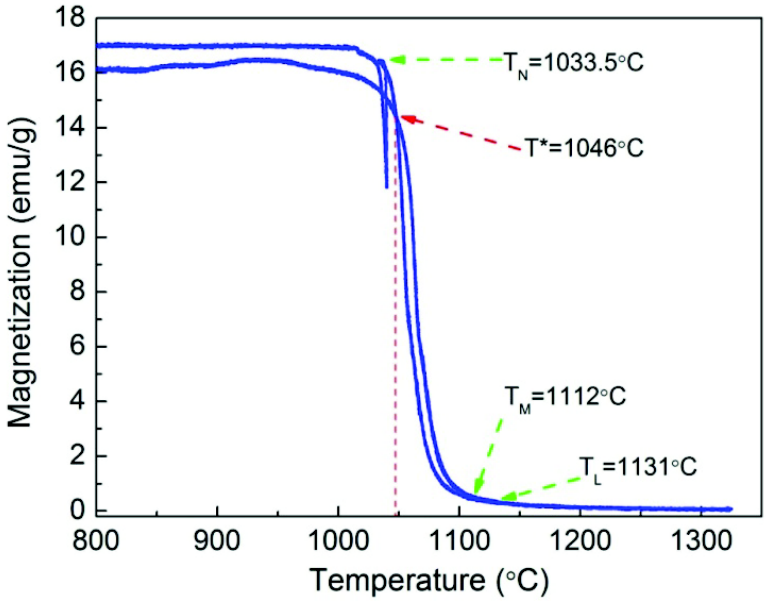

Fig 3-9 Magnetization as a function of temperature of $Co_{83}B_{17}$ alloy during heating and cooling process in 96.8Gauss/cm gradient field. The field intensity is 0.065T and the heating and cooling rate is 5ºC/min

3-10(b)), is quite different. For the alloy overheated at 1325 ºC, the $\chi 1/ -T$ curves during heating and cooling are nearly overlapped. And for the alloy overheated at 1500 ºC, the magnetic susceptibility during cooling shows a different trend, as it is shown in Fig 3-10(b). The curve is firstly overlapped above 1420ºC, and after, the cooling curve keeps linear and deviates from the curve measured in heating process. After the recalescence happens at 1099 ºC, the $1\chi / -T$ curves overlapped again. Kamp et al [KAMP88] have investigated the relationship between short and medium range magnetic ordering and ferromagnetic transitions in Co-B alloys, they found that there existed ordering in the melt above the melting point and the structure of the orderings were close to the solidified phase. And the ordering would disappear only when the temperature was above 1700K. Accordingly the phenomenon in Fig 3-10 can be interpreted as follows. When the overheating temperature is below1420℃ (close to the critical temperature in Ref [KAMP88]), the existence of magnetic ordering in the melt, just as the solidified ferromagnetic phase, gives high magnetization in external magnetic field. Below the critical temperature, the magnetic property of the overheated melt is the same during the heating and cooling process at the same temperature. When the temperature surpasses the critical temperature, 1420℃, vanishing of the ordering leads to perfectly paramagnetic state of the liquid in strong magnetic field. During the cooling process, the magnetic susceptibility is firstly the same as that during the heating at the same temperature. Below the critical

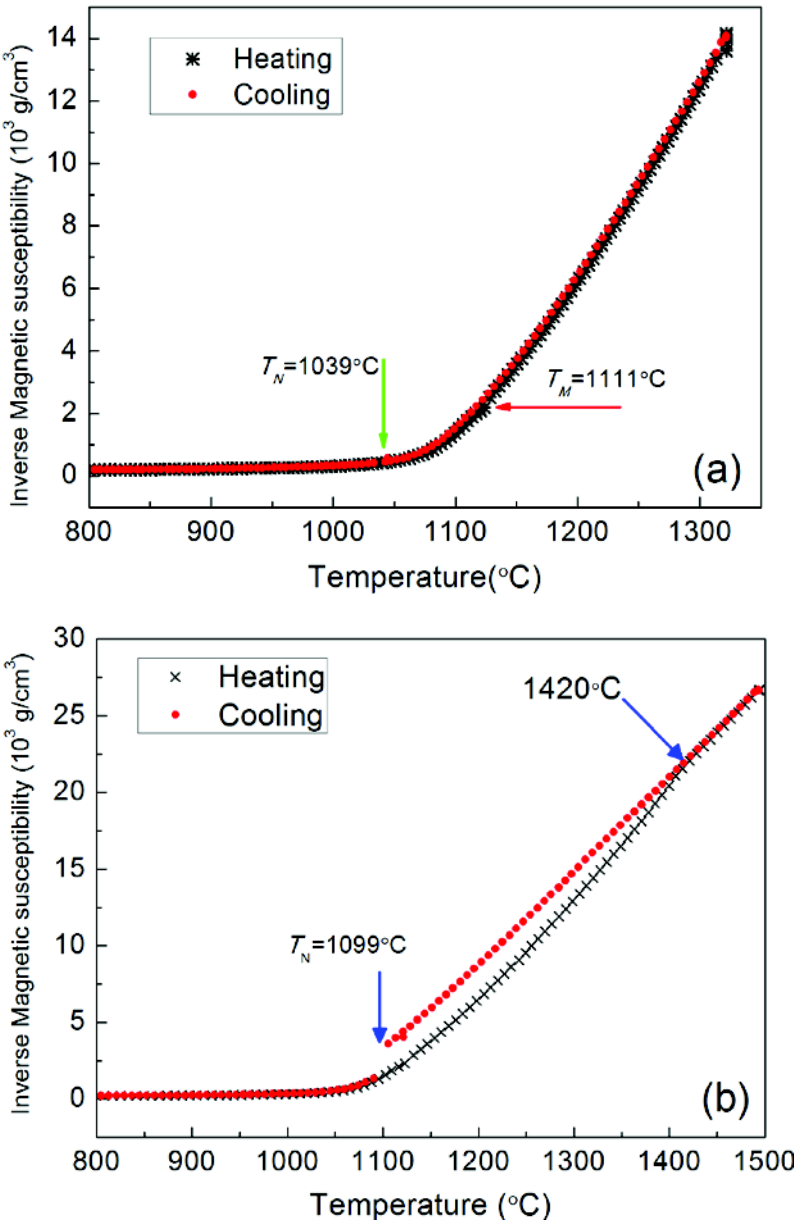

Fig 3-10 Magnetizations as a function of temperature of $Co_{83}B_{17}$ alloy during heating and cooling processed under different overheating temperature. (a) overheated at 1325°C, and (b)overheated at 1500°C. The heating and cooling rate is 5°C/min

temperature, the melt comes into a relatively 'paramagnetic undercooled' state (relatively for the existence of magnetic orderings, but not really the undercooling state of the melt), and there should form a small volume of magnetic orderings. However, when compared with that during the heating process at the same temperature, the scale and the volume of the magnetic ordering are much smaller, leading to nearly paramagnetic state of the melt.

For paramagnetic material, the relations between the magnetization and temperature can be expressed by the Curie-Weiss law (Eq. (3-3)). And the

magnetization divided by field intensity in different magnetic field at the same temperature is constant for paramagnetic materials. Fig 3-11 shows the magnetization divided by magnetic field intensity versus temperature curves of Co-B alloy in different field gradient. It can be seen that the M/B-*T* curves measured at different magnetic field are not overlapped, indicating the alloy is not in ideal paramagnetic state, and with the increasing temperature the discrepancy between the curves measured at different magnetic fields became smaller. With the dissolve of ordering in the melt with the increasing temperature, all the cures will overlapped above the critical temperature for the existence of magnetic ordering, and become fully paramagnetic above 1420°C.

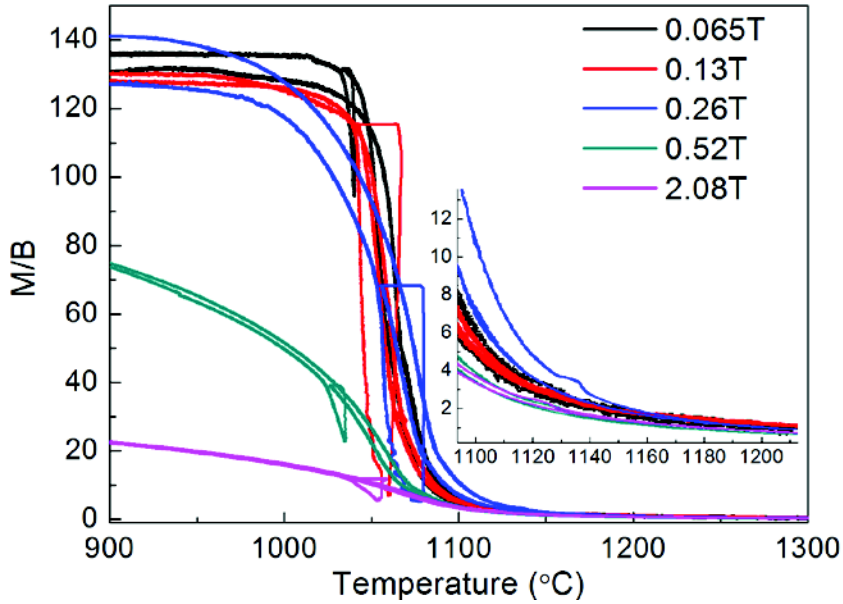

Fig 3-11 M/B vs. temperature curves of $Co_{83}B_{17}$ under different gradient field. The heating and cooling rate is 5°C /min

3.3 Magnetic properties of undercooled binary Co-Sn alloy

The melting point and Curie temperature of $Co_{79.5}Sn_{20.5}$ alloy are 1112ºC and 1050ºC, respectively. What will happen when the alloy melt is directly undercooled approach or far below the Curie temperature becomes an interesting topic. Fig 3-12 is the magnetization curve as a function of temperature of $Co_{79.5}Sn_{20.5}$ alloy measured at 0.26T magnetic field at the heating and cooling rate of 5ºC /min. The same as pure Co, the magnetization curves of $Co_{79.5}Sn_{20.5}$ alloy above the melting point are overlapped. The undercooled $Co_{79.5}Sn_{20.5}$ alloy melt shows quite different behavior, and the linearity of the curve represents the paramagnetic state of the melt even at much lower

temperature below the Curie temperature of solid $Co_{79.5}Sn_{20.5}$ alloy. When the undercooled melt is solidified at 890ºC, ferromagnetic transition happens during the

Table 3-3 Curie-Weiss fitting of the magnetic susceptibility of $Co_{79.5}Sn_{20.5}$ during heating and cooling process，the magnetic field and the magnetic gradient is 0.26T and 387.4Gauss/cm, respectively.

Parameter	χ_0 ($10^{-3}cm^3/g$)	C ($10^{-3}cm^3K/g$)	θ_P (℃)	R-square	$\mu_{eff}(\mu_B)$
Heating (S)	0.005613	2.639	1062	0.9858	1.23
Cooling (L)	-0.01026	15.66	612.1	0.9902	2.99

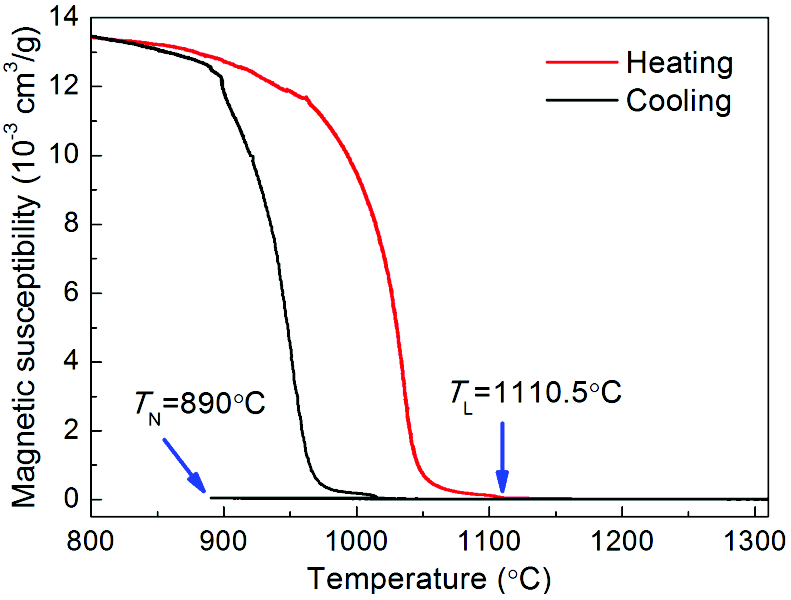

Fig 3-12 Magnetic susceptibility as a function of temperature of $Co_{79.5}Sn_{20.5}$ alloy measured in 387.4 Gauss/cm gradient field, and the field intensity at the sample position is 0.26T. The red and black lines represent the heating and cooling process, respectively. The heating and cooling rate used is 5℃/min.

cooling of the solidified alloy. The paramagnetic Curie temperature is calculated by the heating and cooling curves shown in Fig 3-12, and two paramagnetic Curie temperatures, one for solid $Co_{79.5}Sn_{20.5}$ alloy during heating, θ_P(S)=1062ºC, the other for undercooled $Co_{79.5}Sn_{20.5}$ alloy melt θ_P(L)=612ºC (shown in Table 3-3).

Fig 3-13 is magnetization as a function of temperature for $Co_{76}Sn_{24}$ alloy measured at same field intensity and different overheating temperature. We can see that the magnetization of the curves on heating shows a small difference, which is because the same sample alloy is solidified several times at different undercoolings before heating, showing different phase structure, grain morphology and grain size with different undercooling which will cause the magnetization difference. However,

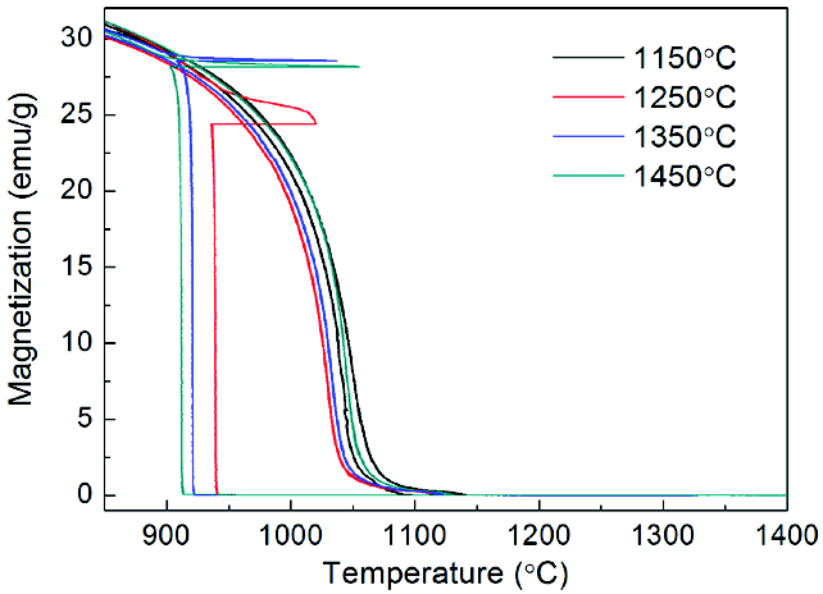

Fig 3-13 Magnetic susceptibility as a function of temperature of $Co_{76}Sn_{24}$ alloy measured under 387Gauss/cm gradient field and different overheating. The heating and cooling rate used is 10℃ /min

when the alloy is heated above the melting point, with the melting of the solid phases, the microstructure difference is eliminated. The melt consists of some orderings and uniform overheated liquid, which means the difference in magnetization caused by microstructure, becomes smaller. The magnetization curves are overlapped during cooling process after holding at different overheats for 30min, showing the same linear decrease of the magnetization before solidification regardless of overheating temperature.

Fig 3-14 is the M/B as function of temperature curves of $Co_{79.5}Sn_{20.5}$ alloy measured at different magnetic field. During the heating process, the discrepancy for M/B-T curves below Curie temperature is very large, while all the curves are overlapped when the temperature is above the melting point, indicating the alloy melt is in paramagnetic state. For the cooling process, the curves are overlapped no matter in overheated or undercooling state, which means $Co_{79.5}Sn_{20.5}$ alloy melt is in paramagnetic state.

3.4 Factors affecting the magnetic properties of the undercooled melt

From above experimental results, it can be concluded that the magnetic properties

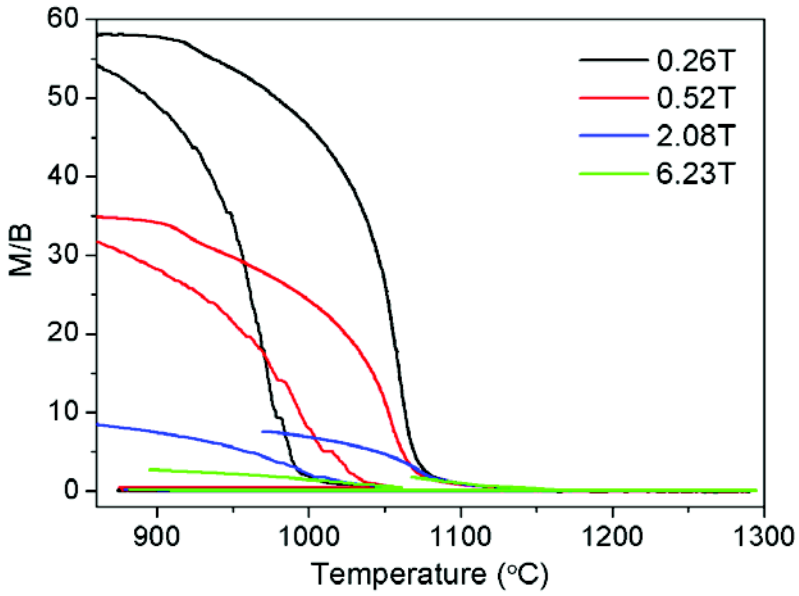

Fig 3-14 Magnetic susceptibility as a function of temperature of $Co_{79.5}Sn_{20.5}$ alloy measured under different gradient fields at the same overheating.

of pure Co, Co-B and Co-Sn alloys show different behaviors in external magnetic field. The difference can be expressed as follows.

The magnetization is different between the undercooled melt and its solid state at the same temperature. The magnetization of undercooled pure Co is larger than that of its solid state, and when the field intensity surpasses certain value, normal field instability effect happens for metallic melt before solidification. A spike pattern can be seen on the surface of the sample, like in ferrofluid when close to external fields. This spike pattern results from a competition between demagnetizing energy that tends to form elongated shapes along the field, and surface energy that tends to give spherical shapes. And for $Co_{83}B_{17}$ and $Co_{79.5}Sn_{20.5}$ alloys, in the present magnetic field range used in this study, the magnetization of the alloy melt is smaller than its solid state at the same temperature.

The effect of overheating on magnetic properties of undercooled melt is different. The magnetic properties of $Co_{83}B_{17}$ alloy are affected by the overheating temperature. When the overheating temperature is below the critical temperature, 1420ºC, the alloy melt behaves like the solid. While the undercooled melt is always in 'paramagnetic undercooled state' before solidification when the overheating temperature surpasses the critical value, and the paramagnetic Curie temperature is much lower than the paramagnetic Curie temperature of the solid state. For pure Co and $Co_{79.5}Sn_{20.5}$ alloy, the overheating has very limited effect on the magnetic properties of the undercooled

melt.

The magnetic properties come from the magnetic moment of atoms, thus the variation of electro orbit and atomic density will lead to the change of magnetic properties. For metals and alloys, the phases and microstructure determine the magnetic properties, take Co-B and Co-Sn alloys for example, αCo is the ferromagnetic phase of these two alloys. However, its behavior under magnetic field is quite different. That is because during the formation of αCo solution, the atomic structure and bonding can be affected by the solute atoms. When the alloy is in overheated or in undercooled state, the structure nature of the metallic melt can determine the magnetic properties of the melt and the magnetic nature of the ordering, e.g. the viscosity of the melt is one of the determine factors which is very important for the formation of ordering structure in the melt. Thus, pure Co, Co-B and Co-Sn alloys melts exhibit different magnetic properties when undercooled in magnetic field.

3.4.1 Magnetic properties of the solid and undercooled liquid

According to the present theory, it is easy to draw the conclusion that the magnetic susceptibility of a matter in solid state is larger than that in liquid state at the same temperature. That is because the melting process breaks the local ordering and atoms neighboring that leads to ferromagnetic interactions. The oscillation in the liquid is not in favor of the formation of stable parallel magnetic domain also. However, from the results in Figs 3-2 and 3-5, we can see that the magnetization of undercooled pure Co melt is larger than that of heated solid Co at the same temperature, and the discrepancy increases with the increasing undercooling. The paramagnetic Curie temperature calculated for undercooled Co melt is 1132.5ºC, which is the highest Curie temperature up to the present.

The magnetic properties of matter can be described by the molecule field theory. Molecular field also called exchange field or Weiss field. According to molecular field theory, there exist strong molecular field in the ferromagnetic material, under the molecular field, the atomic magnetic moments in the matter tend to parallel alignment, and saturated by spontaneous saturation. During spontaneous magnetization of ferromagnetic material, many small areas called magnetic domain are formed. Because the domains have random magnetization direction, the magnetic moments are averaged and macroscopically show no magnetism. Spontaneous magnetization of magnetic material is caused by the static function between electrons, and when a

molecular is formed by the nearby atoms, the electron cloud is overlapped, and the electron will exchange its position. This exchange interaction which reflects the Coulomb repulsion of two nearby electrons, usually on neighboring atoms, is called exchange force. The exchange force let the neighboring atoms form aligned parallel spin. The exchange field is an approximation of the quantum mechanical exchange interaction. On certain assumptions, it is shown that the energy of interaction of atoms i, j, bearing electron spins S_i, S_j can be expressed in a Hamilton function: $H=-2JS_i \bullet S_j$. Where J is the exchange integral and is related to the overlap of the charge distributions of the atoms i, j. When J>0, the ferromagnetic exchange interaction can lead to the formation of magnetic ordering.

When $T<T_C$, the material is in ferromagnetic state. Microscopically the magnetic moments are almost parallel, however, for a real material is composed of magnetic domain. In every domain the localized magnetization is saturated and it is not a must for every domain to ideally parallel with each other. In weak magnetic field, the volume of domains favorably oriented with respect to the filed increase at the expense of unfavorable oriented domains. And in strong external magnetic field, the domain magnetization rotates toward the direction of the field. For pure Co, seen from Fig 3-2 and Fig 3-5, the magnetization is equal to the magnetization of the solid Co during heating process when the undercooled melt is solidified. And the undercooled melt has a larger magnetization than solid at the same temperature. We can explain by the above theories. When pure Co is heated above the melting point, the metal comes into liquid state, and inside there are some short or medium orderings. When an external magnetic field is applied, the ordering structure inside the melt is strengthened. Thus, when the overheating is not too much, even though the temperature is above the Curie temperature, the existence of ordering structure which can be magnetized by external field caused the melt deviates from ideal paramagnetic liquid, and we can see from linearity of the magnetic susceptibility curves in Fig 3-3. When the metal melt comes into the undercooled state, the viscosity increases with the increasing undercooling, and the thermal oscillation decreases with the decreasing temperature. Then the number and scale of the ordering are enhanced in the melt. Thus the magnetization of the melt increases rapidly with the increasing undercooling due to the increasing size and number of ordering structure. The melt is in an ideal isotropy state, and the magneto crystalline anisotropy energy equals 0. The ordering structure can be perfectly aligned by the external magnetic field since there are no blocks such as grain

boundaries in the melt. On contrary, when the undercooled melt is solidified, the alloy microstructure is controlled by the solidification process, such as the undercooling. The formation of grain boundaries and the existence of the magneto crystalline anisotropy energy reduce the energy of the system. And the rapid latent heat release can introduce a strong strain in the alloy which will also destroy the parallel domains formed in the undercooled melt. Thus it is possible for the existence of much more ferromagnetic liquid Co. And for Co-Sn and Co-B, except the ferromagnetic Co, other atoms can affect the formation of magnetic ordering and have a less magnetic alloy.

3.4.2 Effect of overheating on the magnetic properties of the undercooled melt

Even there are no directly relations, present research results indicate that specific ordering is exist in metallic melt which is close to the structure of the crystalline phase structure. Even there still exist some unmelted crystals in the overheated melt. That is to say, there exists a second melting point for the unmelted particles, only when the overheating is surpassing certain value a uniform completely melt can be obtained. In the present study, the magnetization curves of Co-B measured at different overheating show that there exists a critical temperature for this alloy. Below 1420ºC, the magnetic ordering still exists in the melt. Kamp and Methfessel [KAMP88] have investigated the magnetic ordering of overheated $Co_{1-x}B_x(0<x<0.33)$ alloys at different overheating. They have found 1700K is a critical temperature for this alloy, and the magnetic property of the alloy overheated below or above this temperature is quite different. The existence of B in αCo reduce the magnetization of Co, leading to the magnetization of the undercooled melt is lower than its solid state at first. With the increasing undercooling, just as undercooled Co discussed before, the increased viscosity and decreased temperature make a much more strengthened ordering structure which can be magnetized in the melt. However, when the overheating temperature surpasses the critical value, the existence of the ordering structure leads to an ideal paramagnetic liquid. During the cooling process, the ordering is not easy to counter act the thermal driven oscillation and the undercooled melt keeps the paramagnetic state of the liquid before solidification. And for pure Co and Co-Sn alloy, with the experimental overheating, we do not detect the critical temperature, thus the magnetic properties of the undercooled melts are not affected by the

overheating.

3.5 Summary

Based on the modified Faraday balance, the magnetic properties of pure Co, Co-B and Co-Sn are measured, and the main conclusions of this chapter are:

(1) The magnetization of undercooled Co melts increases with the increasing undercooling. The undercooled melt has a larger magnetization than that in solid state at the same temperature. When the temperature is close to the Curie temperature of the melt, the magnetization increased rapidly. Based on Curie-Weiss law, the paramagnetic Curie temperatures calculated based on the solid Co during heating and liquid Co melt during cooling are: $\theta_P(L)$=1132.5ºC, and $\theta_P(S)$=1120.5 ºC, respectivelly.

(2) Under strong external magnetic field, when approaching the Curie temperature, the undercooled Co melt forms unique morphology due to normal field instability effect. A spike pattern can be seen on the surface of the sample, like in ferrofluid when submitted to external fields. This spike pattern results from a competition between demagnetizing energy that tends to form elongated shapes along the field, and surface energy that tends to give spherical shapes.

(3) The magnetic properties of Co-B are affected by the overheating temperature. When the overheating temperature is below 1420ºC, the magnetization of the undercooled melt is close to the solid alloy, and the paramagnetic Curie temperatures determined are: $\theta_P(L)$=1066ºC, and $\theta_P(S)$=1073ºC, respectivelly. When the overheating temperature surpasses 1420℃, the undercooled melt comes into completely paramagnetic state, and the liquid Curie temperature is 1046ºC, the alloy melt cannot undercooled into ferromagnetic state.

(4) The undercooled Co-Sn near eutectic alloy is in fully paramagnetic state, and the magnetic properties of the undercooled melt are not affected by the overheating temperature. The Curie temperatures determined are $\theta_P(L)$=612.1ºC, and $\theta_P(S)$=1062ºC, respectively.

CHAPTER 4 EFFECT OF MAGNETIC FIELD ON THE UNDERCOOLABILITY OF UNDERCOOLED MELT

The investigation of non-equilibrium solidification of undercooled melts in magnetic field started from the research of the effect of magnetic field on the undercoolability of metals and alloys. Based on the research results of the undercooling of Cu [HASE92, ZHAN10b], Ge [ZHAN10b], Sb [ZHAN10a] and Co-Cu [GAO09] alloy in magnetic field, researchers found that the effect of the magnetic field on the undercoolability depended on the alloy characteristics. However, when we analyze the present results, it can be seen that the maximum undercooling of the metals or alloys studied is much smaller than the stable undercooling obtained by the normal undercooling techniques (induction melting or levitation melting method) without magnetic fields, indicating the alloys are not in the thermodynamic stable state. The drawbacks of the facilities cause the nucleation in the undercooled melt before the thermodynamic undercooling limit, and many other factors can also lead to the heterogeneous nucleation. Thus it is difficult to discuss the intrinsic effect of the field on the undercooling. Take pure Cu for example, the undercooling received in Ref. [HASE92] is smaller than 100ºC in 0.5T magnetic field by glass fluxing method and smaller than 200ºC in 10T magnetic field by levitation melting method in Ref.[YASU04], while the maximum undercooling reported is 236ºC [TURN50] and 271ºC [COST89] which is much larger than the value obtained with magnetic field. In this chapter, the undercooling behaviors of diamagnetic pure Cu, ferromagnetic pure Co and near eutectic Co-Sn alloys under static and gradient magnetic field are systematically investigated.

4.1 Effect of magnetic field on the undercoolability

4.1.1 Undercoolability of Cu under strong magnetic field

The heating program used for investigation of the undercooling behaviors of pure Cu in static magnetic field is as follows: Firstly heating at 1ºC/s to 1250ºC, holding

for 10 min, then cooling at 2ºC/s to 800 ºC. After holding for 5 min at 800 ºC, another new heating cycle starts. Fig 4-1 is the typical recalescence curve of pure Cu, the undercooled melt nucleated at T_N and then the temperature increased to T_R, afterwards falling in to the cooling process. The as solidified metal is spherical shape and the surface is ultra bright, indicating the purifying effect of the glass is very nice. In Fig 4-1, T_N=833ºC, and the undercooling calculated by$\Delta T=T_m-T_N$, is 251ºC. After many heating cycles (>150), the undercooling is very stable and the reproduction of the experiment is good.

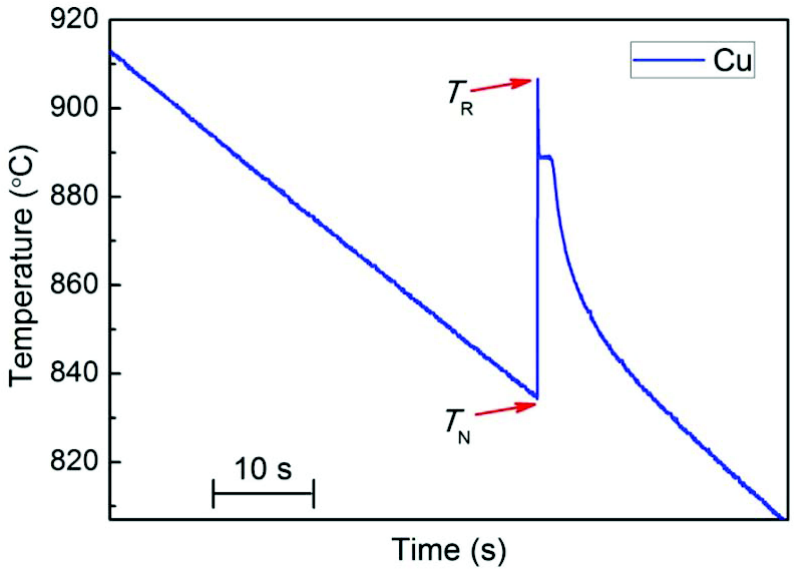

Fig 4-1 Recalescence curve of pure Cu heating under the present furnace in the magnet, ΔT=251℃

Fig 4-2 represents the undercooling as a function of cycling heating times of pure Cu in 0 and 12T static magnetic field. It can be seen that there is a large fluctuation at the beginning when the melt is not stable, and the mean undercooling for the first 15 times cycling is 141.9ºC which is relatively small. With the increasing heating times, from 16th to 42th cycling the mean undercooling increases to 170.1ºC. When a 12T magnetic field is applied at the 43th cycling, the undercooling increases above 200ºC, and the undercooling is rather stable regardless of the cycling times. The mean undercooling increases to 211.6ºC, which is 40.5ºC larger than that without magnetic field. The undercooling suddenly decreases to 180ºC at 54th cycling when the magnetic field is removed. Afterwards the mean undercooling of Cu is always closed to 210ºC with imposing or removing magnetic field and the undercooling slightly increases with the cycling times for Cu without magnetic field. Finally the

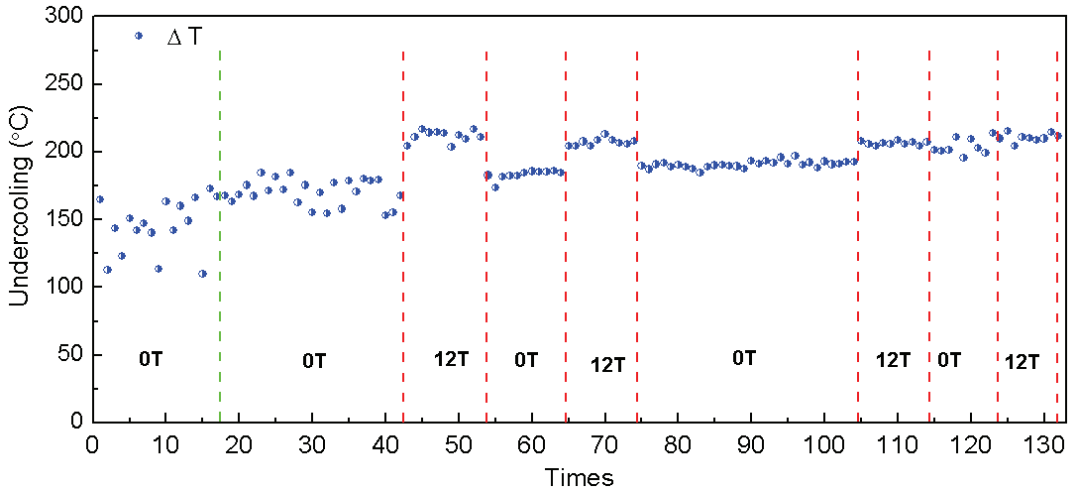

Fig 4-2 Undercooling of Cu at different cycling times under different magnetic fields.

Table 4-1 Parameters used for calculation of the effect of the magnetic field on the Gibbs free energy of undercooled Cu melt

E kJ/mol	ΔH_f J/mol	B	χ^L 10^{-8}	χ^S 10^{-8}	L	σ $10^6\Omega^{-1}m^{-1}$	η (1107K)
30.5[BROO05]	13.03	12T	-9.1	-8.0 [HASE92]	6mm	4.65 (T_m) [GATH83]	8.27mPas

undercooling comes to a stable state regardless of the magnetic field.

The effect of magnetic field on the undercoolability can be analyzed from two sides. The first one is the thermodynamic effect on the nucleation by the application of magnetic field. The second one is some other effects caused by external magnetic field which can affect the purifying effect of the melt, e.g. convection of the melt. The Gibbs free energy of undercooled pure Cu in magnetic field can be expressed as follows:

$$\Delta G = \Delta G_V + \Delta G_M \tag{4-1}$$

$$\Delta G_V = \frac{\Delta H_f \Delta T}{T_m} \tag{4-2}$$

$$\Delta G_M = \Delta G_M^S - \Delta G_M^L = -\frac{1}{2}\mu_0 \Delta \chi_{mol}^{S-L} H_{ex}^2 \tag{4-3}$$

Where ΔG_V, ΔG_M are chemical Gibbs free energy and magnetic Gibbs free energy, ΔH_f, ΔT, T_m, $\Delta \chi^{S-L}$, μ_0, H_{ex} are melting enthalpy, undercooling, melting point, magnetic susceptibility difference between the solid and liquid phase, permeability of vacuum, and the external magnetic field, respectively.

Cu is diamagnetic material, and after solidification the magnetic susceptibility variation is very small. So the calculated (The parameters used for calculation are shown in Table 4-1) magnetic Gibbs free energy, -5.03×10^{-4}J/mol, is relatively small,

and can be neglected compared with the chemical Gibbs free energy (2400J/mol).

The effect of the magnetic field on the suppression of convection effects can be determined by Hartmann number, *Ha*. The value of *Ha* can be used to characterize the effect of magnetic field on the suppression of convection flow in the melt, and the larger the *Ha*, the larger the suppression effect. *Ha* can be calculated by the following equation [HUNT71]:

$$Ha = LB(\sigma / \eta)^{1/2} \tag{4-4}$$

Where L is characteristic length, here, means the diameter of the sample, σ is the electric conductivity, and η is the viscosity of the melt which can be calculated by [BROO05]:

$$\eta = \eta_0 \exp(\frac{E}{RT}) \tag{4-5}$$

Where η_0 is the pre-exponential factor of viscosity, and E is activation energy for viscous flow, which are both constants. Based on the parameters in Table 4-1, *Ha* is calculated as 1707.3, which means the suppression effect of the magnetic field is really very strong. The convection in the melt can cause the fluctuation of heat flow and ordering structure, and also the movement of impurities, thus benefits for the heterogeneous nucleation. In 12T magnetic field, the convection flow in the melt is strongly suppressed by the external field, and the stabilized melt reduces the triggering effect for nucleation. So, when a 12T is applied, the undercooling increases by 40ºC, as we can see in Fig 4-2. Meanwhile, the effect of the magnetic field on the undercooling of the melt is weakened with the increasing heating cycle. During the cycling heating process, the purifying effect of fluxed glass by physical adsorption and interface chemical reaction of impurities can reduce the heterogeneous nucleation sites gradually. After certain cycles, the melt is in a relatively stable state, and the fluxed glass has very limited effects on the maximum undercooling. Before the melt comes to the stable state, there exist impurity elements in the melt waiting for purifying by fluxed glass. At this time, the convection in the melt can accelerate the movement of the impurity elements, stimulating the nucleation and leading to decreased undercooling. Thus when a strong magnetic field is applied, the suppression of convection flow can increase the undercooling. With the cycling processing, the effective nucleation sites decrease due to the purifying effect of the fluxed glass, thus the undercooling of the melt increases. When applying a magnetic field, even if the convection flow is suppressed, the undercooling improvement of the

field becomes less and less, and finally has no obvious effect as the purifying effect of the glass is at its maximum.

Thus it can be concluded that the magnetic field can stimulate the purifying process of fluxed glass and enhance the undercooling process, and it cannot change the nucleation temperature thermodynamically. The strong magnetic field cannot change the maximum undercooling of undercooled Cu melt, and it can accelerate the process for obtaining the maximum undercooling.

4.1.2 Undercoolability of Co under strong magnetic field

Pure Co is a typical ferromagnetic material, and according to Reutzel's results [REUT04], the paramagnetic Curie temperature of solid Co, $\theta_P(S)$, and the paramagnetic Curie temperature of undercooled melt, θ_P (L), are 1400K and 1388K, respectively. Compared with pure Cu, ferromagnetic Co tends to be affected by magnetic field more easily. And when pure Co is deeply undercooled in magnetic field, the effect of magnetic field on the ordering structure especially when close to the Curie point becomes an interesting topic.

Fig 4-3 is temperature profile of pure Co during cooling in 12T magnetic field. The melt solidified when it is undercooled at certain undercooling. It can be seen that recalescence contains two separate processes, meaning two independent nucleation (T_{N1} and T_{N2}) and solidification process. According to Fig 2-4 (a), the magnetic force exerted on paramagnetic or ferromagnetic sample at the maximum field zone is along the radial direction of the field, and the melt is attracted by the force to the direction of the wall of magnet bore. And the force is proportional to the field gradient and magnetization of the melt (Eq.(2-1)). The magnetization of the undercooled melt increases with undercooling (Fig 3-5), thus the melt is divided into two parts by the radial magnetic force exerted on the melt. The two parts solidified separately as indicated by the two recalescence peaks in Fig 4-3. The as solidified sample is in needle like shape (shown in Fig 4-4), which is because the melt was elongated along the axial direction of the field in order to reduce the total energy of the system by the demagnetization effect.

Fig 4-5 is the undercooling and recalescence extent of Co as a function of cyclic heating times in 0 and 12T magnetic field. It can be seen the undercooling of Co is relatively stable with the increasing heating cycle, and the mean undercooling is324±6 ºC. The magnetic field has very limited effect on the undercooling of Co melt.

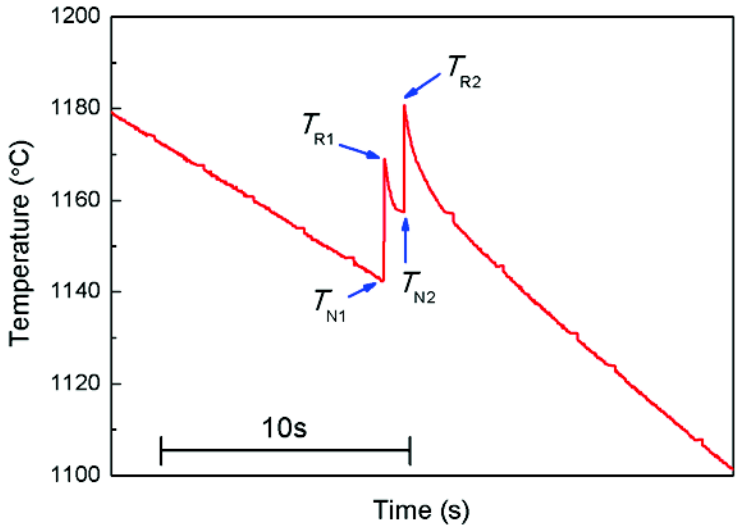

Fig 4-3 Recalescence curve of pure Co heating under the present furnace, ΔT=356°C.

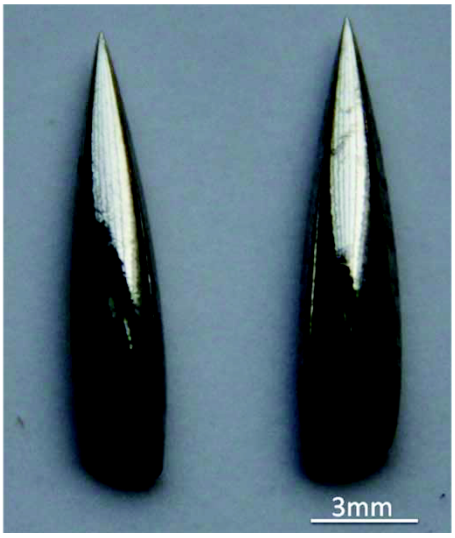

Fig 4-4 Image of solidified undercooled Co under high static magnetic field with intensity 12T showing the undercooled liquid separated into two parts.

According to previous analysis, the application of magnetic field can lead to rapid increase of magnetization. Meanwhile the increasing magnetization of the melt can increase the energy of the whole sample, thus it is elongated along the field direction to reduce the energy due to demagnetization effect. According to the traditional nucleation theory of the undercooled melt, the formation of ordering structure (clusters) in the melt is benefit for nucleation process. Also the catalytic sites can reduce nucleation function, promoting the nucleation process. Before solidification, the undercooled melt is divided into two parts (shown in Fig 4-4), both with a needle like sharp tip, and each part is tightly close to the wall of quartzes tube. The above factors may be good for trigging nucleation, thus decreasing the undercooling.

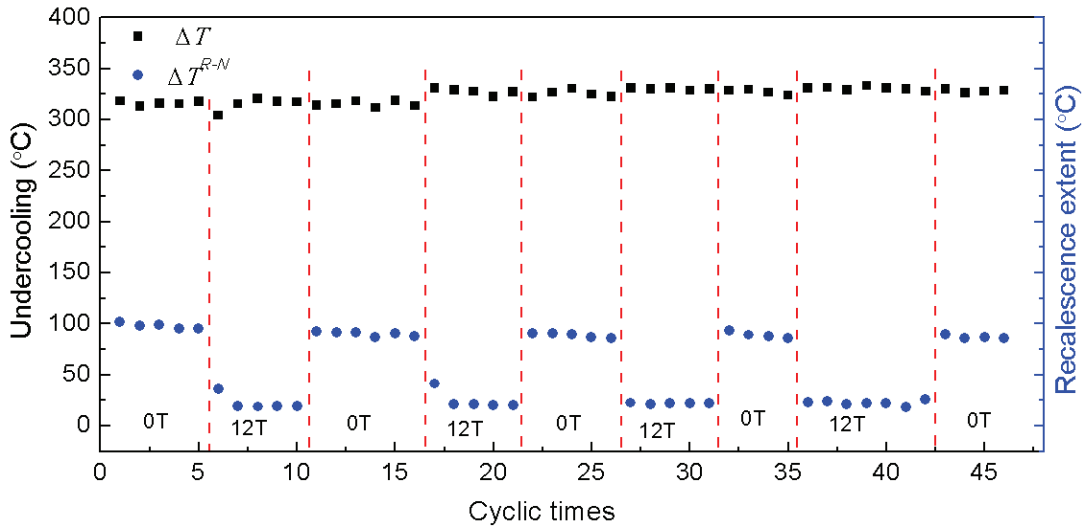

Fig 4-5 Undercooling and recalescence extent of Co at different cycling times under different magnetic fields

However, according to Fig 4-5, the magnetic field has very limited effect on the undercooling, and it doesn't decrease when magnetic field is applied. One possible reason is as follows: the magnetization of undercooled Co melt is larger than that after solidification, thus $\Delta\chi^{S-L}<0$, and the critical nucleation function increases when a magnetic field is applied, which is good for increasing undercooling. The thermodynamic effect and suppressing convection effect of the magnetic field on undercooled Co melt are discussed as below.

Table 4-2 Parameters used for calculation of the effect of the magnetic field on the Gibbs free energy of undercooled Co melt

E kJ/mol	ΔH_f kJ/mol	B	χ^L	χ^S $10^{-3}cm^3g^{-1}$	L	$\sigma 10^5\Omega^{-1}m^{-1}$	η (1448K)
44.4[BATT89]	16.19	12T	0.599	0.4864	3mm	1.02	10.2mPas

Based on Eqs.(4-2) and (4-6), ΔG_V and ΔG_M calculated (the parameters used are shown in Table 4-2) are 2960 J/mol and 5.3 J/mol, respectively. The thermodynamic effect of magnetic field on nucleation of undercooled Co melt can be neglected, and the magnetic Gibbs free energy has very limited effect on the critical nucleation function.

The suppression of convection flow effect by 12T magnetic is also calculated, and the results Ha=113.8, which means the magnetic field also has some effect for suppressing the convection flow, which can promote undercooling. In 12T magnetic field, when Co melt is undercooled at a very large undercooling, due to the increasing magnetization of melt, the surface shape of the sample will be changed just as the

morphology variation of ferrofluid in magnetic field, as it is shown in Fig 4-4. According to classic nucleation theory, the sharp tip on the top of the sample will generate much larger surface tension and increase the energy of the system which is good for nucleation. And the convection suppressing effect of magnetic field is good for obtaining a large undercooling. According to all these factors, the undercooling of Co exhibits no much variation even a strong 12T magnetic field is applied, however, we cannot calculate the effect on undercooling for each factor quantitatively.

The effect of magnetic field on the recalescence extent will be discussed in the following parts.

4.1.3 Undercoolability of Co-Sn under strong magnetic field

Fig 4-6 is the undercooling as a function of cyclic heating times of Co-Sn alloy in 0 and 12T magnetic field. It can be seen that for $Co_{79.5}Sn_{20.5}$ hypoeutectic alloy (Fig 4-6 (a)), $Co_{76}Sn_{24}$ near eutectic alloy (Fig 4-6(b)) and $Co_{72}Sn_{28}$ hypereutectic alloy (Fig 4-6 (c)), with the increasing cyclic heating times, the undercooling in and without magnetic field shows the same trend. After vibration at the first few cycles, the undercooling is stable at certain value, and afterwards keeps constant regardless of cyclic heating times and magnetic field. The mean undercooling for $Co_{79.5}Sn_{20.5}$, $Co_{76}Sn_{24}$ and $Co_{72}Sn_{28}$ alloys are 265ºC, 245ºC and 225ºC, respectively.

After solidification, two phases, ferromagnetic αCo and paramagnetic βCo_3Sn_2 phase are formed in Co-Sn alloys. Compared with αCo, the magnetic Gibbs free energy of βCo_3Sn_2 can be neglected due to the low magnetic susceptibility difference. In the present experiment, when Co-Sn is solidified at the undercoolings shown in Fig 4-6, the solid αCo phase will be in ferromagnetic state due to the low temperature which is blow the Curie point. Thus the magnetic Gibbs free energy should be changed to the following form:

$$\Delta G_M = \Delta G_M^S - \Delta G_M^L = x\Delta G_M^{S_{\alpha Co}} + (1-x)\Delta G_M^{S_{\beta Co_3Sn_2}} - \Delta G_M^L$$

$$= -((1-x)\frac{1}{2}\mu_0\chi_{mol}^{S_{\beta Co_3Sn_2}}H_{ex}^2 + x\int_0^{H_{ex}}\mu_0 M^{S_{\alpha Co}}dH_{ex}) + \frac{1}{2}\mu_0\chi_{mol}^L H_{ex}^2 \quad (4\text{-}6)$$

Where x is αCo phase in mole of one mole Co-Sn alloy. The magnetic Gibbs free energy for ferromagnetic phase is much larger than paramagnetic Gibbs free energy in present calculation, thus for simplicity the following equation is used:

Table 4-3 Parameters used for calculation of the effect of the magnetic field on the Gibbs free energy of undercooled $Co_{79.5}Sn_{20.5}$ melt

T_M	ΔH	B	L	Σ	η
1385K	13.027kJ/mol	12T	5mm	$1.7\times10^{4}\Omega^{-4}m^{-1}$	10mPa s

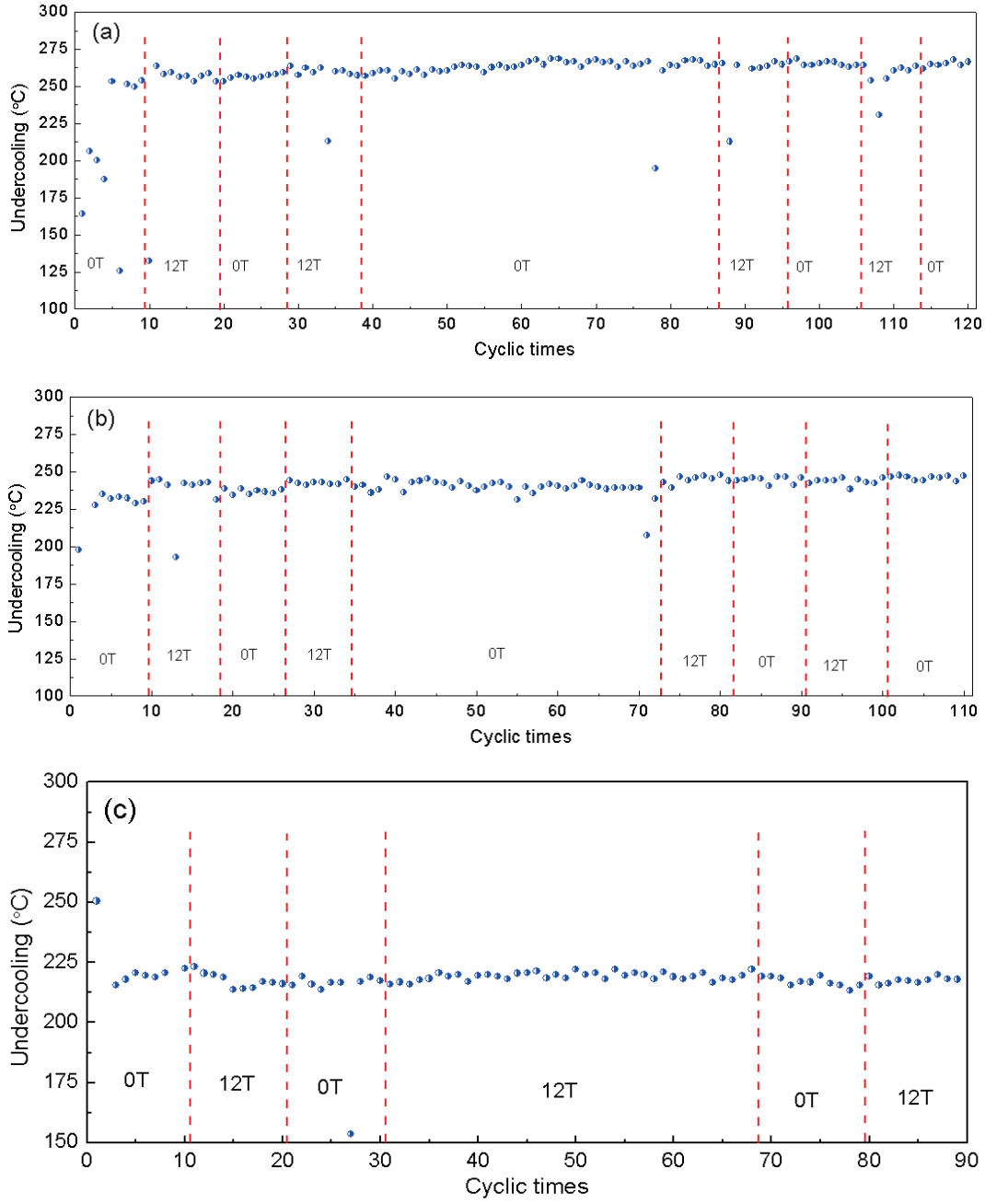

Fig 4-6 Undercooling of Co-Sn alloys at different cycling heating times under different fields. (a)$Co_{79.5}Sn_{20.5}$, (b)$Co_{76}Sn_{24}$ and (c) $Co_{78}Sn_{22}$

$$\Delta G_M \approx -x\int_0^{H_{ex}} \mu_0 M^{S_{\alpha Co}} dH_{ex} \tag{4-7}$$

Calculated by the parameters in Table 4-3, $\Delta G_M(\alpha Co)$=-23J/mol. Compared with

chemical Gibbs free energy ΔG_V=3041J/mol, ΔG_M is so small that its effect on the thermodynamics of nucleation can be neglected. The Hartmann number, *Ha*, calculated for $Co_{79.5}Sn_{20.5}$ is 78, which is much more smaller than the value of Cu in 12T magnetic field, indicating the field does have some effects on the suppression of convection flow, however, the effect is not so strong for avoiding nucleation.

Unlike Co, undercooled Co-Sn melt is in a paramagnetic state, the application of magnetic field cannot make the melt strongly magnetized. The melt is slightly elongated along the direction of the field due to demagnetizing effect, but compared with Co, it's effect on promoting nucleation is still very weak. So the undercooling of Co-Sn alloys is not affected by the external magnetic field, even it is very strong.

4.2 Effect of magnetic field on the recalescence process

The Curie temperature of metallic materials is below their liquid line temperature, thus the magnetic state is constrained in solid state. The atomic movement in solid materials is strictly restricted, and long range magnetic ordering has been proved to exist in liquid alloys, however, until now there are only a few experimental results referring to this topic.

As we have discussed above, magnetic field has no obvious effect on the undercooling of pure Co and Co-Sn binary alloys. The αCo phase precipitates after large undercooling is in ferromagnetic state, and its solidification process will be strongly influenced by the magnetic field. In this section, we have investigated the effect of ferromagnetic phase transition on the recalescence process in magnetic field.

4.2.1 Effect of magnetic field on the recalescence of deeply undercooled Co

When the undercooled melt approaches the nucleation temperature, recalescence happens combined by latent heat release due to rapid solidification. Recalescence accompanies the whole solidification process and determines the volume fraction of the solid phase. T_R (Fig 4-3) is characterized as the maximum temperature after recalescence, and we define $\Delta T^{R\text{-}N}=T_R-T_N$, to describe the recalescence extent of undercooled melt during non-equilibrium solidification, the larger the recalescence extent, the larger the heat releases and temperature increases after nucleation. Strong

magnetic field has no effect on the undercooling of pure Co undercooled melt (marked as '■' in Fig 4-5), which means the nucleation temperature is not affected by magnetic field for Co. However, seen from Fig 4-5 (marked as '●' in Fig 4-5), the recalescence extent is obviously influenced by the magnetic field. Without magnetic field, the recalescence extent is 91ºC, and when a 12T static magnetic field is applied, $\Delta T^{R\text{-}N}$ turned to 23ºC. The application of magnetic field leads to 75% decrease of $\Delta T^{R\text{-}N}$. According to the model proposed by YANG [YANG09a, YANG09b], the maximum temperature after recalescence can be calculated based on the conservation of heat flow and solute. During the recalescence process, the solidification turns from non-equilibrium to equilibrium based on the calculation results of Gibbs free energy difference of solid and liquid phase. When a static magnetic field is applied, the magnetic Gibbs free energy can increase the total energy of the system. Then the heat effect at the same nucleation temperature in magnetic field is reduced, and leads to the decrease of the maximum temperature. However, in the present case the low magnetic Gibbs energy can only take very limited effect on the energy of whole system. Thus abrupt decrease of heat release during recalescence should attribute to other factors. One possible reason is that the growth of grain or dendrites is restricted by the field once the ferromagnetic particles are precipitated. Thus the amount of the temperature increase is weakened because the latent heat release speed is delayed by magnetic field. But as we can see from Fig 4-5, the suppressing effect of the recalescence extent is obvious and stable by the external magnetic field, there must exist an underlying mechanism which can account for the temperature decrease during recalescence.

4.2.2 Effect of magnetic field on the recalescence of deeply undercooled Co-Sn

Fig 4-7 is the curves of ΔT and $\Delta T^{R\text{-}N}$ as a function of cyclic heating times for $Co_{79.5}Sn_{20.5}$ alloy in different magnetic fields. The undercooling is stable regardless of the external magnetic field (Fig 4-7(a)), while the recalescence extent is obviously changed when the field intensity is changed. The mean undercooling is close to 270ºC, which is larger than the value (244ºC) reported by Wei et al [WEI93], indicating the excellent purifying effect of fluxed glass in the present equipment. The effective nucleation sites are removed to the upper limit for fluxing method, and the diversity keeps very little with very good reproducibility during the cyclic process. Under this

condition, the undercooled melt is in a relative stable state, and the effect of the fluxing glass on the nucleation process in magnetic field can be neglected.

For the recalescence extent variations in magnetic field, it can be seen in Fig 4-7(b) that, the field intensity has very limited effect when the intensity is below 4T, and $\Delta T^{R\text{-}N}$ fluctuates around 204ºC. With the increasing field intensity, $\Delta T^{R\text{-}N}$ decreases rapidly. The mean value in 8T is 180 ºC, and in 12T,$\Delta T^{R\text{-}N}$=163ºC which is nearly 40 ºC lower than the mean value without magnetic field. Afterwards, the mean recalescence extent increases again when the field intensity is changed to lower value.

The chemical Gibbs free energy increases with the increasing undercooling of the undercooled melt. When the melt solidifies at the maximum undercooling, latent heat is released rapidly due to the fast crystallization speed. For $Co_{79.5}Sn_{20.5}$ alloy, its maximum undercooling is not affected by magnetic field, which means the latent heat accumulated before solidification is the same, and the heat release/temperature increase effect should be the same if magnetic field has no effect on the recalescence process. In 12T magnetic field, recalescence extent is reduced by 20%, indicating the magnetic field has imposed strong effect on the solidification process, especially for the ferromagnetic phase formed during crystallization (For paramagnetic pure Cu, the recalescence extent is affected only by undercooling irrespective of field intensity). The solidification process of deeply undercooled Co-Sn melt is determined to be less than 60 ms (from T_N to T_R), thus the process for the rapid nucleation and growth combined with latent heat release can be treated as adiabatic. When a magnetic field is applied, the decrease of $\Delta T^{R\text{-}N}$ indicates the heat release during recalescence is reduced which leads to the lowered maximum recalescence temperature, T_R.

The microstructure formed at undercoolings above 200ºC consists of non-regular αCo and βCo_3Sn_2 eutectics for $Co_{79.5}Sn_{20.5}$ alloy. The heat enthalpy for αCo and βCo_3Sn_2 are different, which means the heat release will be different when the volume fraction of these two phases are different. The magnetic properties for αCo and βCo_3Sn_2 are quite different, and in the same magnetic field, the magnetization of αCo is much larger than βCo_3Sn_2 since it is in ferromagnetic state. Fig 4-8 is the microstructure (the dark phase is αCo, and the white phase is βCo_3Sn_2) of $Co_{79.5}Sn_{20.5}$ alloy solidified at the undercooling of 267ºC in different magnetic fields. The volume fraction of αCo phase based on image analysis is 51±2%, 59.5±2%, respectively, indicating external magnetic field can enhance the precipitation of ferromagnetic αCo phase. The formation enthalpy of βCo_3Sn_2 (-16.0kJ/mol [NIES88]) indicating much

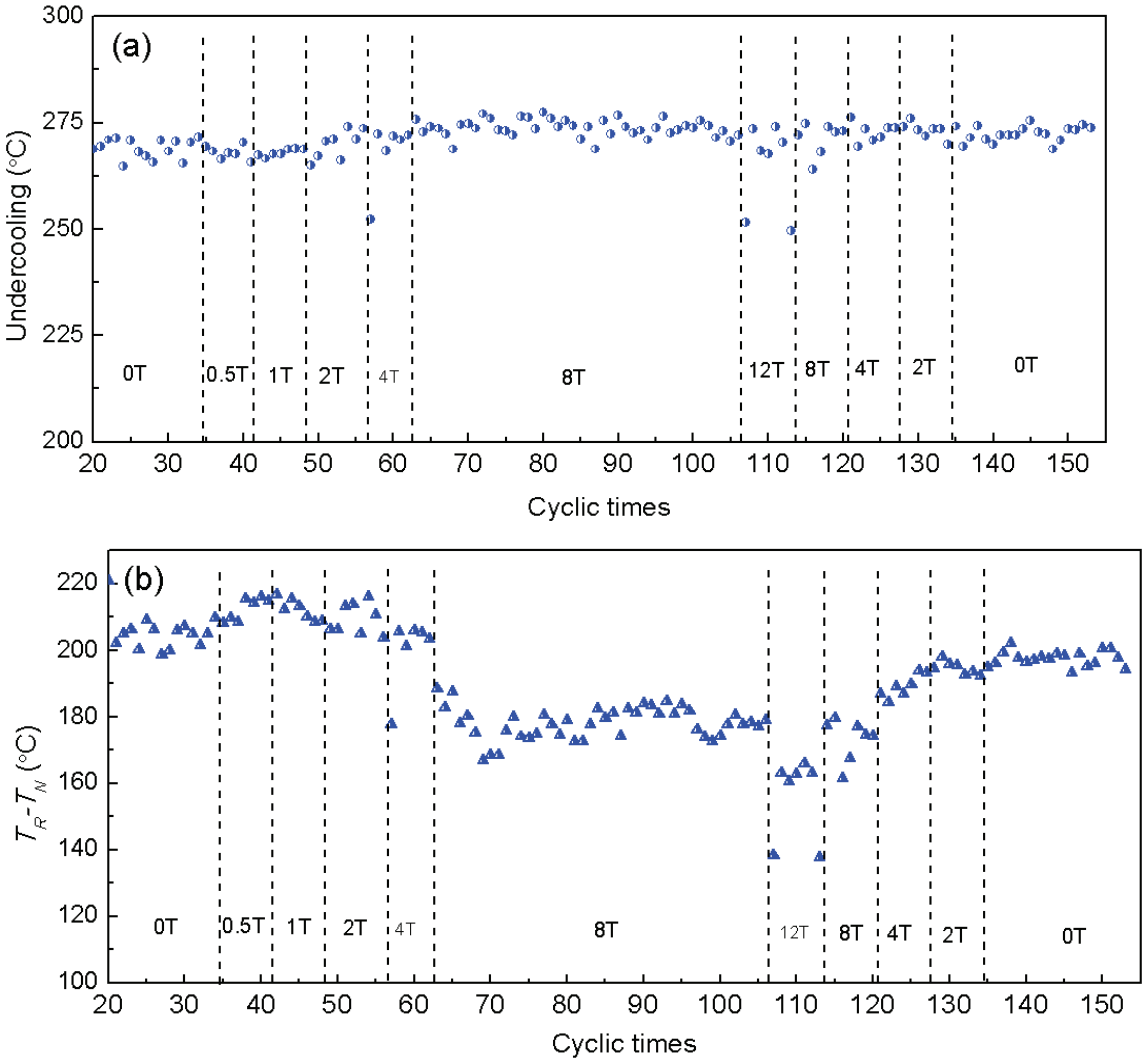

Fig 4-7 (a) Undercooling and (b) recalescence extent of $Co_{79.5}Sn_{20.5}$ alloy as a function of cyclic heating times solidified under different magnetic field

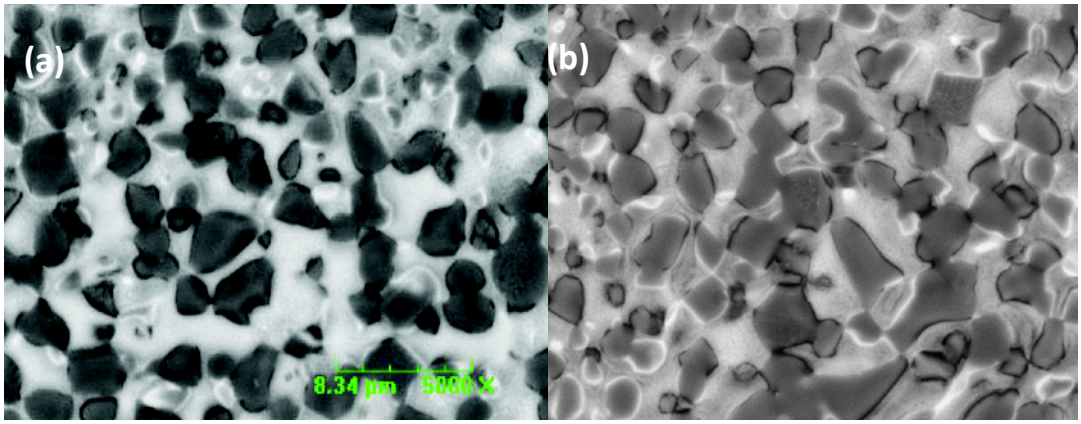

Fig 4-8 Microstructure of $Co_{79.5}Sn_{20.5}$ alloy solidified under different magnetic fields: (a) 0T, $\Delta T^{R\text{-}N}$=202ºC and (b)12T, $\Delta T^{R\text{-}N}$=161 ºC. The undercooling is ΔT=267 ºC

higher heat will release than αCo phase (-11.6kJ/mol[LIU04]), and larger volume fraction of αCo means less βCo_3Sn_2 and less latent heat release. Thus, the external

field causes the reduction of recalescence extent by reducing the volume fraction of βCo_3Sn_2 phase.

4.2.3 The recalescence behavior of Co-Sn alloys with different compositions in strong magnetic field

With the increasing Sn content in Co-Sn near eutectic alloys, the volume fraction of ferromagnetic αCo phase decreases, indicating the effect of magnetic field on recalescence process will be influenced by its composition. Fig 4-9 is $\Delta T^{R\text{-}N}$ as a function of cyclic heating times of $Co_{76}Sn_{24}$ and $Co_{72}Sn_{28}$ alloys in 0 and 12T magnetic field. It can be seen that, the same as $Co_{79.5}Sn_{20.5}$ alloy, the magnetic field typically affects the recalescence extent. Without magnetic field, $\Delta T^{R\text{-}N}$ for $Co_{76}Sn_{24}$ is 150ºC and decreases to 115ºC when undercooled in 12T magnetic field. With the increasing cyclic heating times, the effect of the magnetic field on $\Delta T^{R\text{-}N}$ is weakened, finally stable at 100ºC. As for $Co_{72}Sn_{28}$ alloy, the effect of magnetic field on $\Delta T^{R\text{-}N}$ is much smaller. When a 12T magnetic field is applied, the stable undercooling is 5ºC lowered. Thus we can conclude that with the increasing Sn content or decreasing Co, the magnetic effect on the recalescence behavior becomes smaller. Fig 4-10 is the solidified microstructure of $Co_{72}Sn_{28}$ in 0 and 12T magnetic field. The same as the structure obtained in Fig 4-8, the application of magnetic field increase the volume fraction of the ferromagnetic αCo phase, leading to the decreased heat release during recalescence.

4.3 Effect of gradient magnetic field on the undercoolability

4.3.1 Effect of gradient magnetic field on the undercoolability of Cu

Fig 4-11 illustrates the undercooling and recalescence extent as a function of cyclic heating times of pure Cu in 0 and 9294Gauss/cm (field intensity at sample position is 6.23T) gradient magnetic field. Different from the results obtained in static magnetic field (shown in Fig 4-2), the undercooling of pure Cu in gradient magnetic field has the following characteristics. Firstly, the application of gradient magnetic

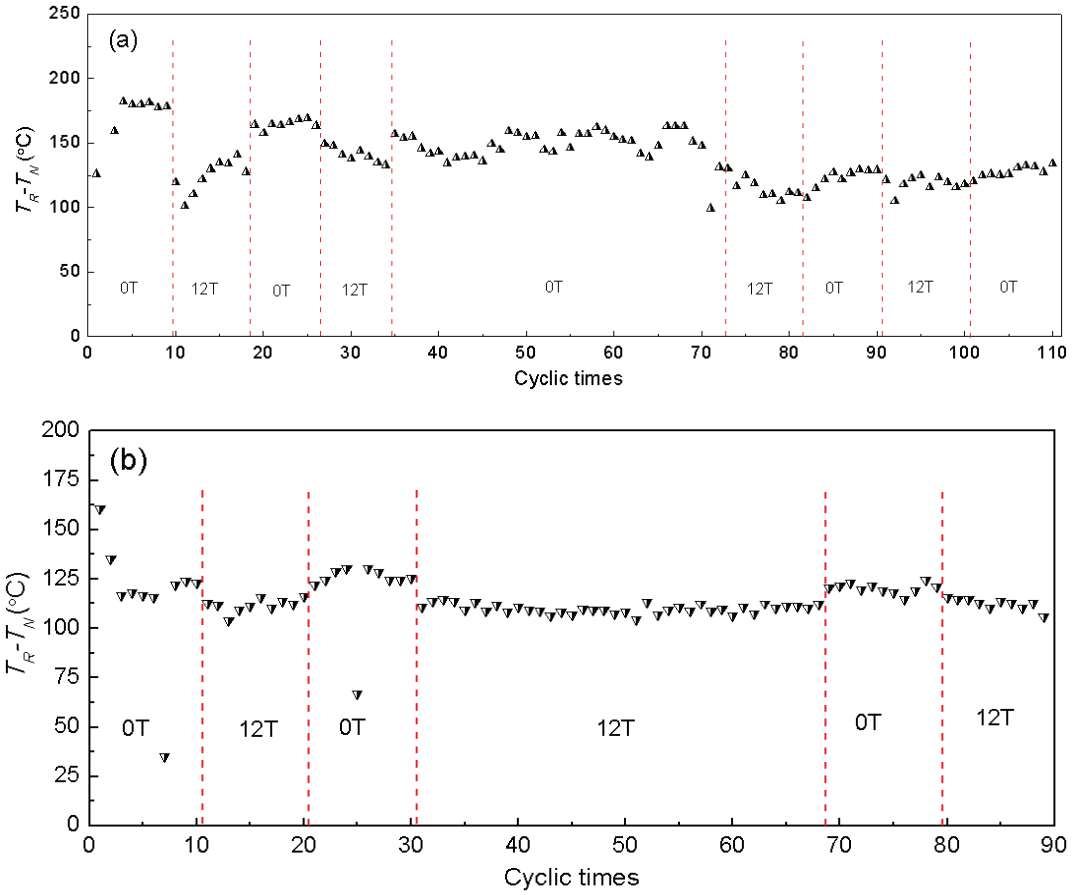

Fig 4-9 $\Delta T^{R\text{-}N}$ vs cycling times of (a)$Co_{76}Sn_{24}$ and (b)$Co_{72}Sn_{28}$ alloys in different magnetic fields.

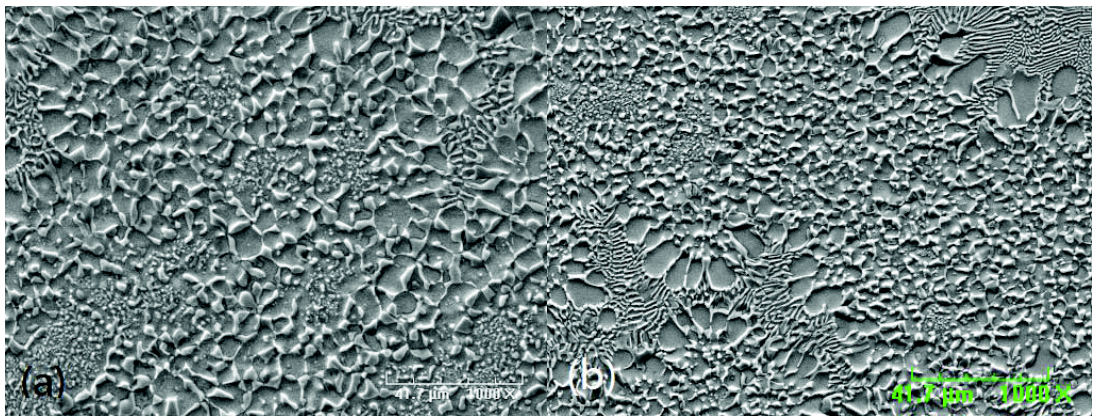

Fig 4-10 Microstructure of undercooled $Co_{72}Sn_{28}$ alloys solidified in (a) 0T, ΔT_a=223℃, $\Delta T^{R\text{-}N}$=120℃ and (b) 12T, ΔT_b=215℃, $\Delta T^{R\text{-}N}$=107℃.

field can obviously increase the stability of the undercooling. Without magnetic field, there is large diversity for the undercooling. Secondly, there is no uniform trend to describe the gradient field effect on the undercooling of Cu. When the gradient field is firstly applied, there are no changes for the undercooling, and the undercooling keeps stable even when the field is removed. When the gradient field is applied again at the 23rd cycle, the undercooling largely increases and a maximum value, 275ºC, is

obtained at the 32nd cycle. Then the undercooling becomes rather unstable when the gradient field is applied and there is no regular law to describe the variations. In static magnetic field, the undercooling can be increased due to the suppression of the convection in the melt until the melt is in a relatively stable state. And the final stable undercooling is not affected by the field intensity and heating times. When a gradient field is applied, the field can directly impose a magnetic force to the undercooled melt. Pure Cu is a diamagnetic material, and the magnetic force exerted on the sample is reversing the direction of gravity. The fluxing glass, mainly B_2O_3, also will move by the force exerted by the gradient field, leading to contact variation between fluxing glass and Cu melt. All the above factors can change the purifying effect of glass slag, thus causing the non-regular undercooling variations of Cu in gradient magnetic field.

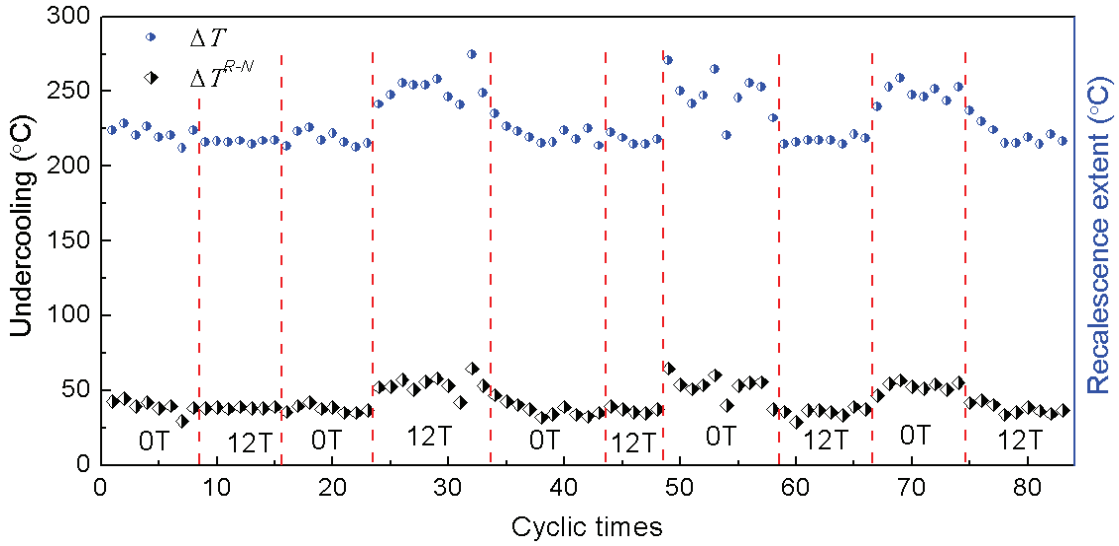

Fig 4-11 Undercooling and recalescence extent of Cu at different cycling times in different magnetic gradient fields, 12T means the maximum field in the magnetic and the field gradient and intensity in the sample position are 6.23T and 9294Gauss/cm, respectively.

4.3.2 Effect of gradient magnetic field on the undercoolability of Co

Fig 4-12 illustrates the undercooling and recalescence extent as a function of cyclic heating times of pure Co in 0 and 9294Gauss/cm (field intensity at sample position is 6.23T) gradient magnetic field. It can be seen that the same as in static magnetic field, the undercooling of pure Co is not affected by gradient magnetic field. However, different from that in static magnetic field, the recalescence extent of pure Co is also not affected by gradient magnetic field. According to the analysis in

Chapter 3, in gradient magnetic field, lotus like morphology with peaks and valleys are formed when pure Co was solidified, indicating the melt is in a rather irregular shape before its solidification and this maybe one of the reason that can cause the difference.

In 9294Gauss/cm gradient magnetic field, the field intensity is 6.23T. Compared with the data in Fig 4-5 which is obtained in 12T static magnetic field, the field has much smaller effect on the sample thermodynamically. That is to say, the field has less effect on avoiding the heterogeneous nucleation in the melt. And when the undercooling melt approaches the Curie point, the increased magnetization causes the increase of static magnetic energy and leads to the severe morphology change. And the sharps formed at the tips of this unique morphology can act as the nucleation sites. So thermodynamically the gradient field can avoid the nucleation while the complicated shape can cause heterogeneous nucleation in the melt.

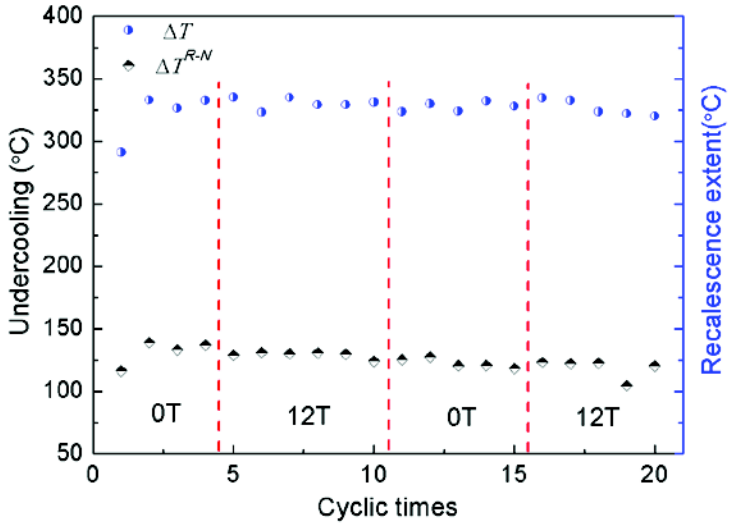

Fig 4-12 Undercooling and recalescence extent of Co at different cycling times in different magnetic gradient fields. 12T means the maximum field in the magnetic and the field gradient and intensity in the sample position are 6.23T and 9294Gauss/cm, respectively

4.3.3 Effect of gradient magnetic field on the undercoolability of Co-Sn

Fig 4-13 illustrates the undercooling and recalescence extent as a function of cyclic heating times of Co-Sn alloys in 0 and 9294Gauss/cm gradient magnetic field. The recalescence behaviors of Co-Sn alloys are obviously affected by the external magnetic field and the undercooling decreases while the recalescence extent increases

when the external gradient field is applied. The variations for different alloys are shown in Table 4-4.

For near eutectic Co-Sn alloy, the volume fraction of ferromagnetic αCo phase decreases with the increasing Sn content. As discussed before, the ferromagnetic phase can play an important role during the recalescence process. In static magnetic field, the undercooling keeps unchanged while in gradient magnetic field, the mean undercooling decreases 23ºC for $Co_{79.5}Sn_{20.5}$. According to the magnetization measurement, $Co_{79.5}Sn_{20.5}$ undercooled melt is still in paramagnetic state, however, the undercooled melt still bears a magnetic force in strong gradient magnetic field which can change the shape of the sample. Fig 4-14 shows the solidified picture of $Co_{79.5}Sn_{20.5}$ alloy in 9294Gauss/cm gradient magnetic field, it can be seen that the

Table 4-4 Undercooling and recalescence extent of Co-Sn alloys under 0 and 9294Gauss/cm gradient field

Alloy Composition	$Co_{79.5}Sn_{20.5}$		$Co_{76}Sn_{24}$		$Co_{72}Sn_{28}$	
Gradient field (Gauss/cm)	0	9294	0	9294	0	9294
ΔT (℃)	265	242	246	232	222	215
$\Delta T^{R\text{-}N}$ (℃)	189	193	177	194	133	148

sample is compressed to a pie shape. Thermodynamically, magnetic field has very limited effect on the variation of the undercooling of Co-Sn alloys, no matter in static or gradient magnetic field. Here, for Co-Sn alloys, the paramagnetic state of the sample let the field exert a compressing force along the field direction while the diamagnetic fluxing glass is levitated at the same gradient field, which means the purifying effect of the glass slag on the undercooled melt is weakened. The increase of the recalescence extent should be the same mechanism as that in static magnetic field, which is attributed to the volume fraction variations caused by the external field.

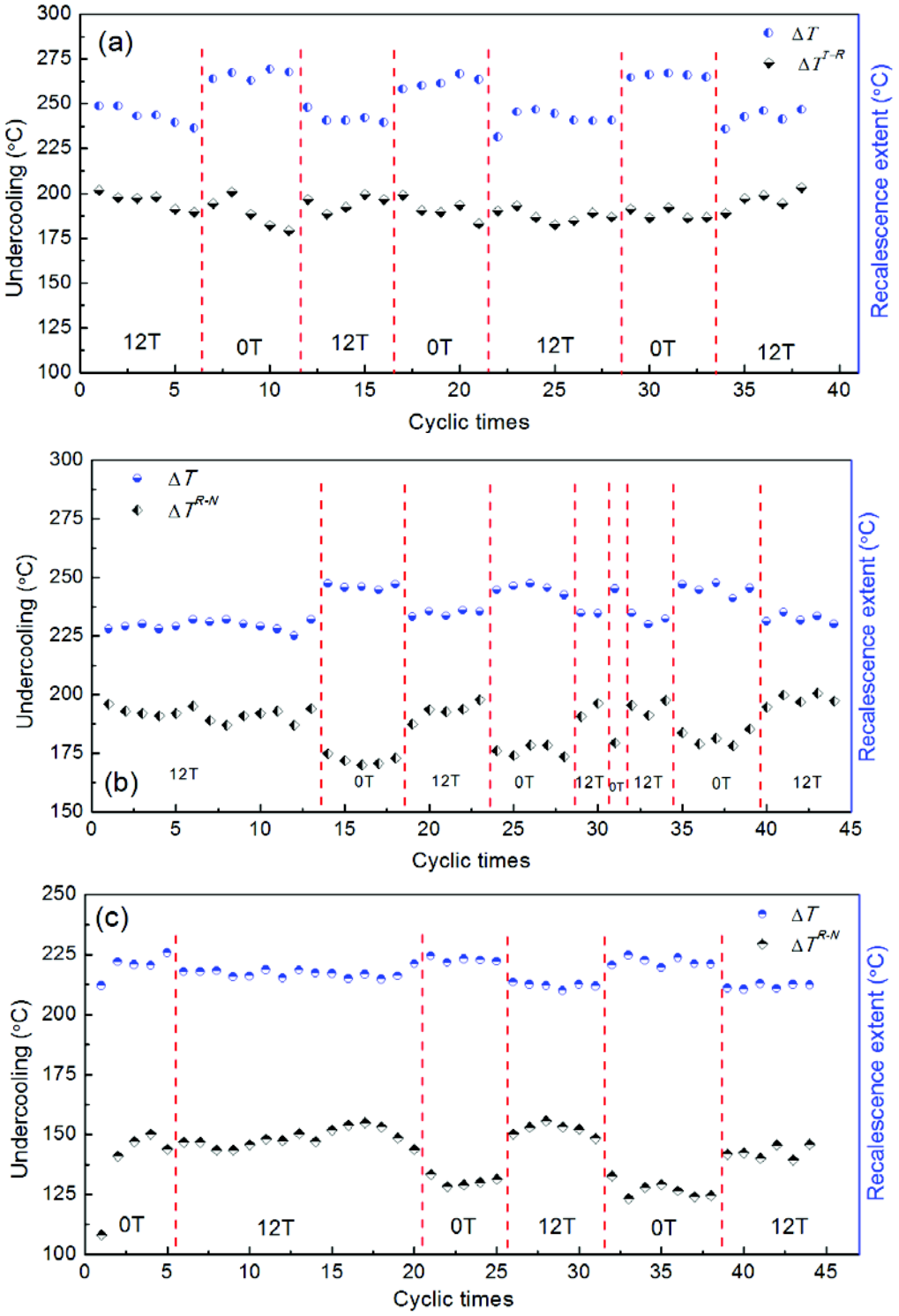

Fig 4-13 Undercooling and recalescence extent of Co-Sn alloys at different cyclic heating times in different gradient magnetic fields (a)$Co_{79.5}Sn_{20.5}$, (b) $Co_{76}Sn_{24}$, (c) $Co_{72}Sn_{28.}$ 12T means the maximum field in the magnetic and the field gradient and intensity in the sample position are 6.23T and 9294Gauss/cm, respectively

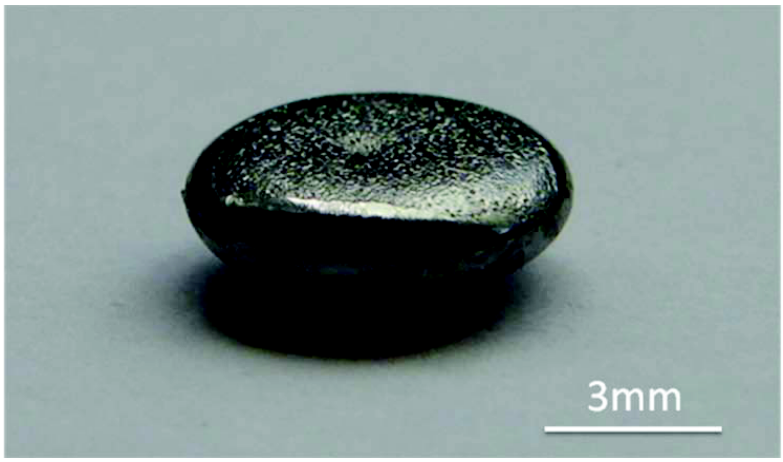

Fig 4-14 Image of $Co_{79.5}Sn_{20.5}$ alloy solidified under 9294Gauss/cm gradient field.

4.4 Mechanism of magnetic field on the nucleation in undercooled melt

Based on the above results and discussions, it can be seen that the strong static/gradient magnetic field can exert different affects for different metals and alloys. For paramagnetic metals and alloys, strong magnetic field can suppress the convection flow in the undercooled melt, thus enhance the undercoolability. And for alloys containing ferromagnetic phase after solidification, the undercooling is affected by the Gibbs free energy difference during solidification and the nature of the magnetic field (e.g. static, gradient) and intensity also can strongly affect the solidification process.

(1) Thermodynamic effect on the undercooled melt in magnetic field

Strong magnetic field can directly change the thermodynamic state of materials, and even the phase transition temperature can be changed by magnetic field due to magnetic susceptibility difference of different phases. When a phase transition process contains a ferromagnetic phase, magnetic field in the order of 10T can obviously change the transition temperature. Depending on the magnetic properties of the melt, the effect of magnetic field on the thermodynamic state of undercooled melt can be classified as follows.

Firstly, the magnetization of melt is larger than the solidified solid phase. In this case, $\Delta\chi^{S-L}<0$, the application of magnetic field can reduce the energy of the system, and enhance the thermodynamic stability of the melt.

Secondly, when the undercooled melt is in paramagnetic state, $\Delta\chi^{S-L}>0$, the application of magnetic field can increase the energy of whole system, which can

promote the nucleation process and reduce the thermal stability of the melt.

Finally, for paramagnetic and diamagnetic materials, since the magnetic susceptibility difference between the solid and liquid phase is very small, magnetic field can affect the undercooling behavior, but the mean undercooling of the stable undercooled melt is nearly unchanged.

(2) Physical effect of magnetic field on the nucleation of undercooled melt

Two main factors are considered here, the suppression of the convection flow in the melt and the movement of glass slag, sample and morphology changes by external magnetic field on purifying effect for heterogeneous nucleation. Magnetic field can control the convection in the melt, and for different metals and alloy, the difference in electric conductivity, magnetic susceptibility and viscosity can affect the suppression effect of magnetic field on convection flow. Depending on the nature of the glass slag and undercooled melt, external field especially for gradient magnetic field can exert magnetic force directly on the sample which can change the purifying effect of glass slag on the removing of the impurities in the melt which can cause heterogeneous nucleation.

4.5 Summary

(1)Strong magnetic field has a strong effect on the nucleation temperature of undercooled melt, and different metals and alloys show different behaviors in 12T magnetic field. For pure Cu, magnetic field can enhance the undercoolability at the beginning, and when the undercooled melt is in a stable state, the magnetic field has no typical effect on its undercooling.

(2)The undercooling of pure Co is not affected by static magnetic field, but its recalescence extent is strongly depressed by static magnetic field. When there is no magnetic field, $\Delta T^{R\text{-}N}\approx$91ºC, and it decreases to 23ºC when solidified in 12T magnetic field.

(3)The undercooling of Co-Sn near eutectic alloys is not affected by static magnetic field, and the recalescence extent decreases when solidified in static magnetic field, and the effect increases with the increasing Co content.

(4)The undercooling of pure Cu shows no stable relation with gradient magnetic field. In gradient magnetic field, the undercooling and recalescence extent of pure Co keep unchanged. Gradient magnetic field can depress the undercooling and enhance the recalescence extent of Co-Sn alloys.

CHAPTER 5 SOLIDIFIED MICROSTRUCTURE OF UNDERCOOLED CO-SN ALLOY IN STRONG MAGNETIC FIELD

Solidification of deeply undercooled melt is an extreme process which is far from equilibrium state. When receiving certain thermodynamic undercooling, rapid solidification known as recalescence happens. Different from equilibrium solidification process, the heat and mass transportation are intrinsically different for non-equilibrium process, and the solidified phases, morphology and distribution, size of the phase are always varies with the undercooling.

According to previous investigation, the application of strong magnetic field can affect the undercoolability and recalescence process of undercooled melt. Also, the magnetization changes with the undercooling. Thus, the magnetic field should also have strong effect on the solidified microstructure. In this chapter, we will systematically investigate the solidification behaviors of Co-Sn alloys in strong magnetic field.

5.1 Cooling curve and solidified microstructure of undercooled Co-Sn eutectic alloys

5.1.1 Cooling curve

According to the phase diagram of binary Co-Sn alloy [OKAM06] (shown in Fig 2-6) the eutectic composition is $Co_{79.5}Sn_{20.5}$. However, some recent research results [LIU09, LIU11a] show that there are still lots of primary αCo phase precipitated at this composition, indicating it is still a hypoeutectic composition, and the eutectic point determined is close to $Co_{76}Sn_{24}$.

Fig 5-1 is the typical solidification temperature curve of hypoeutectic $Co_{79.5}Sn_{20.5}$ alloy. Two recalescence peaks are found for the alloy solidified at low undercoolings (Fig 5-1(a)). The first one (T_{N1}) is the recalescence representing the precipitation of αCo phase, and the second one (T_{N2}) is the solidification of eutectic phase.

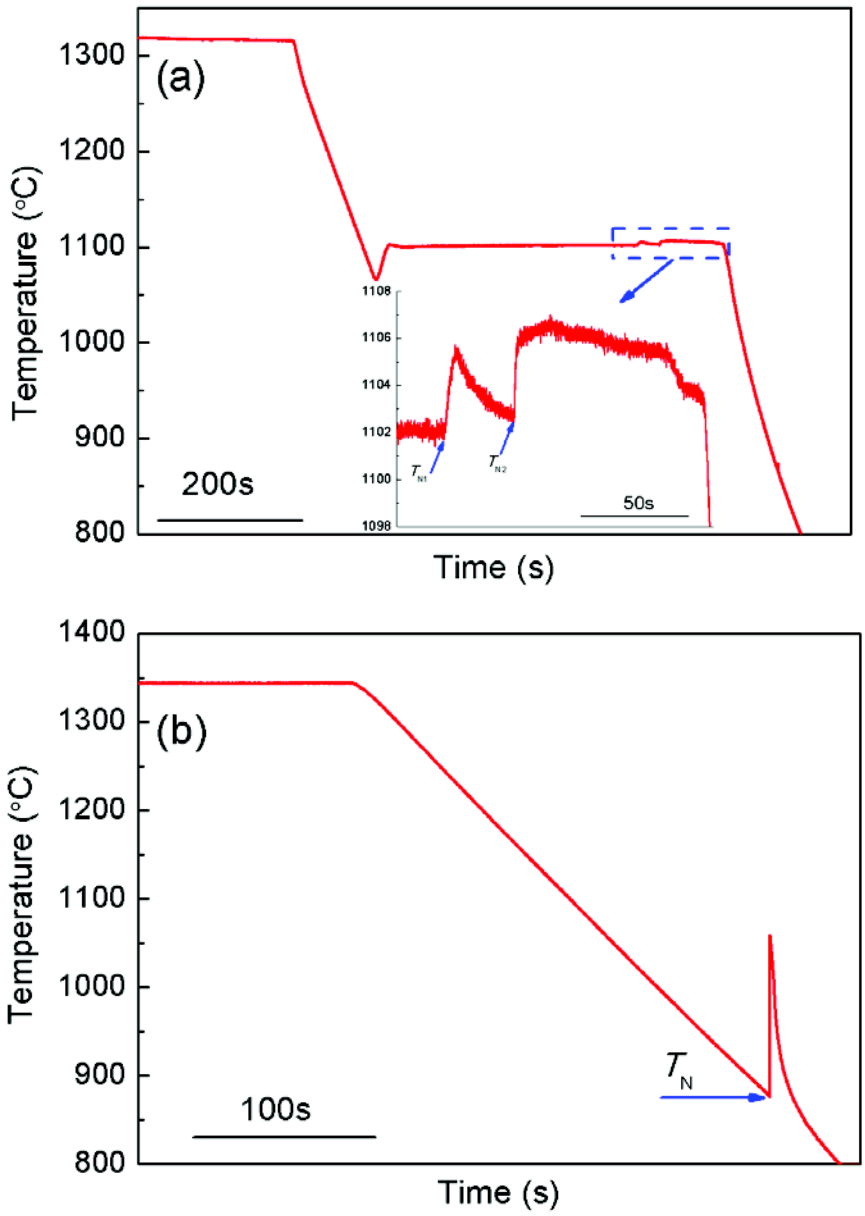

Fig 5-1 Typical solidification curves of Co-Sn alloy solidified under strong magnetic field. (a) Specific undercooling achieved by holding at certain temperature below melting point. (b) Natural cooling curve measured at certain cooling rate

The sharp peak of the first recalescence curve indicates that the nucleation and growth of primary αCo phase is relatively fast while the flat second peak shows the eutectic formation process is very slow due to the temperature increase caused by latent heat release. At large undercoolings, shown in Fig 5-1(b), one strong recalescence is deteced, showing the fast solidification process.

The solidification temperature curves of near eutectic $Co_{76}Sn_{24}$ and hypereutectic $Co_{72}Sn_{28}$ alloys are the same as $Co_{79.5}Sn_{20.5}$ alloy at large undercoolings (Fig 5-1(b)), and the recalescence is composed of a sharp recalescence peak. The temperature

profiles of $Co_{76}Sn_{24}$ and $Co_{72}Sn_{28}$ alloys show only one recalescence peak, as it is shown in Fig 5-2. For $Co_{76}Sn_{24}$ alloy, the composition is close to the eutectic point, thus there is no obvious primary phase formed in the solidification process and there

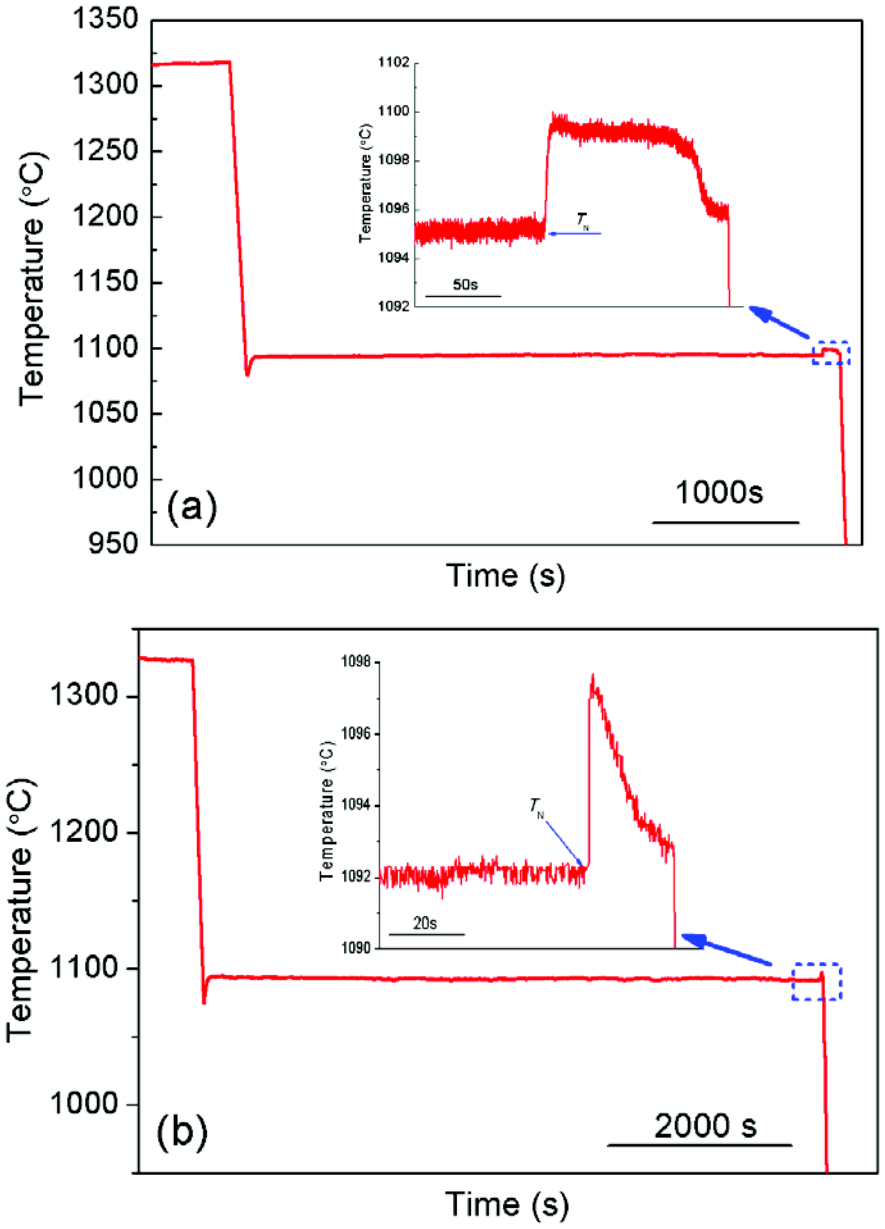

Fig 5-2 Typical solidification curves of Co-Sn alloys, (a) $Co_{76}Sn_{24}$ and (b) $Co_{72}Sn_{28}$

is only one peak denoting the formation of eutectics. But for $Co_{72}Sn_{28}$ alloys, before the formation of eutectic phase, βCo_3Sn_2 phase will pre-precipitate first, however, as it can be seen in Fig 5-2(b) there is only one recalescence peak, indicating the formation of primary βCo_3Sn_2 phase and eutectic phase are nearly at the same time.

When the undercooled alloys are solidified in high magnetic field, according to the results in former chapters, the nucleation and maximum recalescence temperature

can be affected by the application of field. As it was shown in the solidification curves, a typical characteristic was that the shape of the recalescence peak was unchanged while the maximum recalescence peak temperature was altered.

5.1.2 Solidified microstructure

The microstructure of the eutectic phase in Co-Sn binary alloy is αCo and βCo_3Sn_2, and the equilibrium microstructure of Co-Sn hypoeutectic alloys after solidification is primary αCo and regular (αCo+βCo_3Sn_2) eutectics (shown in Fig 5-3(a)). As for Co-Sn hypereutectic alloy, the equilibrium microstructure is βCo_3Sn_2 and regular (αCo+βCo_3Sn_2) eutectics (shown in Fig 5-3(b)).

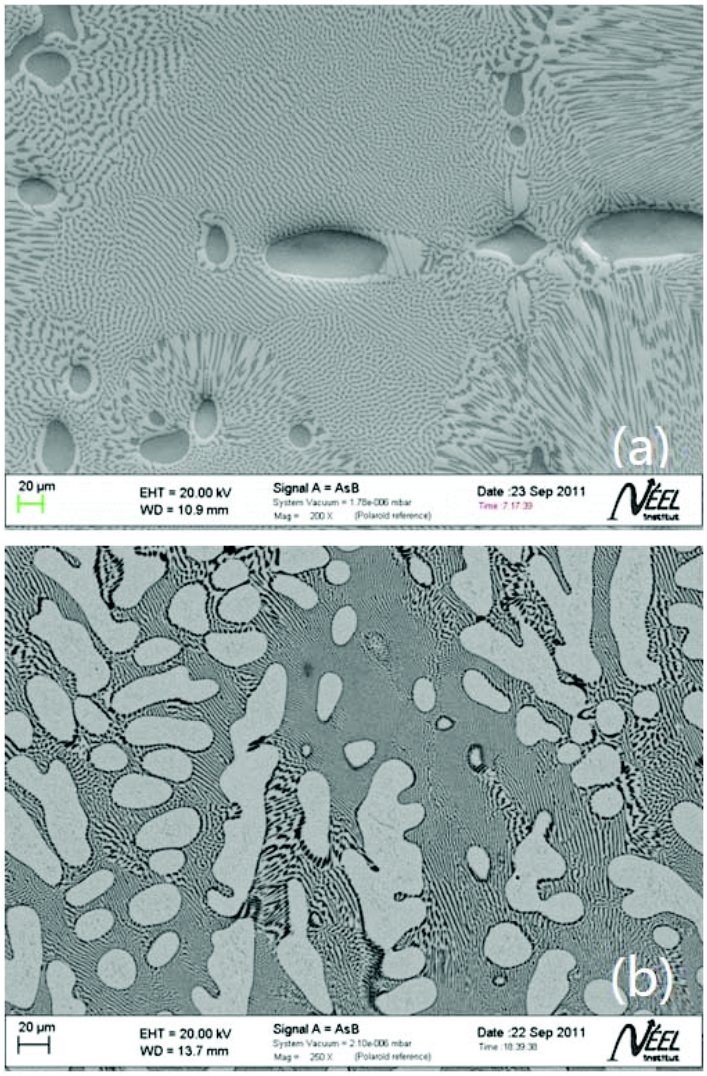

Fig 5-3 Solidified microstructures of Co-Sn alloys, (a) $Co_{76}Sn_{24}$ and (b) $Co_{72}Sn_{28}$. The black phase is primary αCo and the white phase is βCo_3Sn_2.

After Co-Sn alloys solidified, the primary αCo (FCC) phase and βCo_3Sn_2 (HCP) phase undergoes solid phase transitions at lower temperatures, and phases with different crystal structure, εCo (HCP) and αCo_3Sn_2 are formed, respectively. In this chapter, we only discuss about αCo and βCo_3Sn_2 phase, and the formation of εCo and αCo_3Sn_2 have no effect on the morphology and volume fraction of αCo and βCo_3Sn_2 phases.

5.2 Microstructure evolution of undercooled Co-Sn eutectic alloys under magnetic field

The undercooling of undercooled melt determines the solidified microstructure of metals and alloys. When the melt solidifies in strong magnetic field, the final microstructure will be obviously affected by the field, especially when there is a ferromagnetic phase. Compared with other alloys, the Curie temperature of Co alloys can be up to 1121ºC. Due to the difference between the melting point (T_m) and Curie temperature (T_C), $\Delta T=T_m-T_C$, is smaller than other alloy systems, Co-based alloys are the most promising alloys which can be undercooled below their Curie point. The Curie temperature of Co-Sn near eutectic alloys measured is among 1050-1090 ºC, and only a small undercooling (60 ºC below its melting point, 1110 ºC) is required for undercool the alloy below the curie temperature of the solid phase. Here, three alloy composition $Co_{79.5}Sn_{2.5}$, $Co_{76}Sn_{24}$, and $Co_{72}Sn_{28}$ have been studied, and the microstructures evolution with and without magnetic field at different undercoolings are discussed.

5.2.1 Co-Sn hypoeutectic alloy

5.2.1.1 The microstructure evolution of $Co_{79.5}Sn_{20.5}$ alloy without magnetic field

Fig 5-4 is the optical microstructures of $Co_{79.5}Sn_{20.5}$ alloys solidified at different undercoolings. The white phase in the figure is αCo, and the other phase which is etched (by etchant shown in Chapter 2) is βCo_3Sn_2 phase. With the increasing undercooling, as it can be seen from Fig 5-4, the microstructure evolution undergoes

the following processes: At low undercoolings (<40ºC), the microstructure of the alloy is primary αCo+lamellar (αCo+βCo_3Sn_2) eutectic phases. The primary αCo phase (shown in Fig 5-4(a)) is in a regular equiaxed dendrites morphology which is a typical microstructure formed by the remelting of dendrites during recalescence. With the increasing undercooling, the precipitation time between primary αCo and eutectics becomes less and finally there is only one recalescence peak. The remelting of dendrites cannot fully complete and the fragmented dendrites are kept after solidification (shown in Fig 5-4(b)). When the undercooling increases again, the volume fraction of primary αCo phase increases (shown in Fig 5-4(c)), and the alloy still consists of αCo+lamellar (αCo+βCo_3Sn_2) eutectic phases. When the undercooling is larger than 100 ºC, the eutectic colony starts to form and the final microstructure of the as solidified alloys is αCo+lamellar (αCo+βCo_3Sn_2) eutectic phases+eutectic colony. During the solidification process, the eutectic colony is formed before or nearly at the same time as the primary αCo phase, and then grow to big freely colony like structure which composes of anomalous (αCo+βCo_3Sn_2) eutectic phases. After αCo dendrites grow from the periphery of the colony, between the dendrites, lamellar eutectic phases (αCo+βCo_3Sn_2) solidify at last (shown in Fig 5-4(d)). When the alloy solidifies at higher undercoolings, the volume fraction of primary αCo decreases, and finally disappears. The volume fraction of anomalous eutectics increase, and finally the whole sample is dominated by anomalous (αCo+βCo_3Sn_2) eutectic phases (shown in Fig 5-4(e)).

5.2.1.2 The microstructure evolution of $Co_{79.5}Sn_{20.5}$ alloy in 12T magnetic field

Fig 5-5 is the microstructure of $Co_{79.5}Sn_{20.5}$ alloy solidified in 12T magnetic field at different undercoolings. Compared with the microstructure formed without magnetic field, two characteristics are shown in the figure. Firstly, primary αCo phase grows along the direction of magnetic field and forms chain like microstructure. Secondly, the characteristic undercoolings for evolution of αCo phase are altered by the magnetic field, and shift to low undercoolings. It can be seen from Fig 5-5(a) that the primary αCo phase is along the direction of magnetic field. The primary αCo phase is the first phase formed in the undercooled melt. During the recalescence process, the growth of solidified αCo phase is affected by the magnetic field. Due to

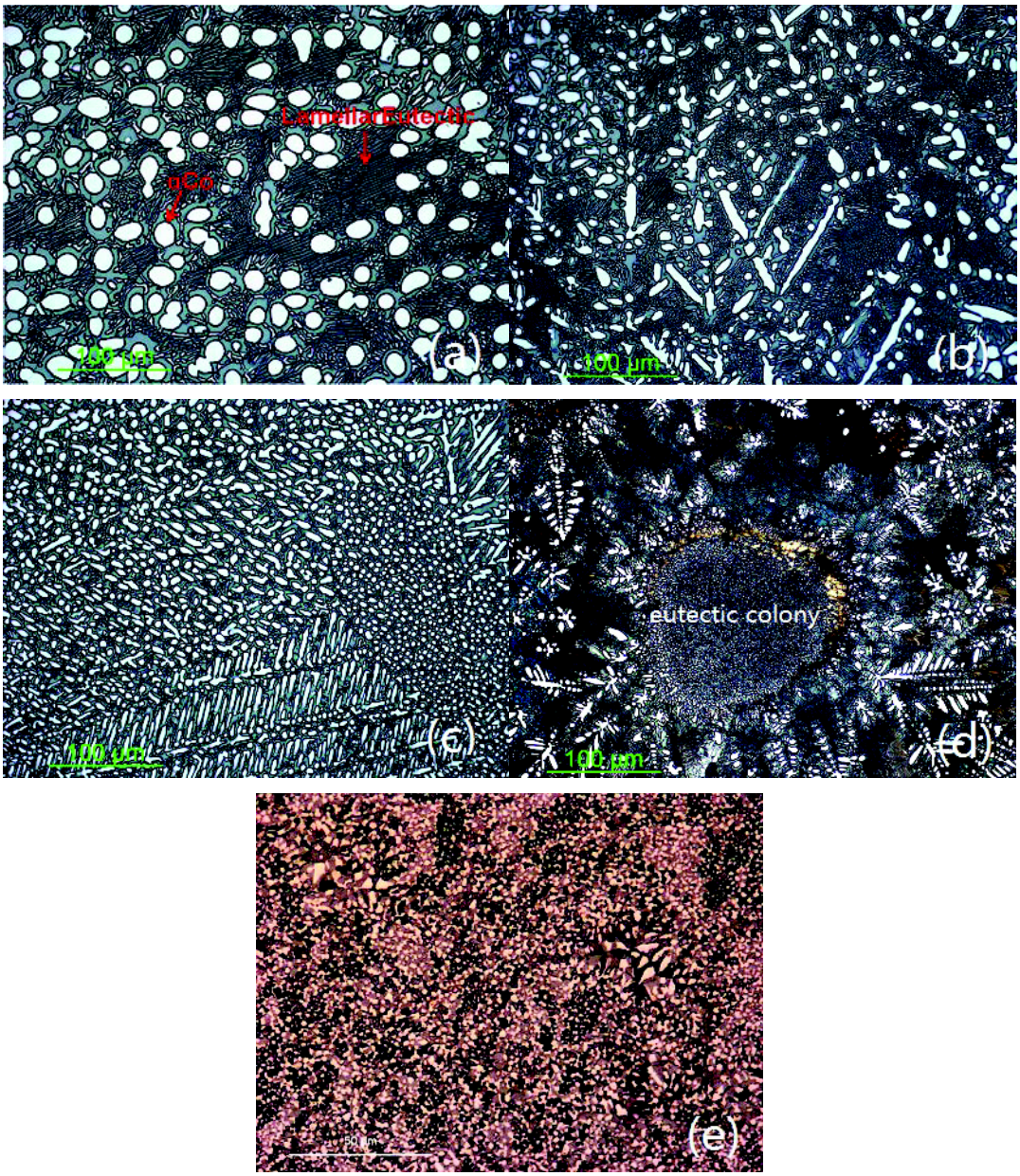

Fig 5-4 Microstructures of $Co_{79.5}Sn_{20.5}$ hypoeutectic alloy solidified at different undercoolings. (a) ΔT=17ºC, (b) ΔT=46ºC, (c) ΔT=77ºC, (d) ΔT=147ºC, (e) ΔT=282ºC.

demagnizing field that depends on shape, the magnetic erengy of the phase is reduced when its shape is elongated along the field line rather than spherical. Also, one can suspect that during growth, atoms or nuclei could be preferentially attracted to the magnetic pole of the ferromagnetic αCo and hence growth is promoted along the field direction. Thus the precipitated αCo will be elongated along the field direction due to the demagnetization effect. When the primary αCo dendrite is fragmented, they can move freely in the remained liquid. And the applied magnetic field can impose directly magnetic force on these dendrites which can force them align along the field direction. Also, fragmented dendrits can stack on each others and form long chains

parallel to the applied field. When the undercooling is larger, the αCo dendrite cannot fully remelt and become much finer. When the undercooling is up to 77ºC, the big anomalous eutectic colony which grows along the direction of magnetic field is observed. At the periphery of the colony, αCo dendrites grow along the field direction. Also, there are many free dendrites grown in the sample. The volume fraction of these free dendrites increases with the increasing undercooling, finally dominates the whole microstructure when the undercooling is up to 200ºC (shown in Fig 5-5(d)).

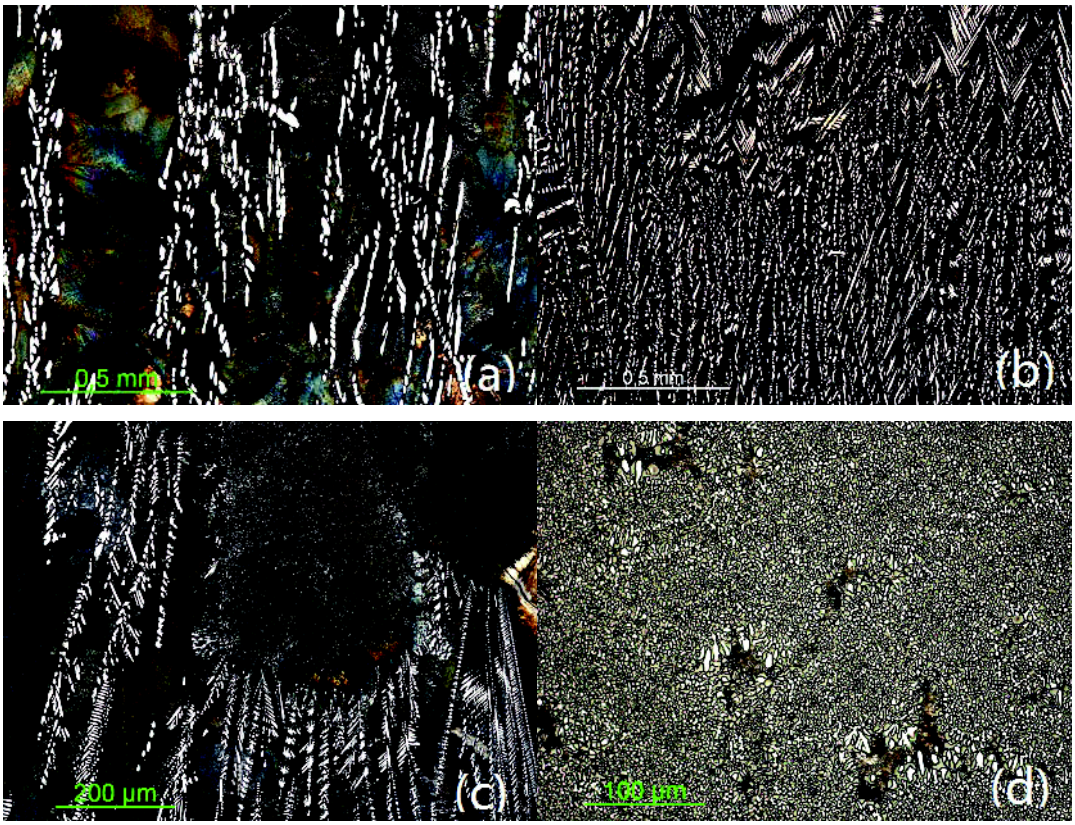

Fig 5-5 Solidified microstructure of undercooled $Co_{79.5}Sn_{20.5}$ alloy under magnetic field with field intensity 12T. (a) ΔT=9℃, (b) ΔT=28℃, (c) ΔT=77℃, (d) ΔT=200℃. The field direction is vertical in the picture.

5.2.1.3 Effect of magnetic field intensity on the microstructure evolution of $Co_{79.5}Sn_{20.5}$ alloy

(1) The primary αCo phase formed in different magnetic field

The ordering clusters are proved to exist in alloy melts. High temperature XRD analysis of $Co_{79.5}Sn_{20.5}$ alloy has found there are two kinds of clusters close to the solidified αCo and βCo_3Sn_2 phase [SUN09]. When $Co_{79.5}Sn_{20.5}$ alloy melt is below the

melting point, the ordering structure in the melt will be strengthened by decreasing temperature. αCo is a ferromagnetic phase which has a much larger magnetization than βCo_3Sn_2 phase in the same magnetic field. When αCo is solidified first in the melt, it is in ferromagnetic state when the temperature is below T_C(S) (ΔT>50ºC). Its high magnetization let its shape and position change by external magnetic field. Fig 5-6 is the microstructure of $Co_{79.5}Sn_{20.5}$ alloy solidified in different magnetic fields at low undercoolings around 10ºC. Without magnetic field, the growth direction of dendrites is controlled by heat flow in the sample, forming the homogenous microstructure in Fig 5-6(a). When 0.5T magnetic field is applied, there are mainly two growth directions for αCo, one is along the direction of magnetic field, and another one should be along the heat flow direction during solidification. When the field intensity increases, αCo finally perfectly grows along the direction of magnetic field.

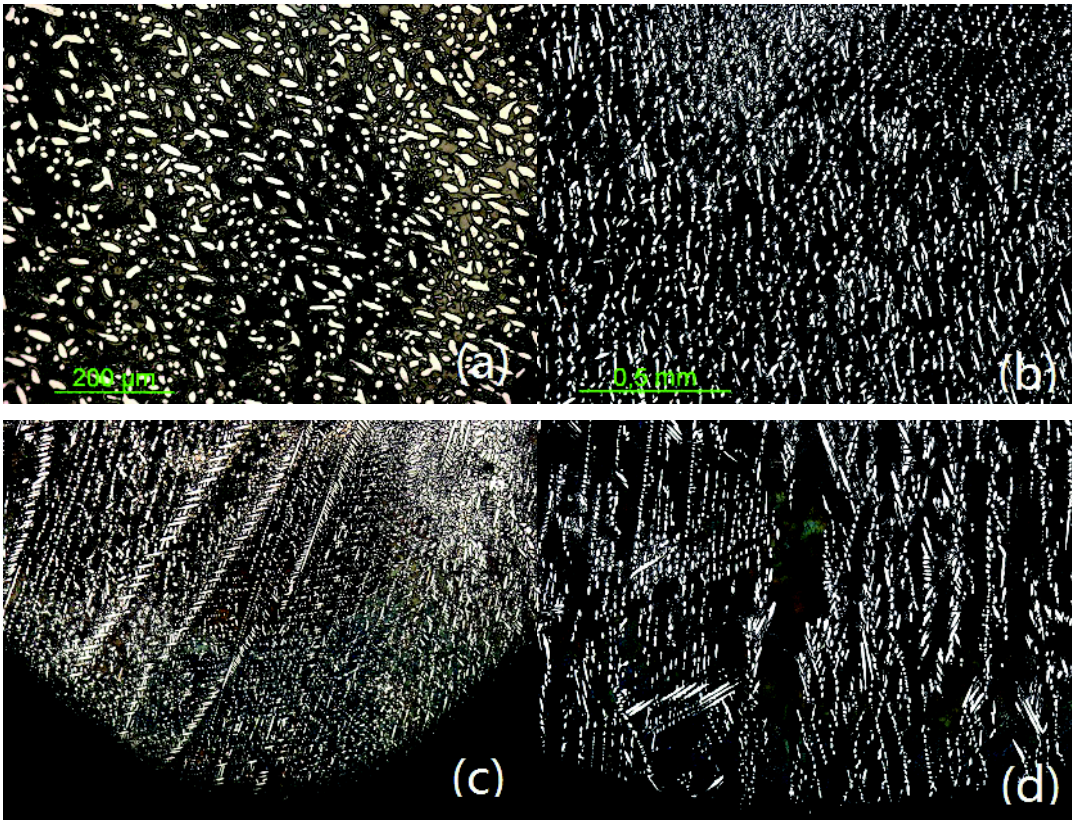

Fig 5-6 Solidified microstructure of undercooled $Co_{79.5}Sn_{20.5}$ alloys under different magnetic fields (a)ΔT=8ºC, 0T; (b) ΔT=8ºC, 0.5T; (c) ΔT=11ºC, 1T; (d) ΔT=8ºC, 8T. The field direction is vertical in the picture.

Fig 5-7 shows the microstructure of $Co_{79.5}Sn_{20.5}$ alloys solidified with different

conditions. For the alloy solidified according to the temperature profile shown in Fig 5-7(a) where the solidification process is controlled at a constant undercooling, the primary Co phase has lost dendritic characteristic due to the remelting of dendrites arms in recalescence process. When the alloy solidifies according to the temperature profile shown in Fig 5-7(c) where the sample is naturally cooled in the furnace after the nucleation of primary αCo phase, the precipitation of the eutectic phase occurs at a lower undercooling, and the dendrites is also aligned along the field direction. Compared with the microstructure shown in Fig 5-7(b), the dendritic microstructure formed after the first recalescence is textured along the field direction, but it does still exist many dendrites that deviate from the direction of the field direction. The growth of grains in magnetic field is affected by two factors, one is grain size and another one is time left for growth rotation ($\tau = \frac{3\pi^2 \mu_0 \eta}{\Delta \chi B^2}$). The time permitted for the rotation of dendrites in Fig 5-7(d) is much smaller than that in Fig 5-7(a), so the effect of magnetic field on the grain alignment is smaller.

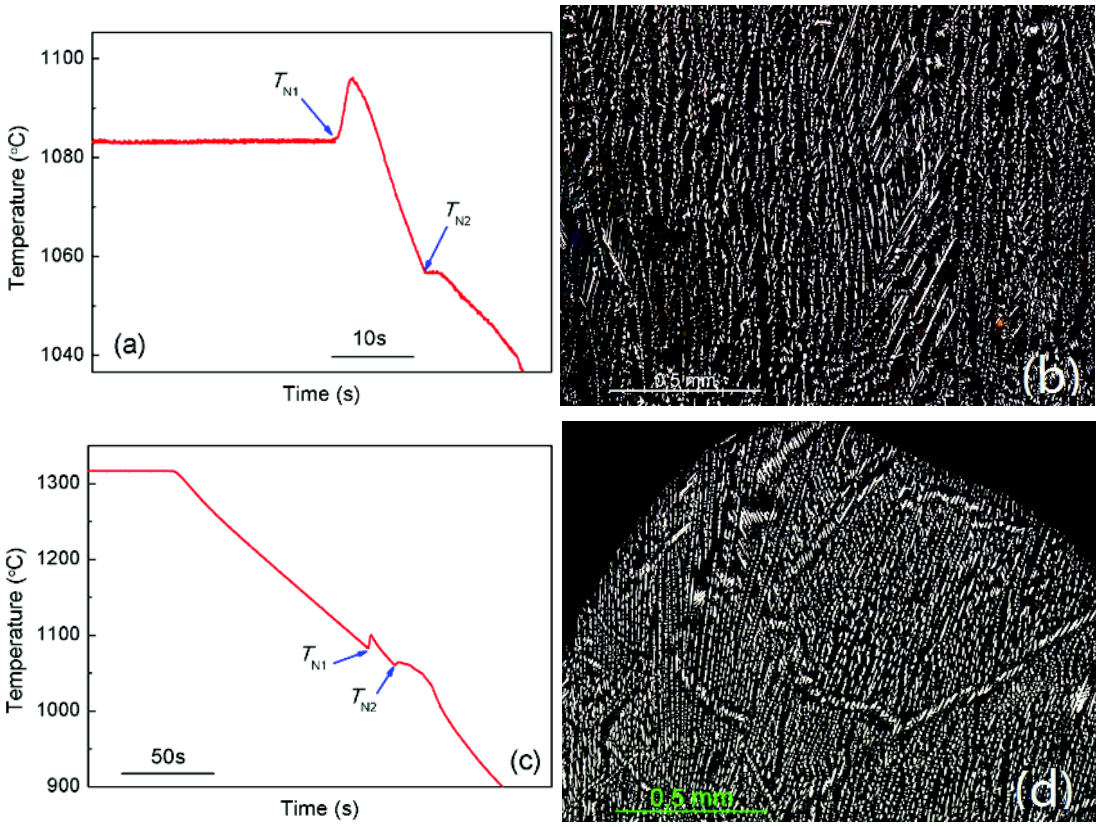

Fig 5-7 Microstructure of undercooled $Co_{79.5}Sn_{20.5}$ solidified under 12T magnetic field. (a, b) Rapid cooling after second recalescence finished, (c, d) Rapid cooling after first recalescence finished. The field direction is vertical in the picture.

(2)The precipitation of secondary αCo phase in strong magnetic field

For Co-Sn hypoeutectic alloys, at large undercoolings, the anomalous eutectic

colony forms firstly in the undercooled melt at large undercoolings, and then secondary αCo phase grows from the periphery of the colony, finally lamellar eutectic precipitates in the remained liquid. Fig 5-8 is the microstructure of $Co_{79.5}Sn_{20.5}$ alloys solidified at undercooling of 150ºC. It can be seen that, secondary αCo phase grows radialy from colony without magnetic field (Fig 5-8(a)). In 4T magnetic field, the growth of the secondary αCo dendrites is constrained in the direction perpendicular to the magnetic field (seen in Fig 5-8(b)). When the field intensity increased to 12T, the volume fraction of anomalous eutectic colony increases and the growth of secondary αCo dendrites is constrained. Then we can conclude that, at the same undercooling, magnetic field enhances the formation of anomalous eutectic colony and reduces the formation of secondary αCo phase.

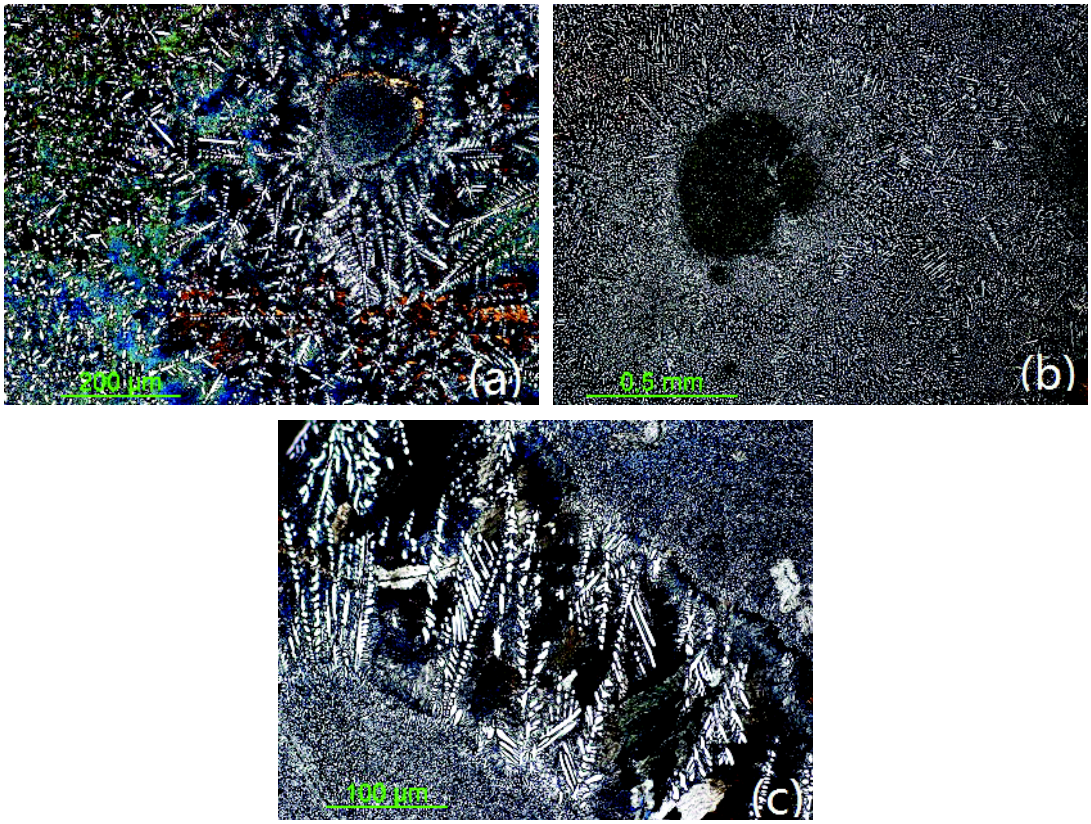

Fig 5-8 Microstructure of undercooled $Co_{79.5}Sn_{20.5}$ alloy: (a)ΔT=150℃, 0T, (b)ΔT= 149℃,4T,(c) ΔT=149℃, 12T. The field direction is vertical in the picture.

5.2.2 Co-Sn near eutectic alloy

5.2.2.1 The microstructure evolution of $Co_{76}Sn_{24}$ alloy without magnetic field

Fig 5-9 shows microstructures of $Co_{76}Sn_{24}$ alloy solidified at different undercoolings. The microstructure evolution processes are as follows. At low undercoolings (ΔT<20ºC), a small volume fraction of primaryαCo phase precipitates first, and then is the formation of regular eutectics, denoting $Co_{76}Sn_{24}$ alloy is close to eutectic point but actually is still hypoeutectic alloy. When the undercooing increases to 25 ºC, seen in Fig 5-9(b), the solidified microstructure is fully lamellar regular eutectics. The anomalous eutectic colony formes at elevated undercoolings, e.g. when ΔT=161ºC, as shown in Fig 5-9(c), and lamellar eutectic grows from the periphery of the colony instead of the secondary αCo dendrites. The volume fraction of eutectic colonies increases with increasing undercooling, and the lamellar eutectics solidify between the colonies.

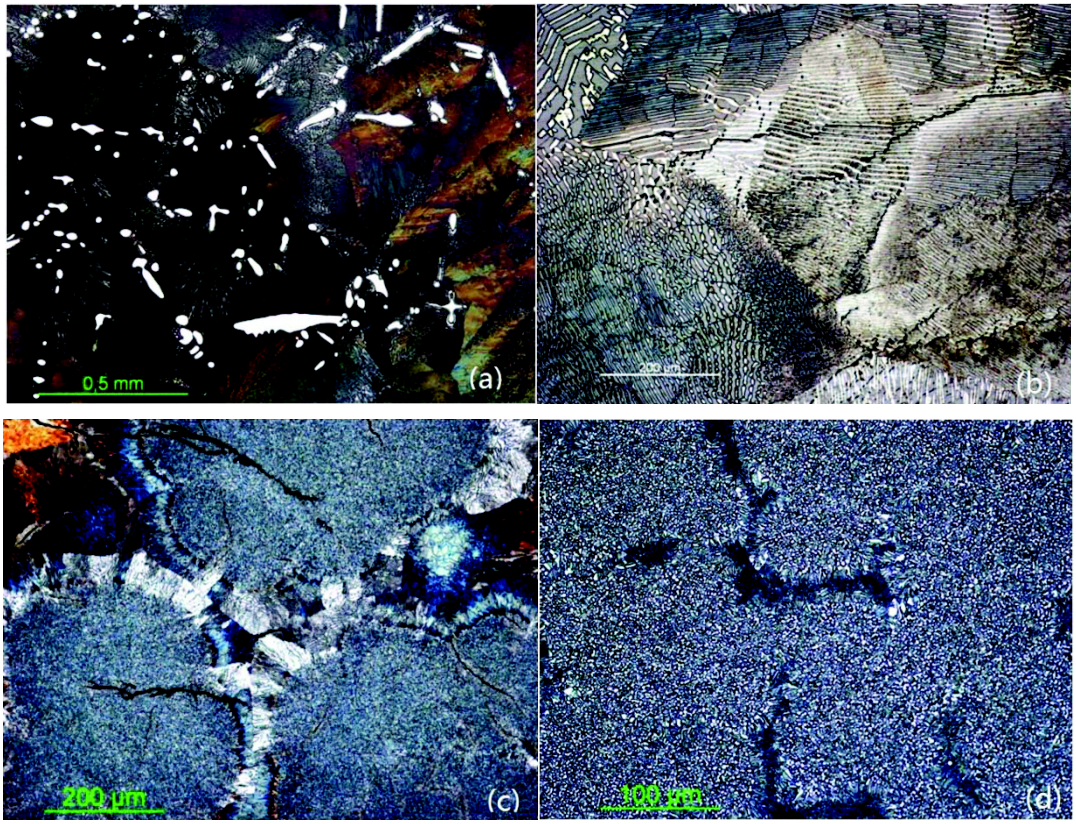

Fig 5-9 Microstructure of undercooled $Co_{76}Sn_{24}$ alloys solidified at different undercoolings, （a）ΔT=15℃,(b) ΔT=25℃,(c) ΔT=161℃,(d) ΔT=216℃.

5.2.2.2 The microstructure evolution of $Co_{76}Sn_{24}$ alloy in 12T magnetic field

Fig 5-10 is the microstructure of $Co_{76}Sn_{24}$ alloys solidified in 12T magnetic field at different undercoolings. At low undercoolings, there is a small volume fraction of αCo phase precipitated along the direction of magnetic field, shown in Fig 5-10(a). With the increasing undercooling, the volume fraction of anomalous eutectics increases and secondary αCo phase precipitates at the end of colonies (Fig 5-10(b)). When the undercooling increases to 108ºC, shown in Fig 5-10(c), the solidified microstructure of $Co_{76}Sn_{24}$ alloy consists only two phases: regular and anomalous eutectics, those colonies growing along the direction of the field. At large undercoolings, the colonies touch each other and there is only a small volume fraction of regular lamellar eutectic forms between them (shown in Fig 5-10(d)).

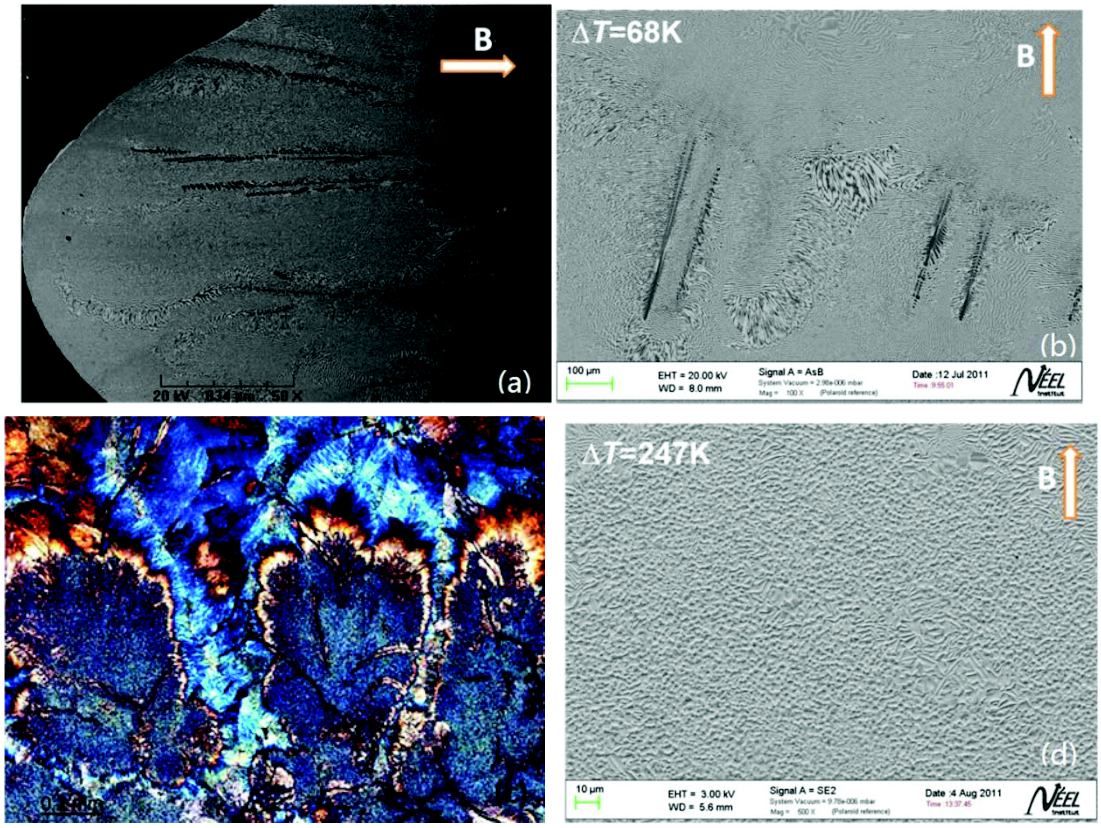

Fig 5-10 Microstructure of undercooled $Co_{76}Sn_{24}$ alloys solidified under 12T magnetic field at different undercoolings: (a)ΔT=29ºC, (b)ΔT= 68ºC, (c) ΔT=108ºC, (d) ΔT=247ºC. The field direction is vertical in the picture (except for (a)).

5.2.2.3 Effect of magnetic field intensity on the microstructure evolution of $Co_{76}Sn_{24}$ alloy

Fig 5-11 shows the microstructure of $Co_{76}Sn_{24}$ alloys solidified in different magnetic fields. It can be seen from the figure that the magnetic field can strongly affect the precipitation temperature of primary αCo phase. Without magnetic field, when the undercooling is 25ºC (shown in Fig 5-11(b)), the solidification microstructure is fully lamellar eutectics. When the sample solidifies in 4T magnetic field, the occurrence temperature for αCo phase extends to above 40ºC (shown in Fig 5-11(c)) and fully lamellar eutectic microstructure is obtained at the undercooling of 52ºC (shown in Fig 5-11(d)). In 12T magnetic field, the αCo phase is still observed at the undercooling of 77ºC (shown in Fig 5-11(e) and fully eutectic microstructure is observed at the undercooling above 100ºC (shown in Fig 5-11(f)).

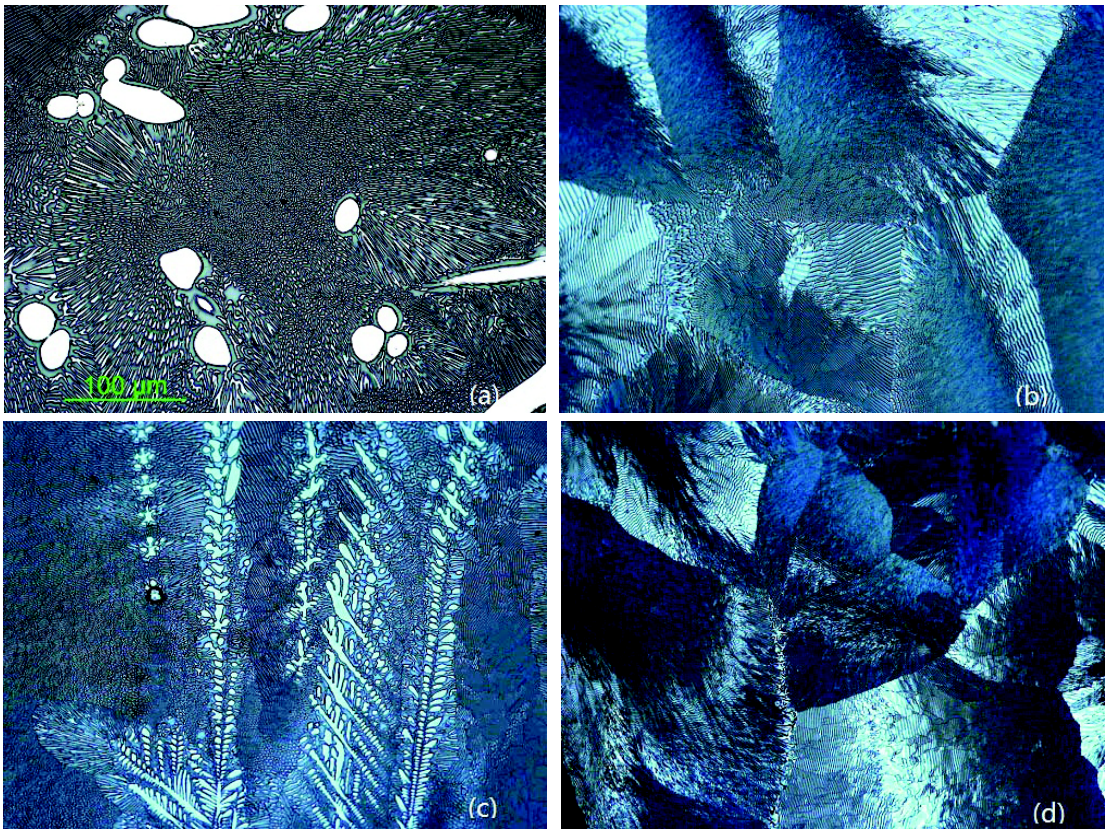

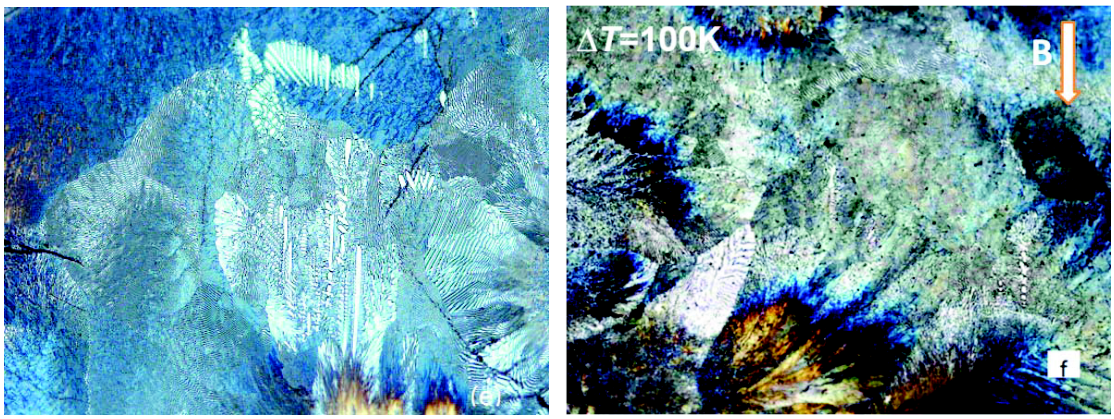

Fig 5-11 Microstructure on longitudinal section (parallel to the magnetic field) of $Co_{76}Sn_{24}$ alloy solidified at different undercoolings under different magnetic field intensity: (a) ΔT=15°C, (b) ΔT=25°C, 0T, (c) ΔT=40°C, 4T, (d) ΔT=52°C, 4T, (e) ΔT=77°C, 12T, (f) ΔT=100°C, 12T. Note that α Co is homogeneously distributed in (a), and the volume fraction decreases and localizes at typical zone of the sample, we only show the area with αCo in (c, e).

Compared with the microstructure solidified without magnetic field, the precipitated αCo phase is strongly affected by external magnetic field. The αCo phase is homogenously distributed in the sample solidified without magnetic field at low undercoolings, while the phase solidified in magnetic field is not homogenous but only exists in some local areas. In Fig 5-11, we only provide for the area with αCo phase, but for the whole sample, other areas are almost eutectic microstructure. The morphology of the αCo phase is also altered by magnetic field. Without magnetic field, αCo phase is typical fragmented dendrites, which is in an equiaxied dendritic morphology. But for the sample solidified in strong external magnetic field, αCo phase can keep the dendritic morphology and be aligned along the magnetic field. At large undercoolings, βCo_3Sn_2 precipitates between the arms of αCo, forming dendrite-eutectic microstructure.

The chemical Gibbs free energy for Co-Sn near eutectic alloys, at large undercoolings, is much larger than magnetic Gibbs free energy, thus it is very difficult to explain the variation of the precipitation temperature of αCo phase in magnetic fields. The investigation on the phase transformation of steel in magnetic field shows that α/γ transition temperature is changed for 1°C2 by the increasing intensity of every 1T magnetic field [GARC10]. This means that the phase transition temperature can be changed 10-20°C in 10T magnetic field. In this study, the precipitation temperature of αCo phase is extended more than 60 °C. According to the theory for the growth of dendrites in undercooled melt, the undercooling is categorized into four parts: ΔT_C, ΔT_t, ΔT_k and ΔT_r. At low undercoolings, the constituent undercooling, ΔT_C,

provides the majority of whole undercooling. Because of the large magnetic susceptibility of αCo than βCo_3Sn_2 phase, magnetic field will impose much stronger effect on the movement of αCo phase. And for ΔT_C, according to Eq.(1-15), it will be strongly affected by the solute distribution coefficient. The magnetic field can enhance or retard the moving speed of αCo phase, and change the value of ΔT_C. At different fields, the variation of ΔT_C for αCo phase will increase with the increasing field intensity while the field has much less effect on the formation temperature of βCo_3Sn_2.

5.2.3 Co-Sn hypereutectic alloy

5.2.3.1 The microstructure evolution of $Co_{72}Sn_{28}$ alloy without magnetic field

Different from the two compositions investigated before, the primary phase formed in $Co_{72}Sn_{28}$ hypereutectic alloy is paramagnetic βCo_3Sn_2 phase. Fig 5-12 shows the microstructure of $Co_{72}Sn_{28}$ hypereutectic alloy solidified at different undercoolings. It can be seen from the figure that the microstructure of $Co_{72}Sn_{28}$ alloy solidified at low undercoolings consists of primary βCo_3Sn_2 dendritic phase and regular lamellar ($\alpha Co+\beta Co_3Sn_2$) eutectic phase. The primary βCo_3Sn_2 dendrites are firstly formed by the remelting of the dendrites during recalescence (seen in Fig 5-12(a)). With the increasing undercooling, the dendrites become finer and the dendritic morphology becomes more obvious since the time left for the rearrangement of fragmented dendrites is smaller at larger undercooling (seen from Fig 5-12(c)). When the undercooling is above 139ºC, shown in Fig 5-12(d), the striped colony consisting of anomalous eutectics is precipitated from undercooled melt. βCo_3Sn_2 dendrites grow from the periphery of the colony, and regular eutectic solidifies from the remained liquid.

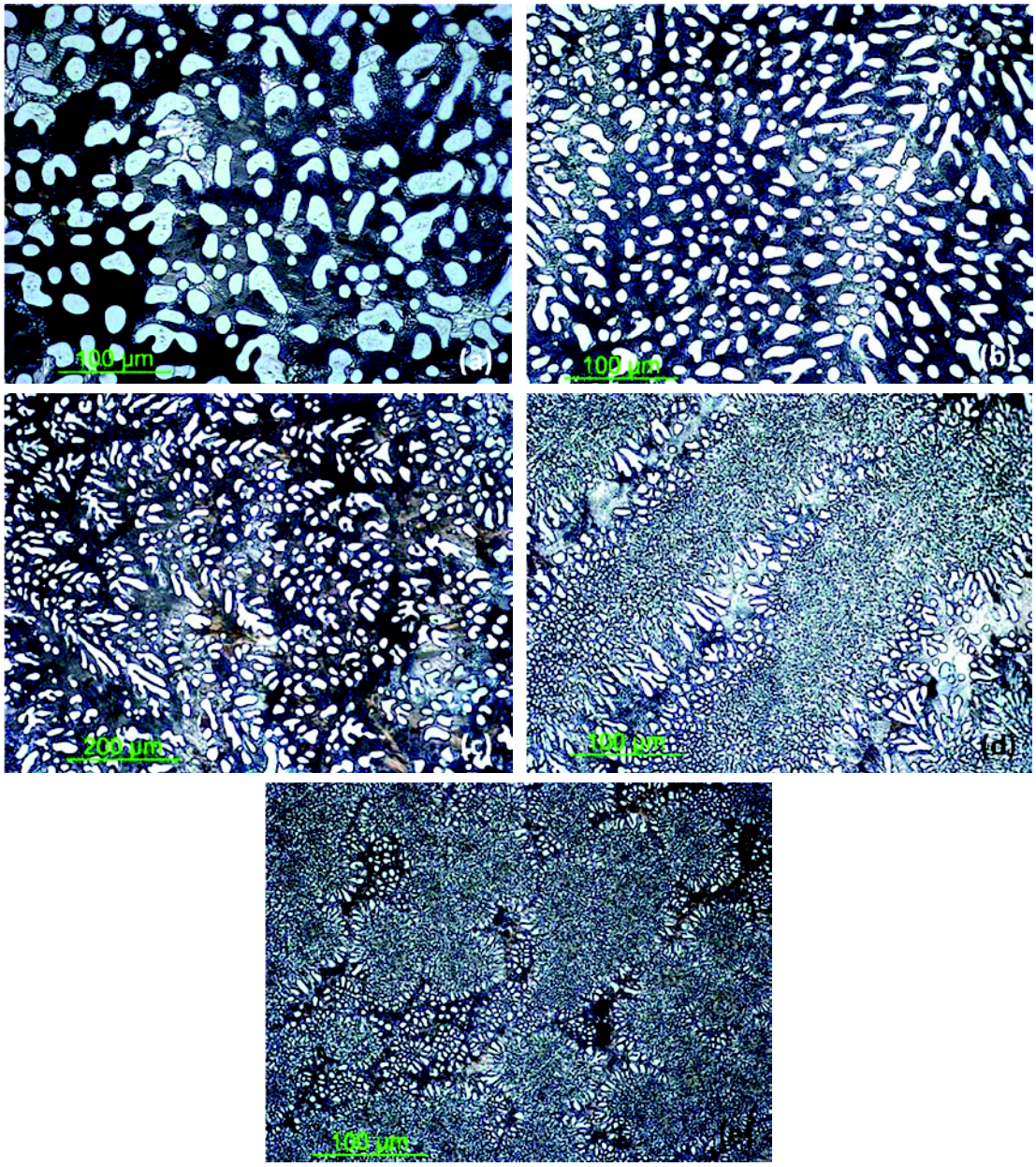

Fig 5-12 Microstructures of the undercooled $Co_{72}Sn_{28}$ alloy solidified at different undercooling conditions, (a) 18℃, (b) 45℃, (c) 105℃, (d) 139℃, (e) 220℃.

5.2.3.2 The microstructure evolution of $Co_{72}Sn_{28}$ alloy in 12T magnetic field

In 12T magnetic field, the solidified microstructure of $Co_{72}Sn_{28}$ alloys is shown in Fig 5-13. Different from hypoeutectic alloy, the primary phase, βCo_3Sn_2, is not obviously aligned along the direction of the field, and is homogenously distributed in the whole sample. The microstructure is close to that formed without magnetic field, but there are still some differences. Firstly, the lamellar eutectics are aligned along the

field direction, seen in Fig 5-13(a). Secondly, the growth direction of anomalous eutectic colony is altered by external magnetic field. Instead of growing freely in the sample, the colony formed in 12T magnetic field grows in a same direction parallel or just has a angle along the direction of magnetic field.

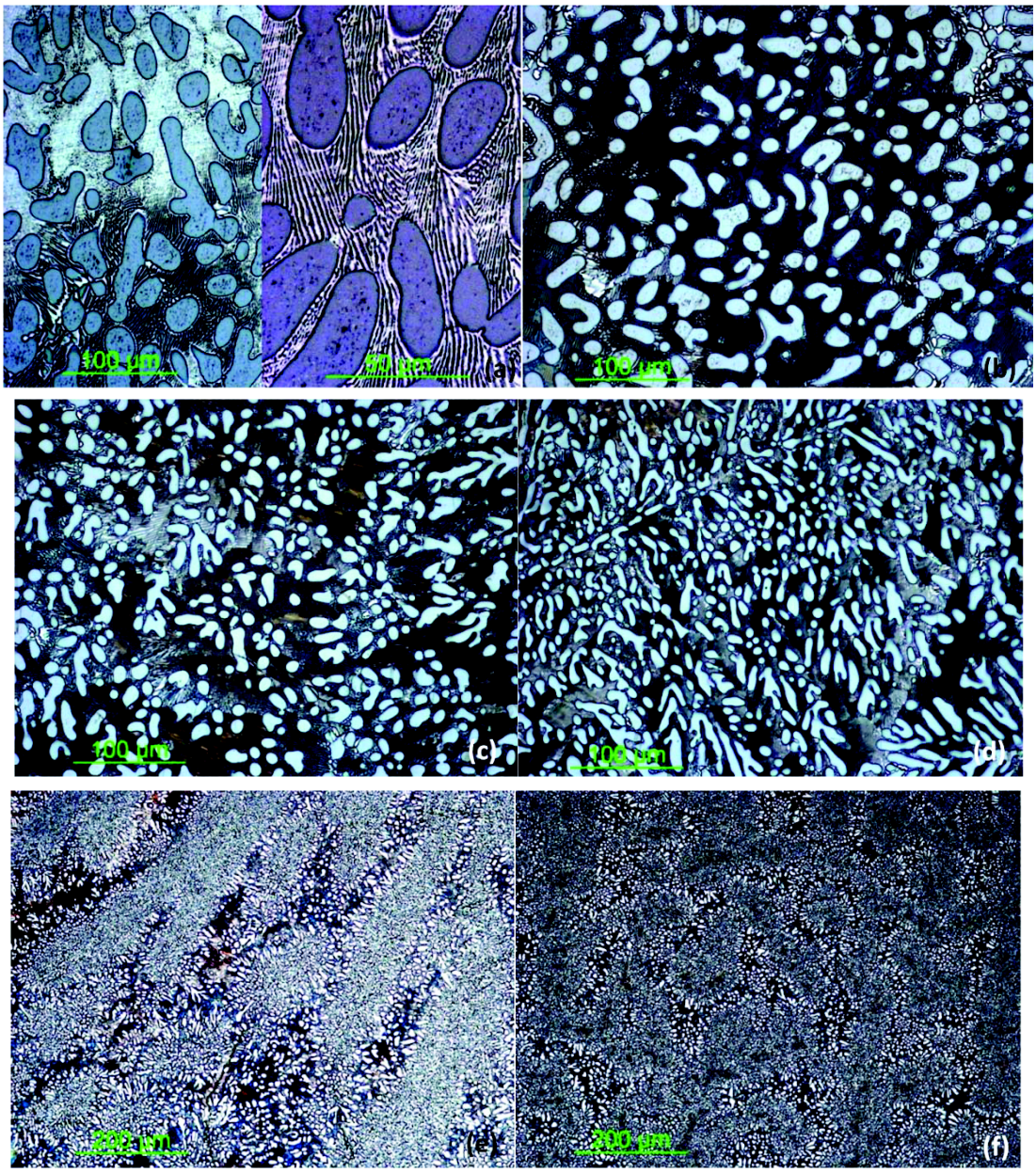

Fig 5-13 Microstructures of the undercooled $Co_{72}Sn_{28}$ alloy solidified at different undercoolings in 12T magnetic field, (a) 18℃, (b) 42℃, (c) 65℃, (d) 109℃, (e) 139℃, (f) 220℃. The field direction is vertical in the picture.

5.3 Texture analysis of undercooled Co-Sn alloys solidified under magnetic field

Fig 5-14 is the XRD patterns of $Co_{79.5}Sn_{20.5}$ solidified at different undercoolings. The peaks detected are the typical phases formed in $Co_{79.5}Sn_{20.5}$ alloys, αCo and βCo_3Sn_2. The pattern also contains the peaks of ξCo and αCo_3Sn_2 phases formed during solid state phase transformation (not shown here). Compared with standard PDF cards of αCo and βCo_3Sn_2, there exists two main peaks at the diffraction angle of 50.5° and 51.6°. With the increasing undercooling, the peaks existing in 51.6º become stronger. The peaks denoting βCo_3Sn_2 phase varies strongly with magnetic field, e.g. the peak in 35.5º ((101) crystal direction) becomes stronger when the undercooling increases while the peak in 70.3º ((103) crystal direction) becomes weaker.

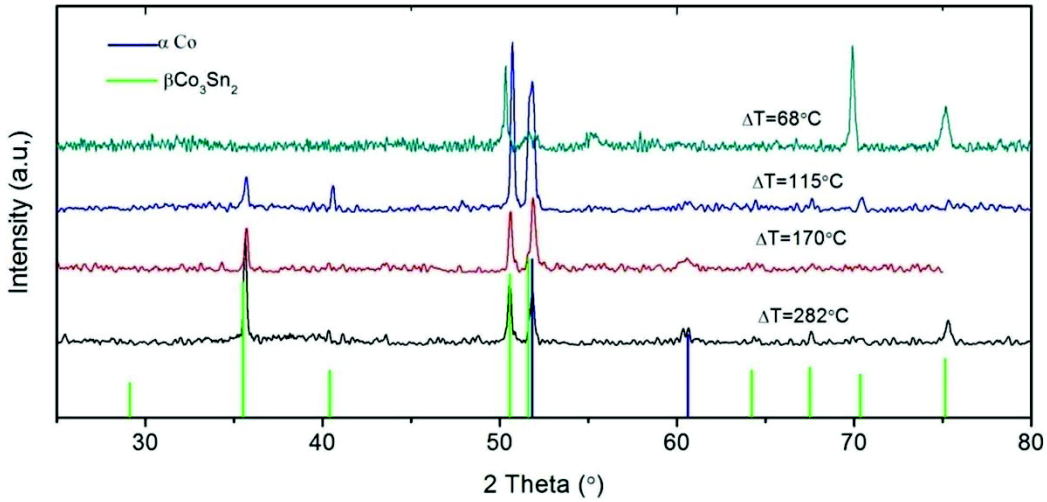

Fig 5-14 XRD patterns of $Co_{79.5}Sn_{20.5}$ alloys solidified at different undercoolings

Figs 5-15 and 5-16 show the EBSD analysis results of $Co_{79.5}Sn_{20.5}$ alloy solidified at undercoolings of 17ºC and 266ºC, respectively. At low undercooling, the orientation of αCo and βCo_3Sn_2 are mainly in three directions (seen from Figs 5-15(b, d) and 5-16(b, d)) while at large undercooling, the pole figure of these two phases are rather scattered without any notable orientation direction. Judging form misorientation angle distribution figure in low (Fig 5-15(e,f)) and high (Fig 5-16(e,f)) undercoolings, the misorientation angle for αCo phase and βCo_3Sn_2 phase formed at undercooling of 17ºC concentrates in 0~25ºC and 0~5ºC, respectively. When ΔT=282ºC, αCo and βCo_3Sn_2 are mainly big angle grains, and among the misorientation angle range, the

crystal orientation obeys statistical distribution. At low undercooling, seen from Fig 5-15(a, b), the αCo phase dendrites grow in the same direction, indicating they are formed by the fragmentation of the same dendrites. At large undercooling, seen from Fig 5-16(a, b), the solidified microstructure is anomalous eutectics, and the grain can grow along any direction they want, thus we have statistical distribution of different grains.

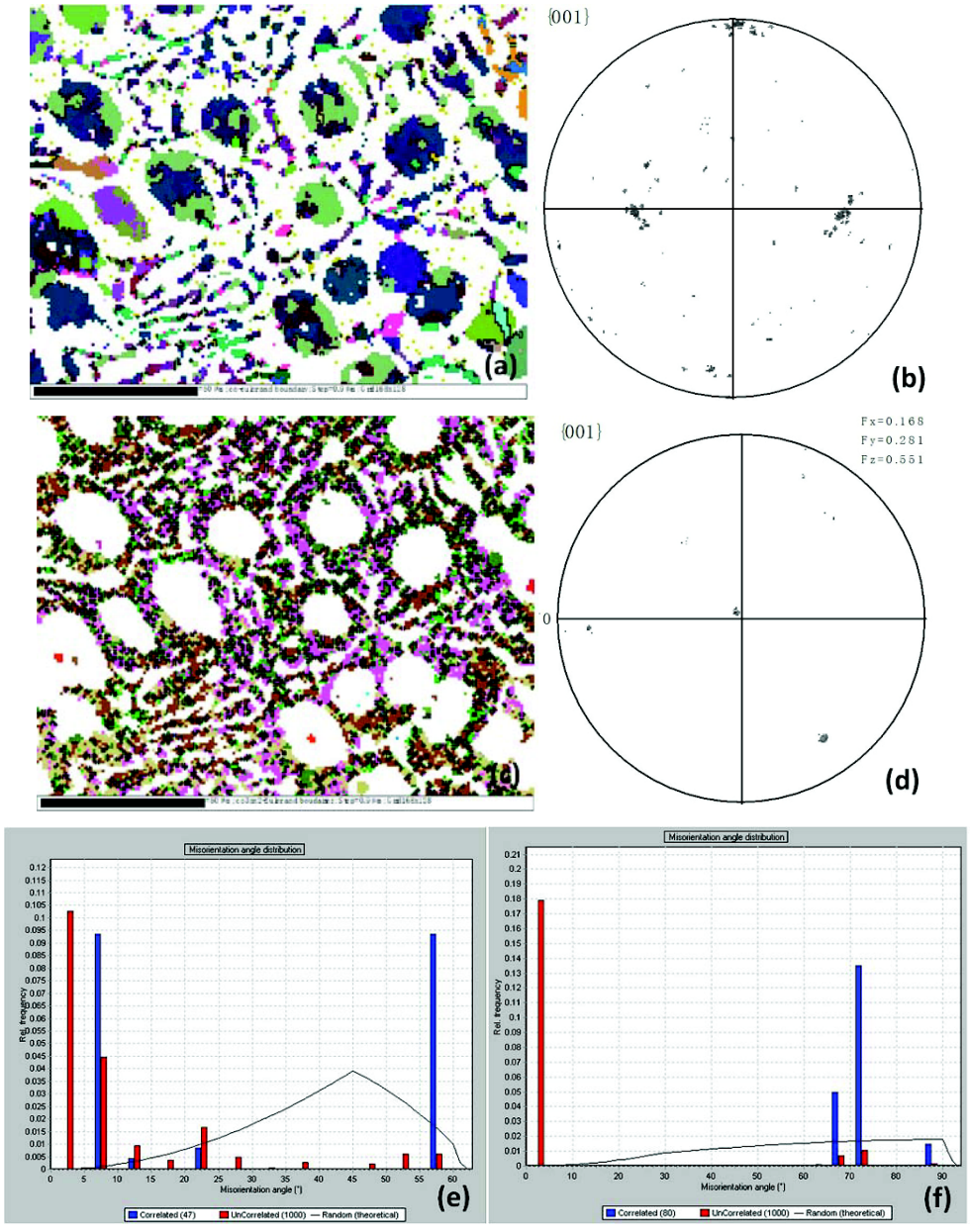

Fig 5-15 EBSD analysis of $Co_{79.5}Sn_{20.5}$ sample with an undercooling of 17℃.(a) EBSD pattern indexed to αCo; (b) (001) pole figure of αCo; (c) EBSD pattern indexed to βCo_3Sn_2 phase; (d) (001) pole figure of βCo_3Sn_2 phase; (e)misorientation angle distribution of αCo grains; (f) misorientation angle distribution of βCo_3Sn_2 phase.

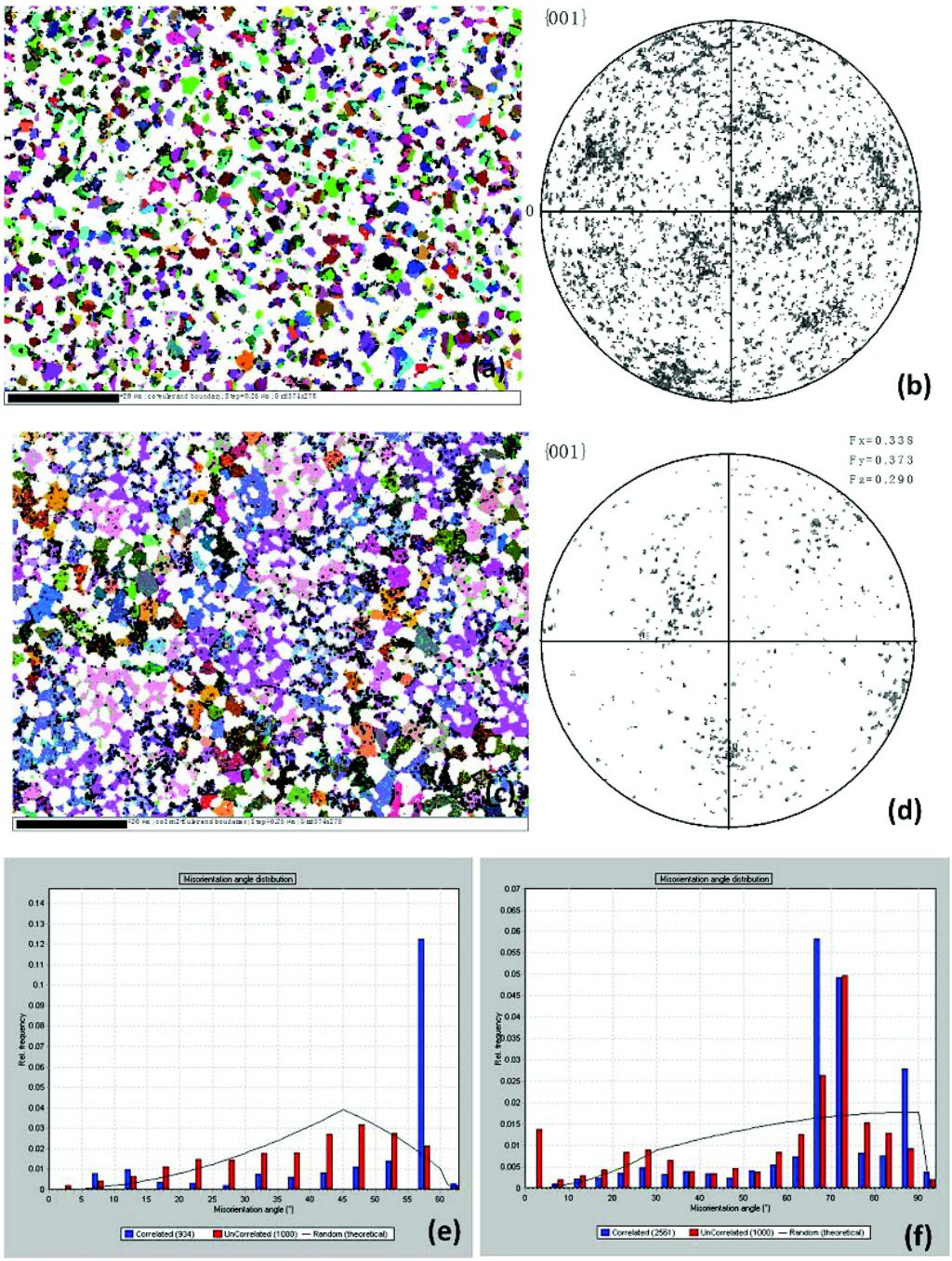

Fig 5-16 EBSD analysis of $Co_{79.5}Sn_{20.5}$ sample with an undercooling of 266℃.(a) EBSD pattern indexed to αCo; (b) (001) pole figure of αCo; (c) EBSD pattern indexed to βCo_3Sn_2 phase; (d) (001) pole figure of βCo_3Sn_2 phase; (e)misorientation angle distribution of αCo grains; (f) misorientation angle distribution ofβCo_3Sn_2 phase

Fig 5-17 shows the XRD patterns of $Co_{79.5}Sn_{20.5}$ alloys solidified at the undercooling of 75ºC in 12T magnetic field. The XRD patterns for the sample solidified along and perpendicular the field direction are not the same. The magnetic susceptibility of αCo phase is much larger than βCo_3Sn_2 phase, and the magnetic field

can align the grain along the field direction. However, αCo cannot be textured by external field due to its FCC crystal structure. Otherwise, for βCo_3Sn_2 phase which has a HCP crystal structure, it can be textured by the field due to the magnetic susceptibility difference in a and c direction of its crystal structure. Fig 5-18 shows the XRD patterns of $Co_{79.5}Sn_{20.5}$ alloys solidified at different undercoolings in 4T magnetic field. There is no much difference compared with the sample solidified without magnetic field. Figs 5-19 and 5-20 are the EBSD analysis results of $Co_{79.5}Sn_{20.5}$ alloys solidified at 17ºC and 271ºC. Different from that formed without magnetic field, the grain formed in the magnetic field at low undercooling, has no typical grain orientation. The grain misorientation angle is not constrained in low angles, seen from the misorientation angle map in Figs 5-19(e,f). And at large undercoolings, magnetic field has no effect on the orientation of αCo phase and βCo_3Sn_2 phase.

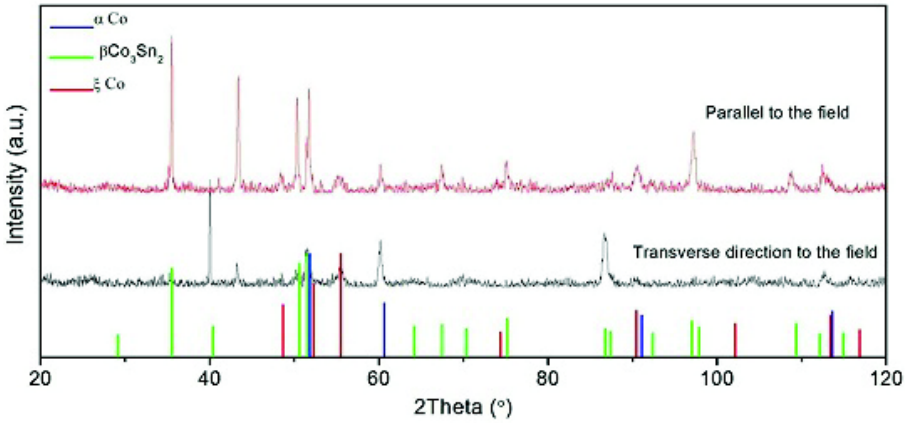

Fig 5-17 XRD patterns of longitude and transverse direction of the solidified $Co_{79.5}Sn_{20.5}$ alloy with undercooling 75℃ under 12T magnetic field

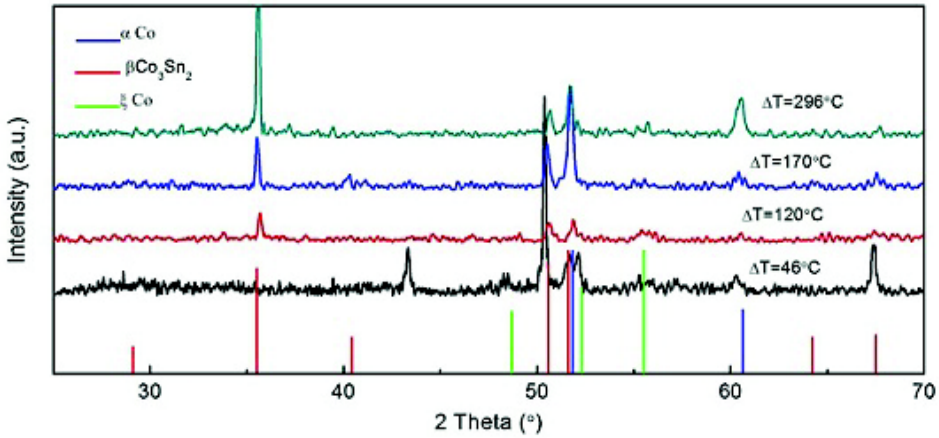

Fig 5-18 XRD patterns of longitude direction of the solidified $Co_{79.5}Sn_{20.5}$ alloys at different undercoolings under 4T magnetic field

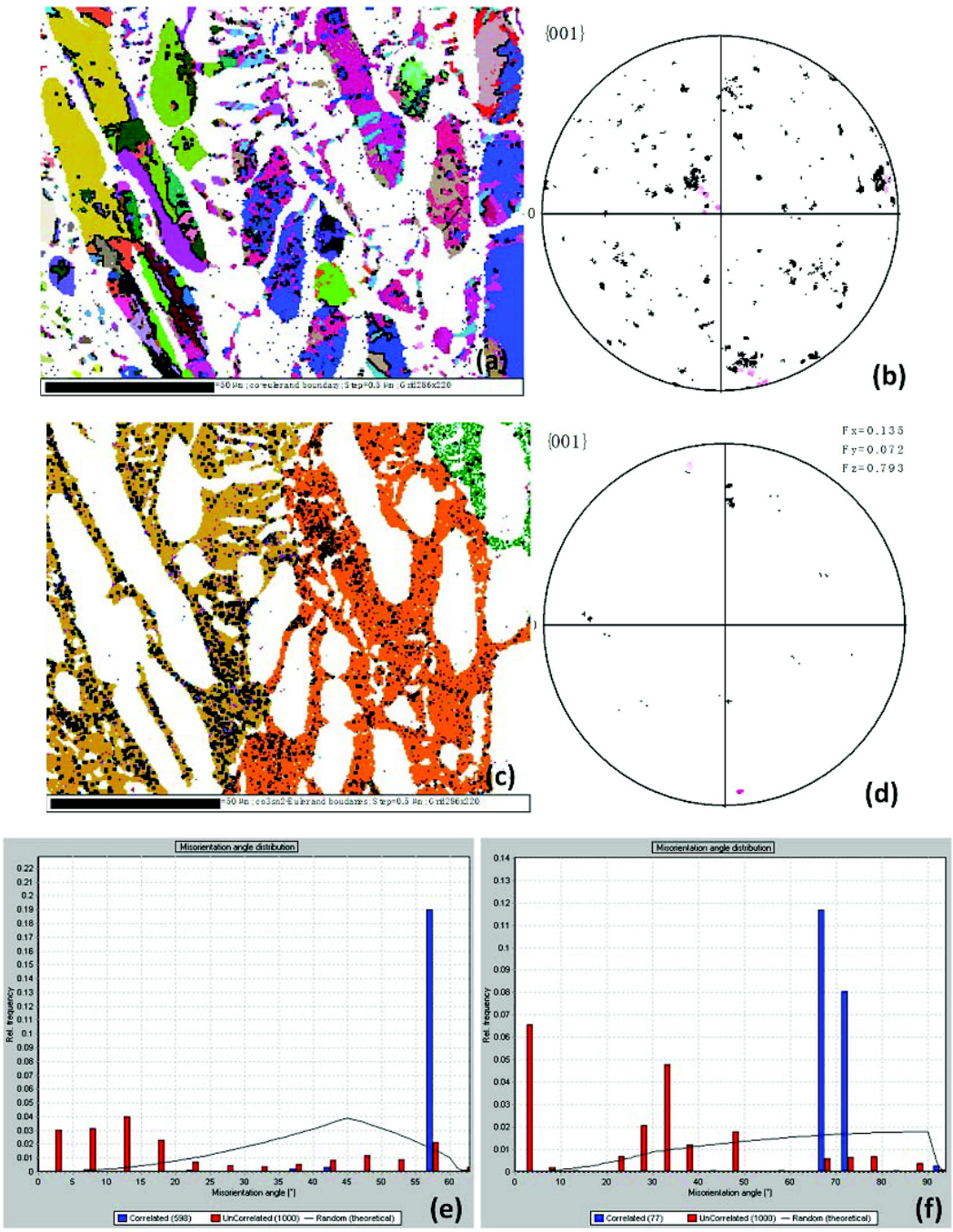

Fig 5-19 EBSD analysis of $Co_{79.5}Sn_{20.5}$ sample solidified under 12T magnetic field at an undercooling of 17℃.(a) EBSD pattern indexed to αCo; (b) (001) pole figure of αCo; (c) EBSD pattern indexed to βCo_3Sn_2 phase; (d) (001) pole figure of βCo_3Sn_2 phase; (e)misorientation angle distribution of αCo grains; (f)misorientation angle distribution of βCo_3Sn_2 phase

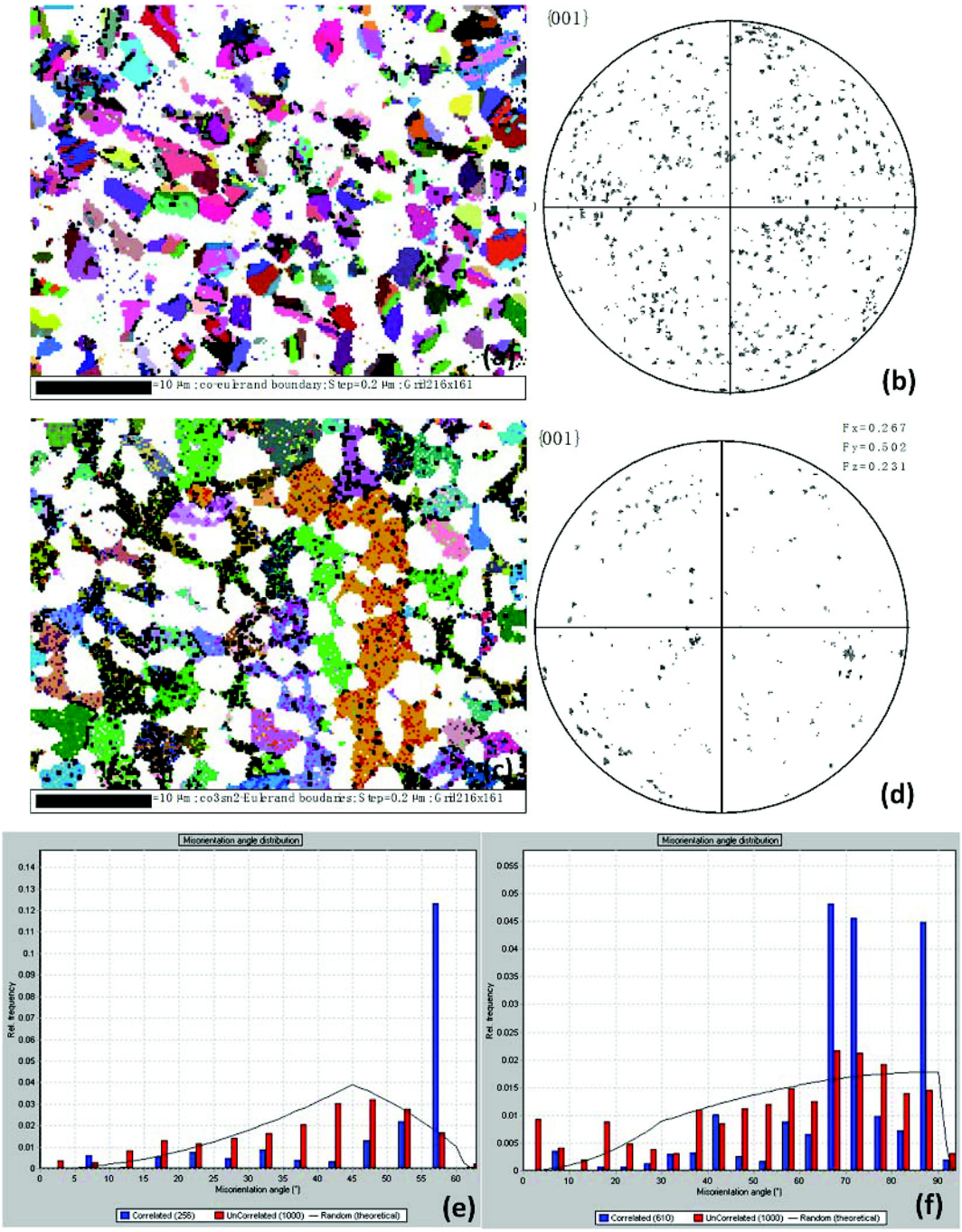

Fig 5-20 EBSD analysis of $Co_{79.5}Sn_{20.5}$ sample solidified under 12T magnetic field at an undercooling of 271℃.(a) EBSD pattern indexed to αCo; (b) (001) pole figure of αCo; (c) EBSD pattern indexed to βCo_3Sn_2 phase; (d) (001) pole figure of βCo_3Sn_2 phase; (e)misorientation angle distribution of αCo grains; (f)misorientation angle distribution of βCo_3Sn_2 phase.

5.4 Summary

In this chapter, the undercooling experiments for Co-Sn alloys were carried out in different magnetic fields and the microstructure evolution process were investigated.

The main conclusions are as follows:

(1) The hypoeutectic $Co_{79.5}Sn_{20.5}$ alloy contains two recalescence peaks solidified at low undercoolings. The first one is the precipitation of primary αCo phase and then the formation of (αCo+βCo_3Sn_2) eutectics. The recalescence curves for near eutectic $Co_{76}Sn_{24}$ alloy and hypereutectic $Co_{72}Sn_{28}$ alloy consist of the same sharp peak.

(2) The microstructure evolution process of $Co_{79.5}Sn_{20.5}$ alloy is as follows. At low undercoolings (<40ºC), the microstructure of the alloy is primary αCo+lamellar (αCo+βCo_3Sn_2) eutectic phases. When the undercooling is larger than 100ºC, the eutectic colony starts to form and the final microstructure of the as solidified alloys is αCo+lamellar (αCo+βCo_3Sn_2) eutectic phases+eutectic colony. When the alloy solidifies at higher undercoolings, the volume fraction of primary αCo decreases, and finally disappears. The volume fraction of anomalous eutectics increases, and finally the whole sample is dominated by anomalous (αCo+βCo_3Sn_2) eutectic phases.

(3) The external magnetic field can enhance the precipitation of αCo dendrite phase in $Co_{76}Sn_{24}$ near eutectic alloy. The primary αCo dendrite grows along the direction of magnetic field, forming chain like structure. The secondary αCo dendrite grows at the periphery of the eutectic colonies, and the critical undercooling for disappearance of αCo dendrite increases with the intensity of magnetic field.

(4) At low undercoolings, the solidified microstructure of $Co_{72}Sn_{28}$ hypereutectic alloy is primary βCo_3Sn_2 dendrite phase and lamellar eutectics. The equiaxed dendritic βCo_3Sn_2 phase is the outcomes of fragmented dendrites during the remelting process in the recalescence. With the increasing undercooling, the equiaxed dendritic βCo_3Sn_2 phase becomes smaller and the dendritic morphology becomes more obviously. The anomalous eutectic colony exists at elevated undercoolings, and the secondary dendritic βCo_3Sn_2 phase is precipitated at the end of the colony. When $Co_{72}Sn_{28}$ hypereutectic alloy is solidified in strong magnetic fields, βCo_3Sn_2 dendrites align weakly along the field direction at low undercoolings, and the lamellar eutectics also is aligned by the external field. When the undercooling is above 100ºC, the anomalous eutectics form and all the colonies are aligned by the external magnetic field.

(5) At low undercooling, the misorientation angle of αCo and βCo_3Sn_2 phase are

between 0~25ºC and 0~5ºC. And at large undercoolings, all the grain boundaries are big angle boundaries, and the misorientation angle obeys a statistical distribution. In 12T magnetic field, αCo phase formed at low undercoolings does not exhibit any orientation, and the misorientation angle distributes widely. The magnetic field has very limited effect on the texturing of αCo and βCo_3Sn_2 phase at large undercoolings.

CHAPTER 6 ANOMALOUS EUTECTIC FORMATION IN UNDERCOOLED CO-SN ALLOYS UNDER STRONG MAGNETIC FIELD

The solidified microstructure of Co-Sn binary near eutectic alloys consists two phases, ferromagnetic αCo phase and paramagnetic βCo_3Sn_2 phase. During the solidification process, the magnetic field can impose quite different effects on these two phases due to the magnetic susceptibility difference. For near eutectic Co-Sn binary alloys, once solidified, αCo phase has much different morphology, including primary dendrites (formed at the beginning of solidification), secondary dendrites (formed at the periphery of anomalous eutectic colony), αCo phase in regular lamellar eutectics and anomalous eutectics. The high magnetization of αCo phase makes it quite easy to be influenced by magnetic field, with effects on phase morphology and volume fraction. In this chapter, we have investigated the effect of magnetic field on the precipitation of αCo phase and the formation mechanisms of anomalous eutectics.

6.1 Precipitation of αCo and its effect on the formation of eutectic microstructure

Fig 6-1 shows the microstructure of $Co_{76}Sn_{24}$ alloy solidified at small undercoolings in 0T and 4T magnetic field. At low undercoolings, they both form primary αCo dendrite phase and regular lamellar ($\alpha Co+\beta Co_3Sn_2$) eutectic phase. Without magnetic field, as seen in Fig 6-1(a), the primary αCo phase has a randomly distributed equiaxed dendritic morphology. In 4T magnetic field, as seen in Fig 6-1(b), the primary αCo phase has equiaxed and dendritic morphologies, and the growth of the secondary arms of the dendrites is strengthened along the direction of magnetic field (see ③ in Fig 6-1(b)).

The primary αCo phase shown in Fig 6-1(b) grows to certain angle (black dasher arrow) with the field direction, and the solidified lamellar eutectic consists two types, one is eutectic grains formed by lamellar eutectics (the area ① shown in Fig6-1), and the other is lamellar eutectics formed based on a αCo dendrite (the area ②

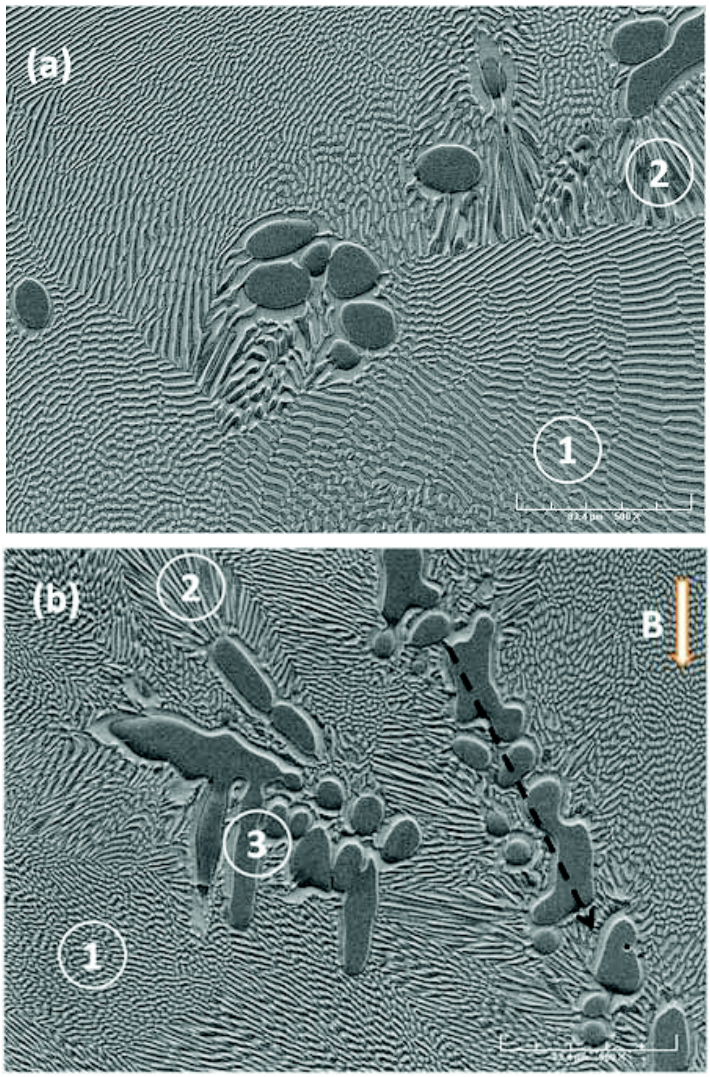

Fig 6-1 Microstructures of solidified $Co_{76}Sn_{24}$ alloy, (a) ΔT=15℃, B=0T, (b) ΔT=10℃, B=4T.

shown in Fig 6-1). The αCo dendrite, just as the bone of the eutectic grain, grows in the center of the grain, and βCo_3Sn_2 phase (between the second arms of αCo dendrite) forms radial like lamellar eutectics.

Fig 6-2 shows the solidified microstructure of $Co_{76}Sn_{24}$ alloy at undercooling of 40ºC in 4T magnetic field. Compared with the microstructure in Fig 6-1(b), αCo dendrite precipitated in the magnetic field has two characteristics. The first kind is close to the characteristics of dendrites shown in Fig 6-1(b), and the second one is a fishbone like dendrite, shown in Fig 6-2 (marked by '1' and '2'), which is the bone of a eutectic grain. It can be seen that the fishbone dendrite is divided into several parts, as it is shown by the arrow marked by '1' in the figure. The trunk of the dendrite separates into two nearly parallel elongated αCo phases (from '2' to the bottom of the

fishbone dendrite). The second arm of the dendrites can directly transform to regular lamellar eutectics, as shown by the arrow marked by '3' in Fig 6-2. The dendrites shown by arrows in the area of '3' and '5' grow along the direction of the secondary dendrites arms marked by the arrow in area '1'. And along the direction of the arrow, the lamellar distance between the eutectics become larger, indicating all these dendrites are formed from the second arms of the dendrite shown in area '1'. The angle between the trunk and the second arm is always equal, and it can be seen from Fig 6-2 that the angle marked by θ_1 is about 40°. When look at the angles between the arms and the trunk, denoting as θ_2 and θ_3, we can see that the value are quite different. Compared with θ_3(70°), θ_2 (40°) is much smaller, and this difference could be caused by the magnetic force which force the arms rotate to the direction of magnetic field.

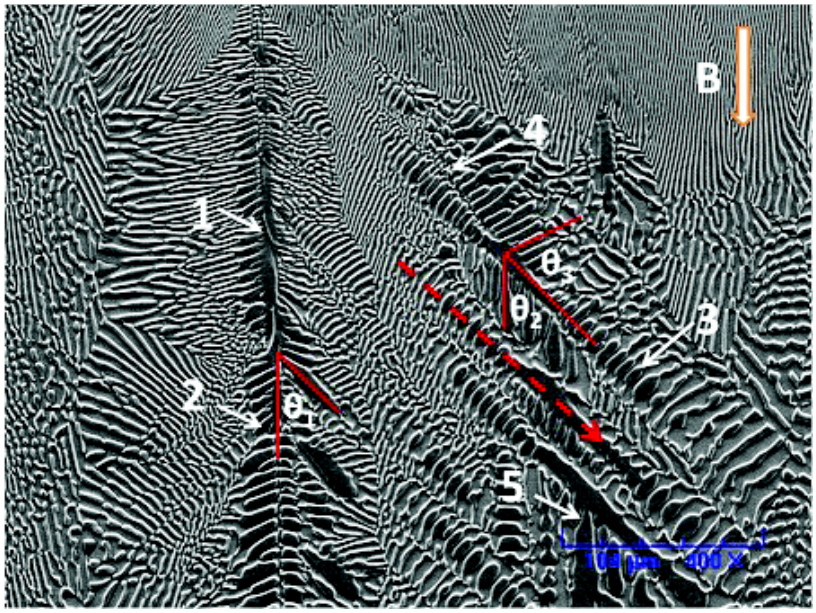

Fig 6-2 Microstructure of $Co_{76}Sn_{24}$ alloy solidified under 4T magnetic field, ΔT=40℃.

The microstructure of $Co_{79.5}Sn_{20.5}$ alloy solidified at the undercooling of 77℃ in 12T magnetic field is shown in Fig 6-3. The αCo dendrite is formed at the periphery of anomalous eutectic colony (area ① in the figure). After the formation of eutectic colony, at the beginning, there is no obvious main trunk for αCo dendrite (marked by arrows '2' and '3'). They are very similar to the parallel elongated αCo dendrites shown in Fig 6-2 (marked by arrow '4'), and have very developed secondary dendrites (marked by arrow '5'). Thereafter the αCo dendrite trunk forms and the secondary arms grow along the direction of the field (marked by arrow '6'). All the

dendrites growing from the colony are parallel with each other.

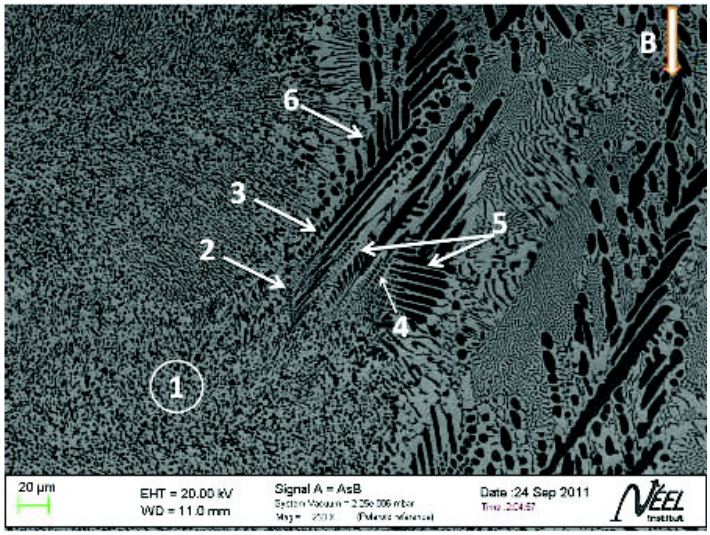

Fig 6-3 Microstructures of $Co_{76}Sn_{24}$ alloys solidified under 12T magnetic field, ΔT=77℃.

6.2 Mechanisms for anomalous eutectic formation in magnetic field

When the undercooling surpasses a certain value, anomalous eutectics are always formed in eutectic alloys systems [GOET98, LI08]. The mechanisms for the formation of anomalous eutectic are still a controversial topic. Based on the investigation of the anomalous eutectic formation in Ni-Sn alloy systems, Li [LI08, LI07a] and Yang [YANG11] find two origins for the formation of anomalous eutectic. The fine grained anomalous eutectic structure stems from partial remelting of eutectic dendrites and subsequent recrystallization of the matrix from the remaining liquid. And the coarse grained anomalous eutectic structure stems from partial remelting of single phase dendrites and delayed crystallization of the matrix from the interdendritic liquid. Li and Kuribayashi [LI03] found there exist anomalous eutectic colony in Co-Sn eutectic alloy system regardless of undercooling, indicating the solidification process is nucleation controlled.

Fig 6-4 shows the typical eutectic microstructure of $Co_{76}Sn_{24}$ alloy. At low undercoolings, the regular lamellar eutectics are formed, as shown in Fig 6-4(a). Anomalous eutectics are preferred for the microstructure solidified at large undercoolings, as shown in Fig 6-4(b). Different from the results by Li and Kuribayashi, we find the formation of anomalous eutectics is strongly affected by undercooling, and there are only lamellar eutectics which are found at low

undercoolings. As the undercooling increases, the anomalous eutectics are observed between the regular eutectics. Fig 6-5 shows the microstructure of $Co_{76}Sn_{24}$ alloy solidified at the undercooling of 62ºC. The lamellar and anomalous eutectics are observed and mixed with each other. The lamellar eutectics grow along the same direction, indicating they are from the same eutectic grain and the anomalous eutectics form the grain boundary of the subgrains in the big eutectic grain. Goetzinger et al [GOET98] find that the anomalous eutectics are the outcomes of the growth of lamellar eutectics. In Fig 6-5, it can be seen that the segments and branches in the lamellar eutectics can directly transform into anomalous eutectics. Meantime, the growth of anomalous eutectics is also unstable at the beginning, and can transform to regular lamellar eutectic. Thus the growth of regular and anomalous eutectics is interlaced in a eutectic grain.

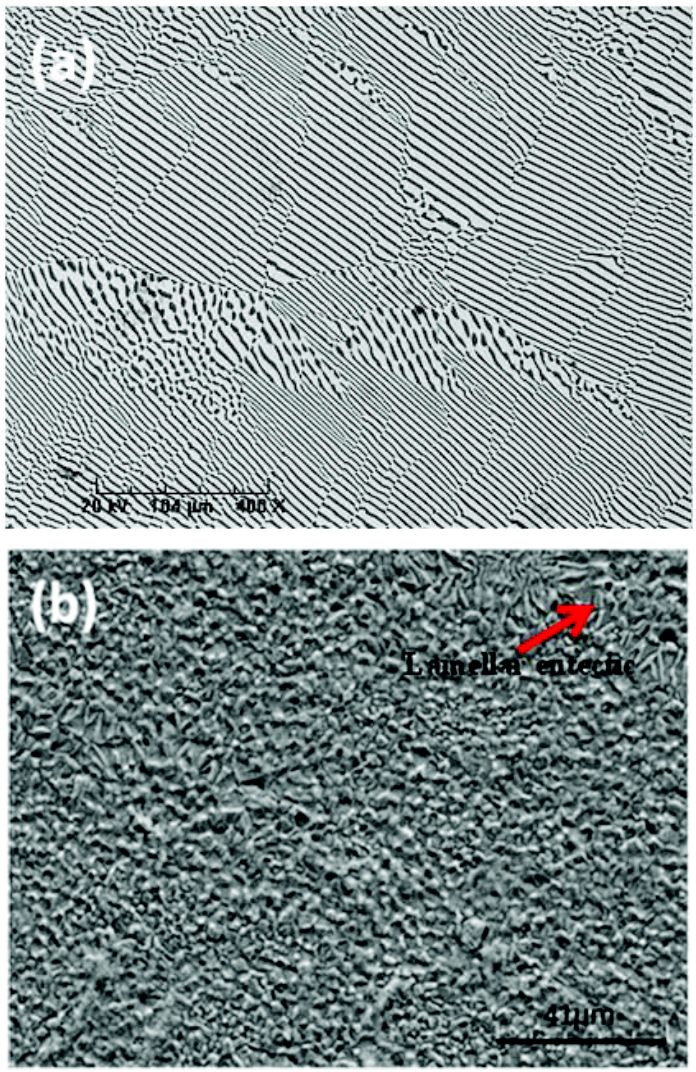

Fig 6-4 Microstructures of solidified $Co_{76}Sn_{24}$ alloy, (a)regular lamellar eutectic, ΔT=29℃ (b)anormalous eutectic, ΔT=235℃

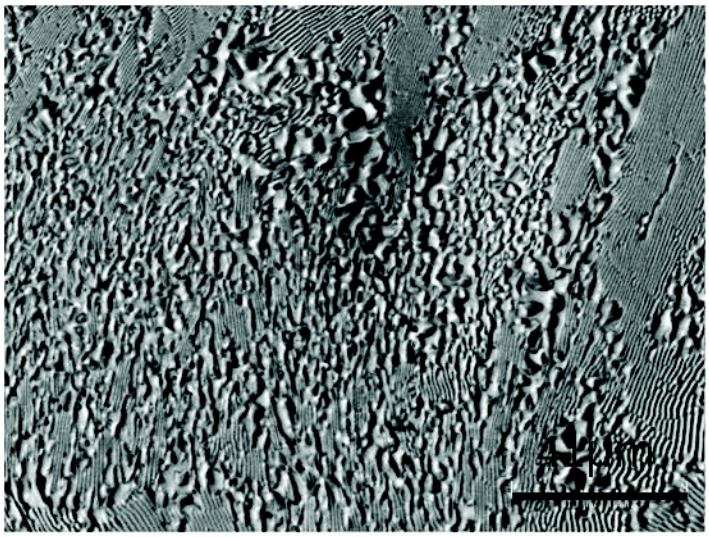

Fig 6-5 Microstructures of solidified $Co_{76}Sn_{24}$ alloy, ΔT=62℃

Fig 6-6 shows the microstructure of $Co_{76}Sn_{24}$ alloy solidified at the undercooling of 16℃ in 12T magnetic field. Unlike the microstructure of $Co_{76}Sn_{24}$ alloy solidified at low undercoolings, there exist anomalous eutectics in the present figure, which means the magnetic field promotes the formation of anomalous eutectics. During the growth of eutectics, regular lamellar eutectics can transform to anomalous eutectic, seen the solid circle in the figure, and also anomalous eutectics can transform to regular lamellar eutectics, seen from the dashed circle in the figure. According to the growth direction of eutectics, lamellar eutectics grow along the direction of magnetic field, and with the growth progresses, the volume fraction of lamellar eutectics decreases.

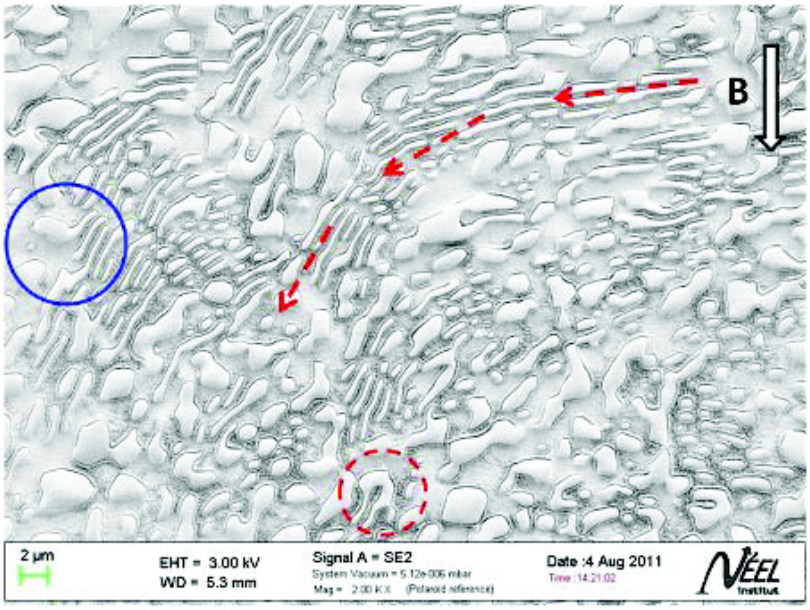

Fig 6-6 Microstructure of solidified $Co_{76}Sn_{24}$ alloy under 12T magnetic field, ΔT=16℃

With the increasing undercooling, relatively large interface energy is stored during the formation of the fine eutectics, thus the reduction of interface energy can act as a driving force for the braking of lamellar eutectics [GOET98]. The neighboring fragments in the undercooled melt can form consecutive bulks by agglomeration and ripening effect. The fragmented lamellar can form consecutive bulks in magnetic field. The tips and branches on top of anomalous eutectics can directly grow into the melt, and reach the formation condition for coupling growth of lamellar eutectics and grow into lamellar eutectics. In strong magnetic field, αCo phase undergoes much stronger effect by the field due to its high magnetic susceptibility, which will destroy the diffusion of solute condition for coupling eutectic growth. Then even in low undercooling, the regular lamellar eutectics can transform to anomalous eutectics in strong magnetic field.

Fig 6-7 is the microstructure of $Co_{76}Sn_{24}$ alloy solidified at undercooling of 105°C. The anomalous eutectics can precipitate from the undercooled melt at large undercoolings (seen from area '1' in Fig 6-7). With the growth of eutectic colony, anomalous eutectics can transform to lamellar eutectics (area '2' in Fig 6-7). Then the melt comes into a mixed growth of regular and anomalous eutectics. Then regular lamellar radial growth eutectics are formed (area '3' in Fig 6-7). With the increasing undercooling, seen from Fig 6-4(b), the mixed growth area for eutectics disappear and regular lamellar eutectics form between eutectics colonies.

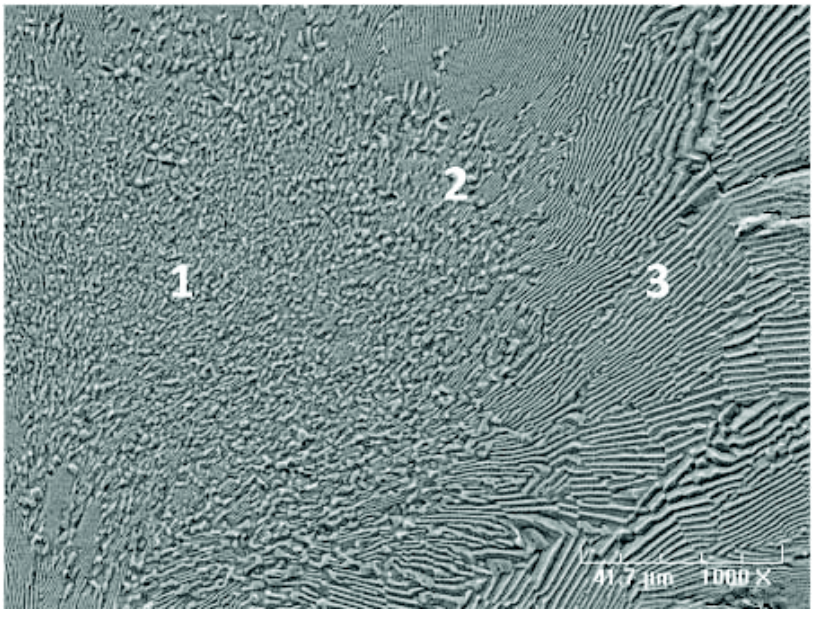

Fig 6-7 Microstructure of solidified $Co_{76}Sn_{24}$ alloy, ΔT=105℃.

The arrangement of αCo phase is very fine and in a rather disorder state in 12T magnetic field. Fine grained anomalous eutectics are formed by eutectic dendrites and recrystallized in the remained liquid. The application of 12T magnetic field promotes the precipitation of ferromagnetic αCo phase, and restrains the precipitation of βCo_3Sn_2 dendrites. Hence the fine grained anomalous eutectics become less after solidification. And for $Co_{72}Sn_{28}$ alloy solidified at the undercooling of 215℃, due to large magnetic force exerted on the αCo phase, the movement of is enhanced thus changing the initial arrangement. Due to the time limit of the fast solidification at large undercooling, αCo phase is solidified before it is aligned by magnetic field, thus forming the structure shown in Fig 6-8(b).

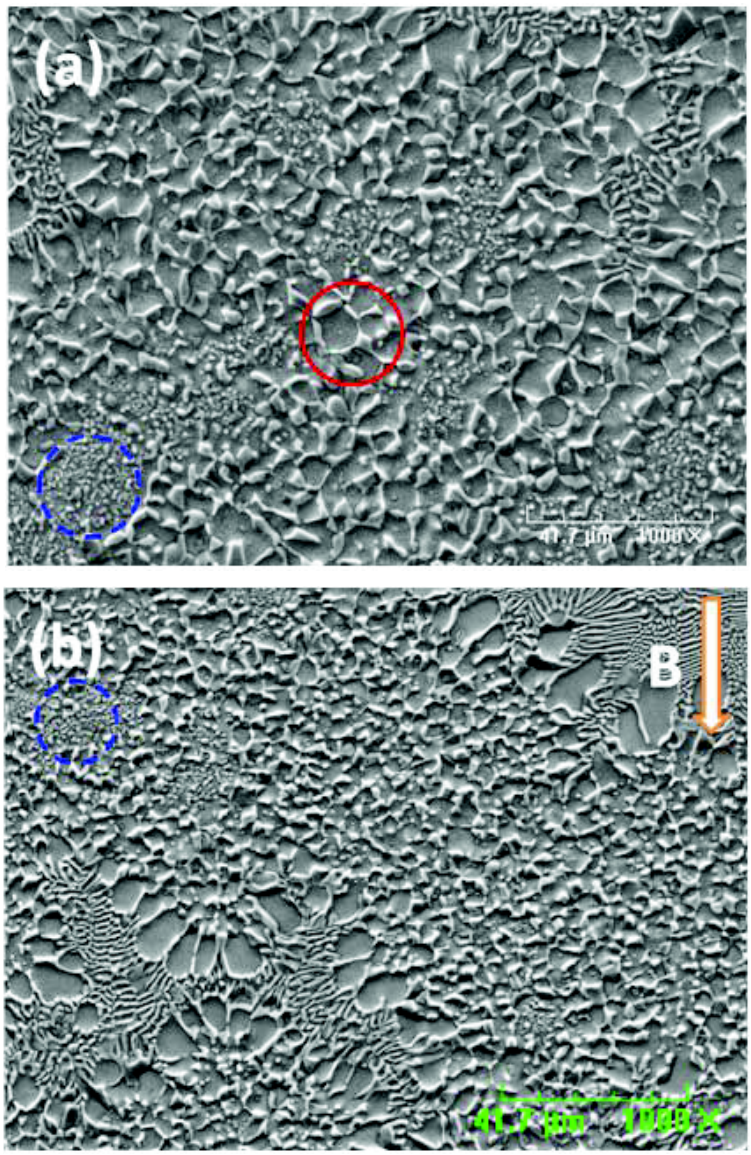

Fig 6-8 Microstructures of solidified $Co_{72}Sn_{28}$ alloy, (a)ΔT=223℃, B=0T, and (b)ΔT=215℃, B=12T.

6.3 Summary

(1) The solidified microstructure of $Co_{76}Sn_{24}$ alloy at low undercoolings in magnetic field has two characteristics. One kind consists in a regular lamellar eutectic grain, and another one is grown from a fishbone like αCo dendrite.

(2) The primary αCo phase is the first precipitated phase in the undercooled Co-Sn melt, which causes the formation of fishbone αCo dendritic phase in the center of eutectic grain and the secondary αCo dendrite phase at the periphery of anomalous eutectic colony.

(3) The magnetic field enhances the formation of anomalous eutectics and eutectic colony in the undercooled melt. The solidified microstructure of $Co_{76}Sn_{24}$ alloy is regular lamellar eutectics at low undercoolings, and anomalous eutectics starts to precipitate between the lamellar eutectics at the undercooling of 62°C. In 12T magnetic field, the undercooling for the existence of anomalous eutectics decreases to 16°C. During the growth of eutectics microstructure, regular and anomalous eutectics can transform to each other.

(4)The solidified microstructure of $Co_{72}Sn_{28}$ alloy solidified in 12T magnetic field at large undercoolings consists of fine grained anomalous eutectics and large amount of fragmented disordered αCo phases.

CHAPTER 7 SUMMARY

This work has been devoted to the investigation of the effect of magnetic field on the magnetic properties and solidification behavior of undercooled Co based alloys in high magnetic field. In this dissertation, we have built an undercooling facility with magnetization measurement system in a superconducting magnet, and have investigated the magnetic properties of the undercooled Co based alloys melt, undercoolability in magnetic field and the solidification microstructure variation at different undercoolings in magnetic field. Results of these are summarized as follows.

1. A new device system for magnetization measurement and solidification of deep undercooled melt in high magnetic fields has been developed in this work. The main advantages of this apparatus are: 1st, we can obtain large undercooling in high fields by glass fluxing technique in combination with cyclical superheating and supercooling method, which is comparable to the maximum undercooling obtained by traditional method. 2nd, we can have a controlled thermal history with linear heating and cooling speed with high accuracy. 3rd, the temperature and magnetization measurement system are fast and on-line, which is very suitable for the investigation of rapid solidification process of deeply undercooled melt.

2. Magnetization of different undercooled metals and alloys show quite different behaviors. (1).The magnetization of undercooled Co melts increases with the increasing undercooling. The undercooled melt has a larger magnetization than that in solid state at the same temperature. When the temperature is close to the Curie temperature of the melt, the magnetization increased rapidly and a spike pattern can be seen on the surface of the sample solidified in magnetic field at large undercooling, like in ferrofluid submitted in external fields. The paramagnetic Curie temperature calculated based on the solid Co during heating and liquid Co during cooling are: θ_P(L)=1132.5°C, and θ_P(S)=1120.5°C. (2). The magnetic properties of Co-B are affected by the overheating temperature. When the overheating temperature is below 1420℃, the magnetization of the undercooled melt was close to the solid alloy, and the paramagnetic Curie temperature determined are: θ_P(L)=1066°C, and θ_P(S)=1073°C. When the overheating temperature surpasses 1420°C, the undercooled melt comes into completely paramagnetic state, and the liquid Curie temperature is 1046°C, the alloy melt cannot undercooled into ferromagnetic state. (3). The

undercooled Co-Sn near eutectic alloy is in fully paramagnetic state, and the magnetic properties of the undercooled melt are not affected by the overheating temperature. The Curie temperature determined are: $\theta_P(L)$=612.1°C, and $\theta_P(S)$=1062°C.

3. The nucleation temperature of undercooled melt can be affected by the strong static magnetic field, and different response happened when a 12T magnetic field was applied for different alloys. (1). The magnetic field is beneficial to the undercooling of pure Cu and this effect was weakened when the melt is in a near equilibrium state. (2).The undercooling of pure Co is not affected by static magnetic field, but its recalescence extent is strongly depressed by static magnetic field. When there is no magnetic field,$\Delta T^{R\text{-}N}$≈91ºC, and it decreases 75% to 23ºC when solidified in 12T magnetic field. (3). The undercooling for Co-Sn alloys also keep unchanged when a strong magnetic field is applied while the recalescence extent is reduced. With the increasing Co content for Co-Sn eutectic systems, the effect of the magnetic field on the recalescence was strengthened. (4). IN gradient magnetic fields, the undercooling of pure Cu shows no stable relation with gradient magnetic field. In gradient magnetic field, the undercooling and recalescence extent of pure Co keep unchanged. Gradient magnetic field can depress the undercooling and enhance the recalescence extent of Co-Sn alloys.

4. The microstructure evolution process of $Co_{79.5}Sn_{20.5}$ alloy is as follows. At low undercoolings (<40ºC), the microstructure of the alloy is primary αCo+lamellar (αCo+βCo_3Sn_2) eutectic phases. When the undercooling is larger than 100ºC, the eutectic colony starts to form and the final microstructure of the as solidified alloys is αCo+lamellar (αCo+βCo_3Sn_2) eutectic phases+eutectic colony. When the alloy solidifies at higher undercoolings, the volume fraction of primary αCo decreases, and finally disappears. And the volume fraction of anomalous eutectics increases, and finally the whole sample is dominated by anomalous (αCo+βCo_3Sn_2) eutectic phases.

5. The external magnetic field can enhance the precipitation of αCo dendrite phase in $Co_{76}Sn_{24}$ near eutectic alloy. The primary αCo dendrite grows along the direction of magnetic field, forming chain like structure. The secondary αCo dendrite grows at the periphery of the eutectic colonies, and the critical undercooling for disappearance of αCo dendrite increases with the intensity of magnetic field.

6. At low undercoolings, the solidified microstructure of $Co_{72}Sn_{28}$ hypereutectic alloy is primary βCo_3Sn_2 dendrite phase and lamellar eutectics. The equiaxed dendritic βCo_3Sn_2 phase is the outcomes of fragmented dendrites during the remelting

process in the recalescence. With the increasing undercooling, the equiaxed dendritic βCo_3Sn_2 phase becomes smaller and the dendritic morphology becomes more obviously. The anomalous eutectic colony exists at elevated undercoolings, and the secondary dendritic βCo_3Sn_2 phase is precipitated at the end of the colony. When $Co_{72}Sn_{28}$ hypereutectic alloy is solidified in strong magnetic fields, βCo_3Sn_2 dendrites align weakly along the field direction at low undercoolings, and the lamellar eutectics also is aligned by the external field. When the undercooling is above 100ºC, the anomalous eutectics form and all the colonies are aligned by the external magnetic field.

7. At low undercooling, the misorientation angle of αCo and βCo_3Sn_2 phase are between 0~25ºC and 0~5ºC. And at large undercoolings, all the grain boudaries are big angle boundaries, and the misorientation angle obeys a stastical distribution. In 12T magnetic field, αCo phase formed at low undercoolings does not exhibit any orientation, and the misorientation angle distributes widely. The magnetic field has very limited effect on the texturing of αCo and βCo_3Sn_2 phase at large undercoolings.

8. The solidified microstructure of $Co_{76}Sn_{24}$ alloy at low undercoolings in magnetic field has two characteristics. One kind consists in a regular lamellar eutectic grain, and another one is grown from a fishbone like αCo dendrite. The primary αCo phase is the first precipitated phase in the undercooled Co-Sn melt, which causes the formation of fishbone αCo dendritic phase in the center of eutectic grain and the secondary αCo dendrite phase at the periphery of anomalous eutectic colony.

9. The magnetic field enhances the formation of anomalous eutectics and eutectic colony in the undercooled melt. The solidified microstructure of $Co_{76}Sn_{24}$ alloy is regular lamellar eutectics at low undercoolings, and anomalous eutectics starts to precipitate between the lamellar eutectics at the undercooling of 62°C. In 12T magnetic field, the undercooling for the existence of anomalous eutectics decreases to 16°C. During the growth of eutectics microstructure, regular and anomalous eutectics can transform to each other.

REFERENCES

[ABOU00] B. Abou, J.E. Wesfreid and S. Roux, "*The Normal Field Instability in Ferrofluids: Hexagon-Square Transition Mechanism and Wavenumber Selection*", Journal of Fluid Mechanics 416, (2000):217-237.

[ALBR97] T. Albrecht, C. Bührer, M. Fähnle, K. Maier, D. Platzek and J. Reske, "*First Observation of Ferromagnetism and Ferromagnetic Domains in a Liquid Metal*", Applied Physics A: Materials Science & Processing 65, (1997):215-220.

[AMOR84] G. Amoretti and J.M. Fournier, "*On the Interpretation of Magnetic Susceptibility Data by Means of a Modified Curie-Weiss Law*", Journal of Magnetism and Magnetic Materials 43, (1984):L217-L220.

[ASAI89] S. Asai, "*Birth and Recent Activities of Electromagnetic Processing of Materials*", Isij International 29, (1989):981-992.

[ASAI07] S. Asai, *"Magnetic Crystalline Alignment"*, ISIJ International 47, (2007):519-522.

[AZIZ82] M.J. Aziz, "*Model for Solute Redistribution During Rapid Solidification*", Journal of Applied Physics 53, (1982):1158-1168.

[BAN08] C.Y. Ban, D.D. Chen, Y. Han, Q.X. Ba and J.Z. Cui, "*Effect of High Magnetic Field on Solidification Structure of Al-2.89%Fe Alloy*", Acta Metallurgica Sinica 44, (2008):1224-1230.

[BATT89] L. Battezzati and A.L. Greer, "*The Viscosity of Liquid Metals and Alloys*", Acta Metallurgica 37, (1989):1791-1802.

[BEAU91] E. Beaugnon and R. Tournier, "*Levitation of Organic Materials*", Nature 349, (1991):470.

[BOET00] W.J. Boettinger, S.R. Coriell, A.L. Greer, A. Karma, W. Kurz, M. Rappaz and R. Trivedi, "*Solidification Microstructures: Recent Developments, Future Directions*", Acta Materialia 48, (2000):43-70.

[BROO05] R. Brooks, A. Dinsdale and P. Quested, "*The Measurement of Viscosity of Alloys： Review of Methods, Data and Models*", Measurement Science and Technology 16, (2005):354.

[BUSC68] G. Busch and H.J. Guentherodt, "*Ferromagnetic Behavior of Liquid Alloys*", Physics Letters A 27, (1968):110-110.

[BUSC03] K. Buschow and F. Boer, *"Physics of Magnetism and Magnetic Materials"*, Springer, 2003.

[CHEN11] C.G. Cheng, L. Yu, W.C. Wan, Z.T. Liu and Y. Jin, "*Effect of Static Magnetic Field on 2024 Aluminum Alloy Solidification Behavior*", Advanced Materials Research 225, (2011):701-705.

[CHRI03] J. Christian, *"The Theory of Transformations in Metals and Alloys"*, Pergamon Press, 2003.

[COEY09] J. Coey, *"Magnetism and Magnetic Materials"*, Cambridge University Press, 2009.

[COST89] M. Costa Agra Mello and C.S. Kiminami, "*Undercoolability of Copper Bulk Samples*", Journal of Materials Science Letters 8, (1989):1416-1417.

[CULL08] B. Cullity and C. Graham. *"Introduction to Magnetic Materials"*, Wiley-IEEE Press, 2008.

[DERA91] P. Derango, M. Lees, P. Lejay, A. Sulpice, R. Tournier, M. Ingold, P. Germi and M. Pernet, "*Texturing of Magnetic-Materials at High-Temperature by Solidification in a Magnetic-Field*", Nature 349, (1991):770-772.

[FEIJ80] L. Feijoo, C.-W. Woo and V.T. Rajan, "*Statistical Calculation for a Model Ferromagnetic Liquid*", Physical Review B 22, (1980):2404.

[FUKU09] T. Fukuda, H. Maeda, M. Yasui and T. Kakeshita, "*Influence of Magnetocrystalline Anisotropy on Martensitic Transformation under Magnetic Field of Single-Crystalline Ni2MnGa*", Scripta Materialia 60, (2009):261-263.

[GAO09] J. Gao, Y. Zhang, T. Fukuda, H. Yasuda, M. Kolbe and J. He, "*Undercooling and Rapid Solidification of Cu84co16 Alloys under a Static Magnetic Field*", Journal ofPhysics:ConferenceSeries 144, (2009):012117.

[GARC09] T. Garcin, "*Thermodynamic and Kinetic Effects of Static Magnetic Field on Phase Transformations in Low-Alloy Steels*", DOCTEUR EN SCIENCES DE L'UNIVERSITE JOSEPH FOURIER – GRENOBLE, 2009.

[GARC10] T. Garcin, S. Rivoirard, C. Elgoyhen and E. Beaugnon, "*Experimental Evidence and Thermodynamics Analysis of High Magnetic Field Effects*

on the Austenite to Ferrite Transformation Temperature in Fe-C-Mn Alloys", Acta Materialia 58, (2010):2026-2032.

[GATH83] G.R. Gathers, "*Thermophysical Properties of Liquid Copper and Aluminum*", International Journal of Thermophysics 4, (1983):209-226.

[GOET98] R. Goetzinger, M. Barth and D.M. Herlach, "*Mechanism of Formation of the Anomalous Eutectic Structure in Rapidly Solidified Ni-Si, Co-Sb and Ni-Al-Ti Alloys*", Acta Materialia 46, (1998):1647-1655.

[HASE92] M. Hasegawa and S. Asai, "*Effects of Static Magnetic Field on Undercooling of a Copper Melt*", Journal of Materials Science 27, (1992):6123-6126.

[HEMM77] P.C. Hemmer and D. Imbro, "*Ferromagnetic Fluids*", Physical Review A 16, (1977):380.

[HERL94] D.M. Herlach, "*Non-Equilibrium Solidification of Undercooled Metallic Metls*", Materials Science and Engineering: R: Reports 12, (1994):177-272.

[HERL07] D.M. Herlach, P. Galenko and D. Holland-Moritz, "*Metastable Solids from Undercooled Melts*", Elsevier, 2007.

[HERL03] D.M. Herlach, D. Holland-Moritz, R. Willnecker, D. Herlach and K. Maier, "*Magnetic Ordering and Crystal Nucleation in Undercooled Co-Based Melts*", Philosophical Transactions A 361, (2003):497-515.

[HIRO95] N. Hirota, T. Homma, H. Sugawara, K. Kitazawa, M. Iwasaka, S. Ueno, H. Yokoi, Y. Kakudate, S. Fujiwara and M. Kawamura, "*Rise and Fall of Surface Level of Water Solutions under High Magnetic Field*", JAPANESE JOURNAL OF APPLIED PHYSICS PART 2 LETTERS 34, (1995):991-991.

[HOLL02] D. Holland-Moritz, T. Schenk, R. Bellissent, V. Simonet, K. Funakoshi, J. Merino, T. Buslaps and S. Reutzel, "*Short-Range Order in Undercooled Co Melts*", Journal of Non-Crystalline Solids 312, (2002):47-51.

[HOLL04] D. Holland-Moritz and F. Spaepen, "*The Magnetic Contribution to the Driving Force for Crystal Nucleation in Undercooled Co-Pd Melts*", Philosophical Magazine 84, (2004):957-966.

[HOLL07] D. Holland-Moritz, D.M. Herlach and F. Spaepen, "*Crystal Nucleation Induced by Magnetic Ordering in Undercooled Melts*", Superlattices

and Microstructures 41, (2007):196-203.

[HUNT71] J. Hunt and J. Shercliff, "*Magnetohydrodynamics at High Hartmann Number*", Annual Review of Fluid Mechanics 3, (1971):37-62.

[JOO00] H.D. Joo, S.U. Kim, N.S. Shin and Y.M. Koo, "*An Effect of High Magnetic Field on Phase Transformation in Fe-C System*", Materials Letters 43, (2000):225-229.

[JOO04] H. Joo, S. Kim, Y. Koo, N. Shin and J. Choi, "*An Effect of a Strong Magnetic Field on the Phase Transformation in Plain Carbon Steels*", Metallurgical and Materials Transactions A 35, (2004):1663-1668.

[KAKE85] T. Kakeshita, K. Shimizu, S. Funada and M. Date, *"Composition dependence of magnetic field-induced martensitic transformations in Fe-Ni alloys"*, Acta Metallurgica 33, (1985):1381-1389.

[KALA78] T.R. Kalaf and T.M. Wu, "*Model Calculation for a Liquid Ferromagnet*", Physical Review B 18, (1978):448.

[KAMP88] P. Kamp and S. Methfessel, "*Magnetism and Short Range Order in Molten* $Co_{1-x}\ B_x$ ", Journal De Physique (1988):1279-1280.

[KANG94a] J. Kang, K. Hoshikawa, M. Tajima and T. Fukuda, "*Effect of Application of a Magnetic Field During Crystal Growth on the Photoluminescence Characteristics of Ge-Doped Liquid Encapsulated Czochralski Grown Gaas*", Journal of Crystal Growth 135, (1994):623-628.

[KANG94b] J. Kang, Y. Okano, K. Hoshikawa and T. Fukuda, "*Influence of a High Vertical Magnetic Field on Te Dopant Segregation in Insb Grown by the Vertical Gradient Freeze Method*", Journal of Crystal Growth 140, (1994):435-438.

[KITT05] C. Kittel and P. McEuen, "*Introduction to Solid State Physics*", Wiley Press, 2005.

[KOCH00] C.C. Koch, "*Experimental Evidence for Magnetic or Electric Field Effects on Phase Transformations*", Materials Science and Engineering A 287, (2000):213-218.

[LI10a] C. Li, H. Yang, Z. Ren, W. Ren and Y. Wu, "*Application of Differential Thermal Analysis to Investigation of Magnetic Field Effect on Solidification of Al-Cu Hypereutectic Alloy*", Journal of Alloys and Compounds 505, (2010):108-112.

[Li10b] C. Li, H. Yang, Z. Ren, W. Ren and Y. Wu, "*On Nucleation Temperature*

of Pure Aluminum in Magnetic Fields", Progress In Electromagnetics Research 15, (2010):45-52.

[LI08] J. Li, X. Li, L. Liu and S. Lu, "*Mechanism of Anomalous Eutectic Formation in the Solidification of Undercooled Ni-Sn Eutectic Alloy*", Journal of materials research. 23, (2008):2139-2148.

[Li07a] J.F. Li, W.Q. Jie, S. Zhao and Y.H. Zhou, "*Structural Evidence for the Transition from Coupled to Decoupled Growth in the Solidification of Undercooled Ni-Sn Eutectic Melt*", Metallurgical and Materials Transactions A 38, (2007):1806-1816.

[LI03] M. Li and K. Kuribayashi, "*Nucleation-Controlled Microstructures and Anomalous Eutectic Formation in Undercooled Co-Sn and Ni-Si Eutectic Melts*", Metallurgical and Materials Transactions A 34, (2003):2999-3008.

[LI07b] X. Li, Y. Fautrelle and Z. Ren, "*Influence of Thermoelectric Effects on the Solid-Liquid Interface Shape and Cellular Morphology in the Mushy Zone During the Directional Solidification of Al-Cu Alloys under a Magnetic Field*", Acta Materialia 55, (2007):3803-3813.

[LI07c] X. Li, Y. Fautrelle and Z.M. Ren, "*Influence of an Axial High Magnetic Field on the Liquid-Solid Transformation in Al-Cu Hypoeutectic Alloys and on the Microstructure of the Solid*", Acta Materialia 55, (2007):1377-1386.

[LI09a] X. Li, Y. Fautrelle, Z.M. Ren, A. Gagnoud, R. Moreau, Y.D. Zhang and C. Esling, "*Effect of a High Magnetic Field on the Morphological Instability and Irregularity of the Interface of a Binary Alloy During Directional Solidification*", Acta Materialia 57, (2009):1689-1701.

[LI06] X. Li, Z.M. Ren and Y. Fautrelle, "*Effect of a High Axial Magnetic Field on the Microstructure in a Directionally Solidified Al-Al2Cu Eutectic Alloy*", Acta Materialia 54, (2006):5349-5360.

[LI09b] X. Li, Z.M. Ren, Y. Fautrelle, A. Gagnoud, Y.D. Zhang and C. Esling, "*Degeneration of Columnar Dendrites During Directional Solidification under a High Magnetic Field*", Scripta Materialia 60, (2009):443-446.

[LIU04] L. Liu, C. Andersson and J. Liu, "*Thermodynamic Assessment of the Sn-Co Lead-Free Solder System*", Journal of Electronic Materials 33, (2004):935-939.

[LIU09] L. Liu, J. Li, S. Zhao and Y. Zhou, "*Redetermination of the Eutectic Composition of the Co-Sn Binary Alloy*", Journal of Phase Equilibria and Diffusion 30, (2009):242-245.

[LIU11a] L. Liu, J. Li and Y. Zhou, "*Solidification Interface Morphology Pattern in the Undercooled Co-24.0 At.% Sn Eutectic Melt*", Acta Materialia 59 (2011):5558-5567.

[LIU07] T. Liu, Q. Wang, A. Gao, C. Zhang, C. Wang and J. He, "*Fabrication of Functionally Graded Materials by a Semi-Solid Forming Process under Magnetic Field Gradients*", Scripta Materialia 57, (2007):992-995.

[LIU11b] T. Liu, Q. Wang, A. Gao, H. Zhang and J. He, "*Effects of a High Magnetic Field on the Phase Equilibria of Mn-Sb System During Solidification Process*", Journal of Alloys and Compounds 509, (2011):5822-5824.

[LIU11c] T. Liu, Q. Wang, H.W. Zhang, C.S. Lou, K. Nakajima and J.C. He, "*Effects of High Magnetic Fields on Solidification Microstructure of Al-Si Alloys*", Journal of Materials Science 46, (2011):1628-1634.

[MOLO04] D.A. Molodov and A.D. Sheikh-Ali, "*Effect of Magnetic Field on Texture Evolution in Titanium*", Acta Materialia 52, (2004):4377-4383.

[MORE93] R. Moreau, O. Laskar, M. Tanaka and D. Camel, "*Thermoelectric Magnetohydrodynamic Effects on Solidification of Metallic Alloys in the Dendritic Regime*", Materials Science and Engineering: A 173, (1993):93-100.

[MOTA90] S. Motakef, "*Magnetic Field Elimination of Convective Interference with Segregation During Vertical-Bridgman Growth of Doped Semiconductors*", Journal of Crystal Growth 104, (1990):833-850.

[MULL63] W.W. Mullins and R.F. Sekerka, "*Morphological Stability of a Particle Growing by Diffusion or Heat Flow*", Journal of Applied Physics 34, (1963):323-329.

[MULL64] W.W. Mullins and R.F. Sekerka, "*Stability of a Planar Interface During Solidification of a Dilute Binary Alloy*", Journal of Applied Physics 35, (1964):444-451.

[NAKA69] Y. Nakagawa, "*Comments on Ferromagnetic Behaviour of Liquid Alloys*", Physics Letters A 28, (1969):494-495.

[NIES88] A.K. Niessen, A.R. Miedema, F.R. de Boer and R. Boom, *"Enthalpies of*

Formation of Liquid and Solid Binary Alloys Based on 3d Metals: *Iv. Alloys of Cobalt"*, Physica B+C 151, (1988):401-432.

[OKAM06] H. Okamoto, "*Co−Sn (Cobalt-Tin)*", Journal of Phase Equilibria and Diffusion 27, (2006):308-308.

[OREP83] G. Oreper and J. Szekely, "*The Effect of an Externally Imposed Magnetic Field on Buoyancy Driven Flow in a Rectangular Cavity*", Journal of Crystal Growth 64, (1983):505-515.

[PLAT94] D. Platzek, C. Notthoff, D. Herlach, G. Jacobs, D. Herlach and K. Maier, "*Liquid Metal Undercooled Below Its Curie Temperature*", Applied Physics Letters 65, (1994):1723.

[REN06] Z.M. Ren, X. Li, Y.H. Sun, Y. Gao, K. Deng and Y.B. Zhong, "*Influence of High Magnetic Field on Peritectic Transformation During Solidification of Bi-Mn Alloy*", Calphad-Computer Coupling of Phase Diagrams and Thermochemistry 30, (2006):277-285.

[RESK95] J. Reske, D.M. Herlach, F. Keuser, K. Maier and D. Platzek, "Evidence *for the Existence of Long-Range Magnetic Ordering in a Liquid Undercooled Metal*", Physical Review Letters 75, (1995):737.

[REUT04] S. Reutzel and D.M. Herlach, "*Magnetic Properties of Undercooled Co-Based Alloys*", Materials Science and Engineering A 375-377, (2004):552-555.

[RIVO09] S. Rivoirard, "*Texturing Hard Nd-Fe-B Powdered Ribbons in High Magnetic Field*", Journal of Physics: Conference Series 156, (2009):012009.

[ROSE66] R. Rosensweig, "*Buoyancy and Stable Levitation of a Magnetic Body Immersed in a Magnetizable Fluid*", Nature 210, (1966):613-614.

[ROSE87] R.E. Rosensweig, *"Magnetic Fluids"*, Annual Review of Fluid Mechanics 19, (1987):437-461.

[ROSE96] R.E. Rosensweig, "*Negative Viscosity in a Magnetic Fluid*", Science 271, (1996):614.

[SAVI81] E. Savitsky, R. Torchinova and S. Turanov, "*Effect of Crystallization in Magnetic Field on the Structure and Magnetic Properties of Bi-Mn Alloys*", Journal of Crystal Growth 52, (1981):519-523.

[SCHE02] T. Schenk, D. Holland-Moritz, V. Simonet, R. Bellissent and D.M. Herlach, "*Icosahedral Short-Range Order in Deeply Undercooled*

Metallic Melts", Physical Review Letters 89, (2002):075507.

[SUN09] J. Sun, H. Zheng and X. Shi, "*Structure Correlation of Co79.5Sn20.5 Eutectic Alloy between Liquid and Solid States*", Sci China Ser E-Tech Sci 52, (2009):3674-3677.

[TEWA94] S. Tewari, R. Shah and H. Song, "*Effect of Magnetic Field on the Microstructure and Macrosegregation in Directionally Solidified Pb-Sn Alloys*", Metallurgical and Materials Transactions A 25, (1994):1535-1544.

[TILL53] W.A. Tiller, K.A. Jackson, J.W. Rutter and B. Chalmers, "*The Redistribution of Solute Atoms During the Solidification of Metals*", Acta Metallurgica 1, (1953):428-437.

[TOUR00] R. Tournier, S. Pavard, D. Bourgault and C. Villard, "*Bulk Bi2212 Texturing Bu Solidification in a High Magnetic Field and Hot Forging*", Advances in Superconductivity Xii (2000):527-529.

[TOUR07] R.F. Tournier, *"Presence of intrinsic growth nuclei in overheated and undercooled liquid elements"*, Physica B: Condensed Matter 392, (2007):79-91.

[TOUR12] R.F. Tournier, "Thermodynamic and kinetic origins of the vitreous transition", Intermetallics, In Press.

[TRIV86] R. Trivedi and W. Kurz, "*Morphological Stability of a Planar Interface under Rapid Solidification Conditions*", Acta Metallurgica 34, (1986):1663-1670.

[TURN50] D. Turnbull, "*Formation of Crystal Nuclei in Liquid Metals*", Journal of Applied Physics 21, (1950):1022-1028.

[TURN69] D. Turnbull, "*Under What Conditions Can a Glass Be Formed?*", Contemporary Physics 10, (1969):473 - 488.

[UTEC66] H.P. Utech and M.C. Flemings, "*Elimination of Solute Banding in Indium Antimonide Crystals by Growth in a Magnetic Field*", Journal of Applied Physics 37, (1966):2021-2024.

[VAKA84] I.A. Vakarchuk, G.V. Ponedilok and Y.K. Rudavskii, "*Theory of Liquid Magnets*", Theoretical and Mathematical Physics 58, (1984):291-302.

[VOLL84] D. Vollhardt, *"Normal ^{3}He: an almost localized Fermi liquid"*, Reviews of Modern Physics 56, (1984) 99-120.

[WANG09] Q. Wang, A. Gao, T. Liu, F. Liu, C. Zhang and J. He, "*Solidified*

Microstructure Evolution of Mn-Sb near-Eutectic Alloy under High Magnetic Field Conditions", Journal of Materials Research 24, (2009):2332.

[WEB1] http://www.cryogenic.co.uk

[WEB2] http://en.wikipedia.org/wiki/Ferrofluid

[WEI93] B. Wei, D.M. Herlach, F. Sommer and W. Kurz, "*Rapid Solidification of Undercooled Eutectic and Monotectic Alloys*", Materials Science and Engineering: A 173, (1993):355-359.

[WEST10] M.C. Weston, M.D. Gerner and I. Fritsch, "*Magnetic Fields for Fluid Motion*", Analytical chemistry 82, (2010):3411-3418.

[XION08] X.Y. Xiong and T.R. Finlayson, "*Phase Transformation Sequence and Magnetic Properties of Melt-Spun Smco-Based Alloy after Isochronal Heat Treatment*", Journal of Applied Physics 104, (2008):103910-103917.

[YANG11] C. Yang, J. Gao, Y. Zhang, M. Kolbe and D. Herlach, "*New Evidence for the Dual Origin of Anomalous Eutectic Structures in Undercooled Ni-Sn Alloys: In Situ Observations and Ebsd Characterization*", Acta Materialia 59, (2011)3915-3926.

[YANG09a] W. Yang, F. Liu, H. Liu, H.F. Wang, G.C. Yang and Y.H. Zhou, "*Numerical Description for the Recalescence of Bulk-Undercooled Cu70ni30 Alloy*", Journal of Crystal Growth 311, (2009):3225-3230.

[YANG09b] W. Yang, F. Liu, H.F. Wang, Z. Chen, G.C. Yang and Y.H. Zhou, "*Prediction of the Maximal Recalescence Temperature Upon Rapid Solidification of Bulk Undercooled Cu70Ni30 Alloy*", Journal of Alloys and Compounds 470, (2009):L13-L16.

[YASU05] H. Yasuda, I. Ohnaka, R. Ishii, S. Fujita and Y. Tamura, "*Investigation of the Melt Flow on Solidified Structure by a Levitation Technique Using Alternative and Static Magnetic Fields*", Isij International 45, (2005):991-996.

[YASU01] H. Yasuda, I. Ohnaka, O. Kawakami, M. Yamamoto, K. Ueno and K. Kishio, "*Effect of a High Magnetic Field on Monotectic Solidification*", Pricm 4: Forth Pacific Rim International Conference on Advanced Materials and Processing, Vols I and Ii (2001):289-292.

[YASU04] H. Yasuda, I. Ohnaka, Y. Ninomiya, R. Ishii, S. Fujita and K. Kishio,

"*Levitation of Metallic Melt by Using the Simultaneous Imposition of the Alternating and the Static Magnetic Fields*", Journal of Crystal Growth 260, (2004):475-485.

[ZELD43] Y.B. Zeldovich, "*On the Theory of New Phase Formation: Cavitation*", Acta Physicochim. URSS 18, (1943):1-22.

[ZHAN10a] Y. Zhang, J. Gao, Y. Zhou, D. Herlach and J. He, "*Undercooling Behavior of Glass-Fluxed Sb Melts under Gradient Magnetic Fields*", Journal of Materials Science 45, (2010):1648-1654.

[ZHAN10b] Y. Zhang, Y. Zhou, J. Gao and J. He, "*Undercooling of Pure Cu and Ge Melts in a Static Magnetic Field*", Materials Science Forum 649, (2010):281-286.

[ZHAN05] Y.D. Zhang, C. Esling, J.S. Lecomte, C.S. He, X. Zhao and L. Zuo, "*Grain Boundary Characteristics and Texture Formation in a Medium Carbon Steel During Its Austenitic Decomposition in a High Magnetic Field*", Acta Materialia 53, (2005):5213-5221.

[ZHOU11a] S. Zhou, R. Hu, L. Jiang, J. Li, H. Kou, H. Chang and L. Zhou, "*Microstructure Evolution in Undercooled Co80Pd20 Alloys*", Journal of Materials Science 46, (2011):5495-5502.

[ZHOU11b] S. Zhou, R. Hu, J. Li, H. Chang, H. Kou and L. Zhou, "*Stress Induced Deformation in the Solidification of Undercooled Co80Pd20 Alloys*", Materials Science and Engineering: A 528, (2011):973-977.

Abstract

This work is devoted to the investigation of the magnetic field effect on the magnetic properties and solidification behavior of undercooled Co based alloys in high magnetic field. Co based alloys are promising candidates to be undercooled below or approaching their Curie point in strong magnetic field due to their small temperature difference between liquid line and Curie point. In this dissertation, a high temperature undercooling facility with magnetization measurement system is built in a superconducting magnet, and is used for in situ measurement of the magnetization of the undercooled melts and to studying the undercoolability and solidification microstructure evolution in magnetic field. The deep undercooled Co melt is strongly magnetized in magnetic fields, and its magnetization is even larger than the magnetization of heated solid at the same temperature. The magnetization of undercooled Co-B near eutectic alloy is related with overheating temperature while the undercooled Co-Sn melt is always in paramagnetic state. Mean undercooling and recalescence extent of different metals and alloys are affected by external magnetic field. In uniform magnetic field, the undercooling of Cu is enhanced while the undercoolings of Co and Co-Sn keep constant. However, the recalescence extents of Co and Co-Sn alloys are reduced, and with the increasing Co content, the effect becomes larger. Magnetic field promotes the precipitation of αCo dendrite phase and the formation of anomalous eutectics in solidified microstructure of undercooled Co-Sn alloys. The microstructure evolution processes are affected by magnetic field depending on the field intensity and undercooling. This work opens a new way to investigate the magnetic properties of deeply undercooled metallic melts and non-equilibrium solidification in strong magnetic fields.

Résumé

Ce travail est dédié à l'étude de l'effet des champs magnétiques sur les propriétés magnétiques et le comportement à la solidification d'alliages à base de Cobalt en surfusion sous champ magnétique intense. Les alliages à base Co sont d'excellents candidats pour obtenir une surfusion en dessous ou proche du point de Curie sous champ intense en raison du faible écart entre ce point de Curie et la température du liquidus. Dans cette étude, un dispositif haute température de surfusion intégrant une mesure magnétique a été construit dans un aimant supraconducteur, et est utilisé pour la mesure in situ de l'aimantation de liquides surfondus et pour l'étude du sur-refroidissement et de l'évolution de la microstructure de solidification en champ intense. Le cobalt liquide en surfusion est fortement magnétique sous champ, et son aimantation est même supérieure à celle du solide au chauffage à la même température. L'aimantation de l'alliage proche eutectique Co-B en surfusion dépend de la température de surchauffe, tandis que le Co-Sn en surfusion est toujours paramagnétique. La surfusion moyenne et l'étendue de la recalescence de différents métaux et alliages est affectée par un champ externe. En champ magnétique uniforme, la surfusion du Cuivre est amplifiée, tandis que la surfusion du Cobalt et de Co-Sn reste identique. Cependant, l'étendue de la recalescence du Cobalt et de Co-Sn est réduite, et l'effet est d'autant plus important pour des teneurs supérieures en Cobalt. Le champ magnétique promeut la précipitation de la phase dendritique αCo et la formation d'eutectique anormal dans la microstructure des alliages Co-Sn surfondus. Les processus d'évolution de la microstructure sont affectés par le champ magnétique, et dépendent de l'intensité du champ et de la surfusion. Ce travail offre de nouveaux horizons dans l'étude des propriétés magnétiques d'alliages métalliques en forte surfusion et dans l'étude de la solidification hors équilibre sous champ magnétique intense.